TECHNISCHE UNIVERSITÄT MÜNCHEN
FAKULTÄT FÜR MEDIZIN

Elucidation of the molecular mechanisms underlying *aryl hydrocarbon receptor-interacting protein* (*AIP*)-dependent tumorigenesis in the pituitary

Eva-Maria Bogner

Vollständiger Abdruck der von der Fakultät für Medizin der Technischen Universität München zur Erlangung des akademischen Grades eines Doktors der Naturwissenschaften genehmigten Dissertation.

Vorsitzende: Prof. Dr. Stephanie E. Combs

Prüfer der Dissertation:

1. Prof. Dr. Michael J. Atkinson

2. Prof. Dr. Nina H. Uhlenhaut

Die Dissertation wurde am 06.05.2020 bei der Technischen Universität München

eingereicht und durch die Fakultät für Medizin am 01.12.2020 angenommen.

Statutory Declaration:

I declare that I have authored this thesis independently, that I have not used other than the declared sources/resources, and that I have explicitly marked all material which has been quoted either literally or by content from the used sources.

Munich, ……

Eva-Maria Bogner

Eidesstattliche Erklärung:

Ich erkläre an Eides statt, dass ich die vorliegende Arbeit selbstständig verfasst, keine anderen als die angegebenen Quellen/Hilfsmittel benutzt, und die den benutzten Quellen wörtlich und inhaltlich entnommene Stellen als solche kenntlich gemacht habe.

München, ……

Eva-Maria Bogner

Table of Contents

Abstract

Mutations of the aryl hydrocarbon receptor interacting protein (AIP) are associated with a subset of aggressive pituitary adenomas (PAs) that are commonly resistant to therapy. Although a multitude of cases with AIP mutations (*AIP*mut+) have been described, the molecular mechanisms underlying AIP-associated tumorigenesis are unclear. AIP is able to interact with a variety of proteins, which led to the assumption that upon AIP mutation tumorigenesis is mediated by a loss of protein-protein interactions. The most extensively studied interaction partner of AIP is the aryl hydrocarbon receptor (AhR), which is able to regulate miRNA expression. This, together with the fact that it has been previously reported that miRNAs may play a crucial role in PA development and progression, led to the assumption that miRNA expression is altered in *AIP*mut+ compared to *AIP*mut- PAs and this dysregulation may cause the distinctive phenotype of *AIP*mut+ patients. Therefore, we aimed to elucidate whether human *AIP*mut+ and *AIP*mut- tumors are associated with different miRNA signatures and, if so, whether the differentially expressed miRNAs impair cellular function of PA cells and can possibly lead to tumorigenesis of these cells.

We identified a novel subset of miRNAs that were differentially expressed between *AIP*mut+ and *AIP*mut- human pituitary tumors. We were able to link the upregulation of two miRNAs, miR-145 and miR-34a, directly to the overexpression of mutant AIP (AIP-R271W) in *Aip*-/- MEFs. Both candidate miRNAs were functionally characterized *in vitro* in rat GH3 cells, which surprisingly revealed that overexpression of miR-34a, frequently described as a tumor suppressor miRNA, increased pro-tumorigenic behavior of transfected cells in terms of cell viability, proliferation, migration, colony formation and apoptosis as well as *in vitro* therapy response and intracellular signaling. Target prediction for miR-34a led to the identification of *Gnai2*, encoding Gαi2, as a promising candidate target gene. *Gnai2* was validated as a direct target of miR-34a and Gαi2 levels were significantly reduced in *AIP*mut+ compared to *AIP*mut- patient samples.

In conclusion, this study might help to shed light on the complex cellular processes that lead to tumorigenesis in *AIP*mut+ PAs by adding the downregulation of Gαi2 by miR-34a, which is in turn up-regulated in *AIP*mut+ PAs, as a possible pathway. miR-34a was shown to act as an oncomiR in PA cells, thus reinforcing the concept that miR-34a plays a pro- or anti-oncogenic role in tumors depending on the cellular context. While miR-34a may not represent an ideal therapy target due to possible pro- and anti-tumorigenic actions, Gαi2 is worthy of further investigation as a putative target for PA therapy in *AIP*mut+ patients.

Zusammenfassung

Mutationen in AIP (aryl hydrocarbon receptor-interacting protein) liegen einem Teil aggressiver Hypophysenadenomen (HA) zu Grunde, die häufig resistent gegenüber Therapien sind. Obwohl bereits eine Vielzahl an Fällen von HA mit AIP Mutationen (*AIP*mut+) bekannt sind, sind die molekularen Mechanismen, auf der die AIP-abhängige Tumorentstehung beruht, noch nicht aufgeklärt. AIP ist in der Lage mit einer Vielzahl von Proteinen zu interagieren, was zu der Annahme führet, dass die mit AIP Mutationen einhergehende Tumorentwicklung mit einem Verlust der Protein-Protein-Interaktionen zusammenhängt. Der am besten untersuchte Interaktionspartner von AIP ist AHR (aryl hydrocarbon receptor), der miRNA Expression regulieren kann. Dies, zusammen mit der Tatsache, dass bereits gezeigt wurde, dass miRNAs eine wichtige Rolle in der Entstehung und dem Verlauf von HA spielen, lies uns vermuten, dass die Expression von miRNAs in *AIP*mut+ HAs dysreguliert ist und dies den speziellenen Phänotyp von *AIP*mut+ Patienten erklären könnte. Daher zielten wir mit unserer Studie darauf ab zu klären, ob miRNAs, die in eine abweichende Expression in *AIP*mut+ im Vergleich zu *AIP*mut- HA aufweisen, die Funktionen von HA Zellen beeinträchtigen und möglicherweise zur Tumorentstehung in diesen Zellen führen.

Wir konnten eine für HA neuartige Menge an miRNAs ermitteln, die zwischen *AIP*mut+ and *AIP*mut- Tumoren differenziell exprimiert sind. Mehrere miRNAs konnten im Patientengewebe validiert werden und anschließend wurde die Hoch-Regulierung zweier miRNAs, miR-145 und miR-34a, direkt auf die Überexpression von mutiertem AIP (AIP-R271W) in MEF *Aip*-/- zurückgeführt. Beide Kandidaten wurden einer funktionellen *in vitro* Charakterisierung in GH3 Zellen unterzogen, die überraschenderweise offenbarte, dass miR-34a, die normalerweise als Tumor Suppressor miRNA beschrieben wird, das onkogene Verhalten der Zellen fördert. Dies geschah in Bezug auf Viabilität, Proliferation, Migraition, Bildung von Kolonien und Apoptose, sowie das *in vitro* Ansprechen auf Medikamente und den Effekt auf intrazelluläre Signalwege. Daher wurden im Anschluss die Zielgene für miR-34a vorhergesagt, was zur Identifizierung von *Gnai2* (Gαi2) als vielversprechenden Kandidaten führte. Der direkte funktionelle Zusammenhang zwischen *Gnai2* und miR-34a wurde nachgewiesen und es konnte weiterhin gezeigt werden, dass die Expression von Gαi2 in *AIP*mut+ Patientengewebe reduziert war.

Zusammenfassend könnte diese Studie dabei helfen, die komplexen zellulären Prozesse aufzuklären, die zur Tumorentstehung in *AIP*mut+ HA führt, da wir die reduktion der Expression von Gαi2 durch miR-34a, welches wiederum in *AIP*mut+ HAs überexprimiert ist, nachweisen

konnten. Diese Interaktion kann möglicherweise die onkogenen Eigenschaften von HA Zellen beeinflussen. Desweiteren konnte gezeuigt werden, dass miR-34a als „oncomiR“ in HA Zellen funktioniert, was das Konzept, dass miR-34a in Abhängigkeit von dem zellulären Kontext eine pro- oder anti-onkogene Rolle in Tumoren spielen kann. miR-34a stellt auf Grund seiner dualen Rolle in der Tumorentstehung kein optimales Zielmolekül für eine zukünftige Therapie dar. Gαi2 hingegen ist eine interesannte Zielstruktur, die für mögliche Therapien in Betracht gezogen werden sollte.

Abbreviations

%	percent
(q)RT-PCR	quantitative reverse transcription polymerase chain reaction
(v/v)	volume per volume
(w/v)	weight per volume
°C	degree Celsius
µ	micro- (10^{-6})
AA	amino acid
Ab	antibody
AB-block	avidin-biotin block
AC	adenylate cyclase
ACTH	adrenocorticotropic hormone
ad.	Adjust to
ADH	antidiuretic hormone
AGO protein	argonaute protein
AhR	aryl hydrocarbon receptor
AHRE	aryl hydrocarbon response elements
AIP	aryl hydrocarbon receptor interacting protein
*AIP*mut-	*AIP* mutation negative
*AIP*mut+	*AIP* mutation positive
AMB	amphotericin B
ANOVA	analysis of variance
APS	ammonium persulfate
ARA9	aryl hydrocarbon receptor activated protein 9
ARNT	aryl hydrocarbon receptor nuclear translocator
ATP	denosine triphosphate
B2m	β_2 microtubulin
BAX	Bcl-2-associated X protein
BBC3/PUMA	BCL2 Binding Component 3
BCA	bicinchoninic acid
BCL2	B-cell lymphoma 2
bidest.	bidestillatus
bp	base pair
BSA	bovine serum albumin
c	centi- (10^{-2})
$CaCl_2$	calcium chloride
cAMP	cyclic adenosine monophosphate
CCNA2	cyclin-A2
CDK	cyclin-dependent kinase
CDKN1B	cyclin-dependent kinase inhibitor 1B
cDNA	complementary DNA
cGMP	cyclic guanosine monophosphate
ChIP	chromatin immunoprecipitation
CHX	cycloheximide
CLL	chronic lymphocytic leukemia
CMV	cytomegalovirus
CNC	Carney Complex
CO_2	carbon dioxide
CRH	corticotropin-releasing hormone
Ct	cycle threshold
DA	dopamine agonist
Da	Dalton
DAB	3,3'-diaminobenzidine
DAPI	4′,6-diamidino-2-phenylindole
dATP	deoxyadenosine triphosphate
dCTP	deoxycytidine triphosphate
dGTP	deoxyguanosine triphosphate
DMEM	Dulbecco's modified eagle's medium
DMSO	dimethyl sulfoxide
DNA	deoxyribonucleic acid
dNTP	nucleoside triphosphate
DTT	dithiothreitol
dTTP	deoxythymidine triphosphate

E.coli	*Escherichia coli*
e.g.	exempli gratia (for example)
E2F3	E2F transcription factor 3
EDTA	ethylenediaminetetraacetic acid
ELISA	enzyme linked immunosorbent assay
EPOX	epoxomicin
ERK1/2	extracellular signal-regulated kinases ½
EXP5	exportin 5
FBS	fetal bovine serum
FC	fold change
FDR	false discovery rate
FFPE	formalin-fixed paraffin embedded
FIPA	familial isolated pituitary adenomas
FS cells	folliculostellate cells
FSH	follicle stimulating hormone
FSK	forskolin
g	relative centrifugal force/gramm
GH	growth hormone
GHRH	growth hormone–releasing hormone
GNAI2/Gαi2	Guanine Nucleotide Binding Protein (G Protein), Alpha Inhibiting Activity Polypeptide 2
GNAI3/Gαi3	Guanine Nucleotide Binding Protein (G Protein), Alpha Inhibiting Activity Polypeptide 3
GNAO1/Gαo1	Guanine Nucleotide Binding Protein (G Protein), Alpha Activating Activity Polypeptide O
GNAQ/Gαq	Guanine Nucleotide Binding Protein (G Protein), Q Polypeptide
GNAS/Gαs	Guanine Nucleotide Binding Protein (G Protein), Alpha Stimulating Activity Polypeptide 1
GnRH	gonadotropin-releasing hormone
g protein	guanine nucleotide binding protein
GPCR	G-protein coupled receptor
GPR101	G protein-coupled receptor 101
Gα13	Guanine Nucleotide-Binding Protein Subunit Alpha-13
Gαq	Guanine Nucleotide-Binding Protein G(Q) Subunit Alpha
h	hour
H&E	haematoxylin and eosin
HBSS	Hank's balanced salt solution
HEK293 cells	human embryonic kidney 293 cells
hluc	*Firefly* luciferase
HMGA ½	High-mobility group protein ½
hRluc	*Renilla* luciferase
HS	horse serum
I	homo sapiens
HSP90	heat shock protein 90
i.e.	id est (that is)
IF	immunfluorescence
IFS	isolated familial somatotropinomas
IGF-1	Insulin-like growth factor-1
IHC	immunhitochemistry
k	kilo- (10^3)
kb	kilo base
l	liter
LB	lysogeny broth/Luria broth
LH	luteinizing hormone
LOH	loss of heterozygosity
m	meter/milli- (10^{-3})
M	molar
MEF	mouse embryonic fibroblast
MEN1	multiple endocrine neoplasia type 1
MEN4	multiple endocrine neoplasia type 4

MENX	multiple endocrine neoplasia-like syndrome X
min	minute
miRNA	microRNA
mM	milli molar
mmu	mus musculus
mRNA	messenger RNA
mut	mutant
n	number/nano- (10^{-9})
n.s.	not significant
NaOAc	sodium acetate
NFPA	Non-functioning pituitary adenoma
NGS	normal goat serum
nt	nucleotide
Oct	octreotide
OCT-LAR	octreotide-long-acting repeatable
OD	optical density
Opti-MEM	optimized modified eagle's medium
ORF	open reading frame
OT	oxytocin
P/S	penicillin/streptomycin
PA	pituitary adenoma
PAM16/Magmas	presequence translocated-associated motor subunit PAM16/ mitochondria-associated granulocyte macrophage CSF-signaling molecule
PAP	pituitary adenoma predisposition
PBS	phosphate buffered saline
PCC	pheochromocytoma
PCR	polymerase chain reaction
PDE	phosphodiesterase
PFA	paraformaldehyde
pH	minus the decimal logarithm of the hydrogen ion activity in solution
PKA	cAMP-dependent protein kinase A
PLAG1	Pleiomorphic Adenoma Gene-Like 1
Pol II	polymerase II
PPIase	peptidyl-prolyl *cis-trans* isomerase
pre-miRNA	precursor miRNA
pri-miRNA	primary miRNA
PRKAR1A	protein kinase cAMP-dependent Type I regulatory subunit alpha
PRL	prolactin
PT	Pertussis toxin
PTTG	pituitary tumor-transforming gene
RB1	Retinoblastoma 1
RIPA	radio-immunoprecipitation assay
RISC	RNA-induced silencing complex
RNA	ribonucleic acid
rno	rattus norvegicus
rpm	rounds per minute
RT	room temperature
SDS	sodium dodecyl sulphate
SDS-PAGE	discontinuous sodium dodecyl sulphate polyacrylamide gel electrophoresis
sec	second
SEM	standard error of the mean
Smad3	mothers against decapentaplegic homolog 3
Sox5	SRY-Box 5
SOX7	SRY-Box 7
SRY	sex determining region Y
SSA	somatostatin analog
SSTR	somatostatin receptor
TBE	tris/boric acid/EDTA
TBP	TATA binding protein
TBS-T	tris-buffered saline with tween 20
TCDD	2,3,7,8-tetrachlorodibenzo-p-dioxin
TE	Tris-EDTA

TEMED	N,N,N',N'-tetramethylethane-1.2.iamine	V	volt
		vs	versus
TGFβ	Transforming growth factor β	W	watt
T-MF	transformed mycosis fungoides	WB	western blot
TPR	tetratricopeptide repeat	WST-1	water soluble tetrazolium 1
TRH	thyrotropin-releasing hormone	wt	wild-type
Tris	2-Amino-2-(hydroxymethyl) propane-1,3-diol	XAP2	hepatitis B virus X-associated protein 2
TSH	thyroid-stimulating hormone	X-LAG	X-linked acrogigantism
u	unit	XRE	xenobiotic response element
UTR	untranslated region	yrs	years
UV	ultraviolet	ZAC1	See PLAG1

1. Introduction

1.1. Pituitary adenomas

1.1.1. The pituitary gland and the endocrine system

The pituitary gland or hypophysis is an endocrine gland, existing in all vertebrate species, located at the base of the brain. The pituitary is often referred to as the “master gland” due to the ability of its different hormones to target multiple organs of the body, thereby regulating a variety of body functions [1].

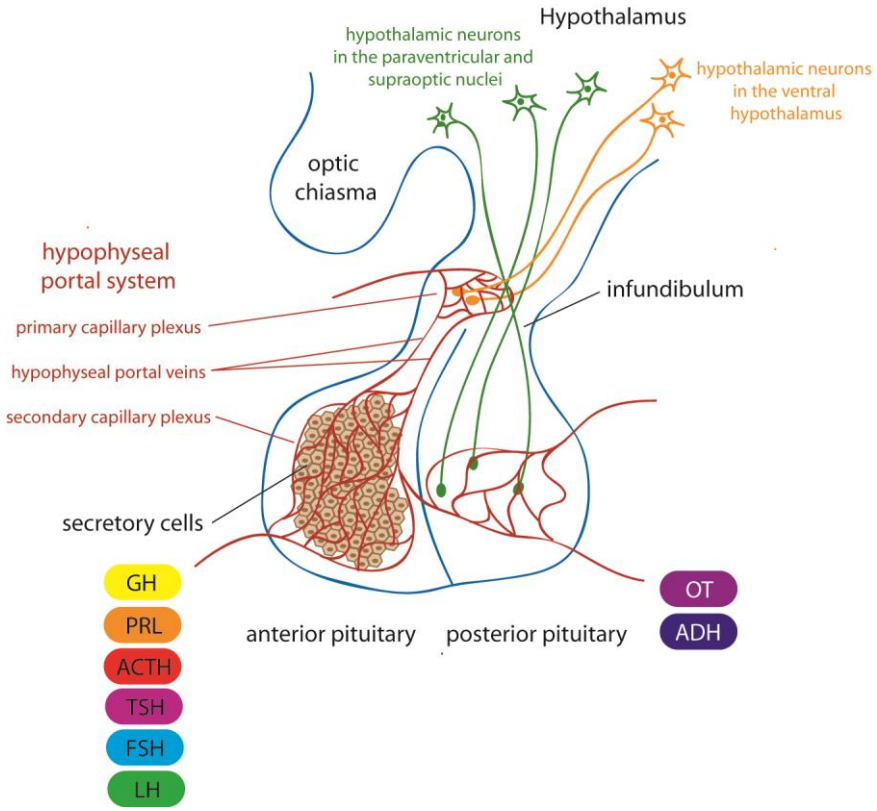

Figure 1: Schematic representation of the pituitary gland. The posterior pituitary receives direct nervous input from the paraventricular and supraoptic nuclei of the hypothalamus and subsequently releases Oxytocin (OT) and antidiuretic hormone (ADH) from axon terminals of neurosecretory cells. The anterior pituitary is stimulated or inhibited by regulatory hormones produced in the arcuate nucleus of the hypothalamus and transported to the anterior pituitary via the hypophyseal portal system. These hormones lead to the release/retention of the respective pituitary hormones. ACTH: Adrenocorticotropic hormone; ADH: antidiuretic hormone; FSH: Follicle-stimulating hormone; GH: Growth hormone; LH: Luteinizing hormone; OT: Oxytocin; PRL: Prolactin; TSH: Thyroid-stimulating hormone;
Figure: Eva-Maria Bogner

The pituitary is composed of two functionally distinct structures, that are both of ectodermal origin: 1) the adenohypophysis, or anterior pituitary, derived from oral ectoderm, 2) the neurohypophysis

or posterior pituitary, which originates from neural ectoderm [1]. The infundibulum, or pituitary stalk, connects the pituitary to the brain (Figure 1). The hypothalamus serves to integrate the nervous system with the endocrine systems in the anterior or posterior pituitary compartment. In the hypothalamus, neurosecretory cells of the paraventricular nuclei predominantly produce oxytocin (OT) while antidiuretic hormone (ADH, Vasopressin) is synthesized predominantly in the supraoptic nuclei. Both hormones are transported to and released from axon terminals innervating the posterior pituitary [2-4]. Two classes of regulatory hormones (releasing or release-inhibiting) are secreted in the arcuate nucleus of the hypothalamus and transported to the anterior pituitary via the hypophyseal portal system. In the anterior pituitary these regulatory hormones bind to G-protein coupled receptors which regulate the intracellular levels of cAMP and therefore cause either release or retention of hormones produced by the anterior pituitary (Figure 1) [4, 5]. Hormones that are released from the different parts of the pituitary, and their respective target organs and functions are listed in Table 1 and Table 2.

Table 1: Hormones released from the posterior pituitary. Structure of origin, target organs and subsequent functions are listed [2].

Pituitary hormone	Structure of origin	Target organ	Function in target organ
Oxytocin (OT)	Paraventricular nucleus of the hypothalamus	Uterus, Mammary glands	Uterine contraction (during childbirth), breast milk production
Antidiuretic hormone (ADH, Vasopressin)	Supraoptic nucleus of the hypothalamus	Kidney	Regulation of water reabsorption

The anterior pituitary comprises of a mixture of five different secretory cell types that each synthesize and secrete specific hormones (Table 2). The secretory cells are located in the pars distalis of the anterior pituitary and can be classified into alpha (also referred to as acidophil) and beta cells (basophil). Both, GH releasing somatotroph and PRL secreting lactotroph cells are acidophil, whereas TSH secreting thyrotroph, ACTH secreting corticotroph and LH/FSH secreting gonadotroph cells belong to the basophil cell group. The difference in staining behavior of the respective cell types can be explained by the differences in the protein structures of the hormones that are stored in the secretory granules of the cells. Somatotroph cells are the most abundant secretory cells in the anterior pituitary (50 %) followed by lactotrophs (10-30 %), gonadotrophs (20 %), corticotrophs (10 %) and thyrotrophs (5 %) [6]. In addition, folliculostellate (FS) cells can be found in the anterior pituitary, although these have no neuroendocrine functions. FS cells are morphologically similar to astrocytes with an astral cell body and long cytoplasmatic processes

interspersed within the surrounding neuroendocrine cells [7]. The roles of FS cells in the pituitary include support and signal mediation, and they may potentially possess stem cells characteristics [8].

Table 2: Hormones of the hypothalamus and the anterior pituitary. Hypothalamic release (+)/retention (-) hormones, their target cell type in the pituitary, pituitary hormone, target organs and subsequent functions are listed. ACTH: Adrenocorticotropic hotmone; CRH: Corticotropin-releasing hormone; FSH: Follicle stimulating hormone; GH: Growth hormone; GHRH: Growth hormone-releasing hormone; GnRH: Gonadotropin-releasing hormone; LH: Luteinizing hormone; PRL: Prolactin; TRH: thyrotropin-releasing hormone; TSH: Thyroid stimulating hormone;

Hypothalamic hormone	TRH (+)	CRH (+)	GnRH (+)	GHRH (+) Somatostatin (-)	Dopamine (-)
Pituitary cell	Thyrotroph cells	Corticotroph cells	Gonadotroph cells	Somatotroph cells	Lactotroph cells
Pituitary hormone	TSH	ACTH	LH/FSH	GH, Somatotropin	PRL
Target organ	Thyroid gland	Adrenal gland	Gonads (Ovaries and testes)	Bone, Cartilage	Mammary glands
Function in target organ	Thyroid hormone production	Glucocorticoid production	Regulation of fertility	Regulation of growth	breast milk production

1.1.2. Clinical manifestations of pituitary adenomas (PAs)

Pituitary adenomas (PAs) are mainly monoclonal neoplasms [9, 10], which means that most PAs are derived from a single cell that underwent malignant transformation followed by uncontrolled clonal expansion. This ancestral cell can be of any cell type in the pituitary [9]. PAs can be either functioning, i.e. producing an excess of the respective pituitary hormone, or non-functioning lacking aberrant hormone secretion. Non-functioning PAs (NFPAs) have mainly a gonadodroph cell origin (>80 %). They tend to be diagnosed at a later time point compared to functioning PAs since they do not elicit the pronounced symptoms of hormonal excess that can usually be observed in patients with functional PAs. Nevertheless, patients with NFPAs often suffer from symptoms due to the bulk of the tumor, such as visual impairment caused by compression of the optic chiasm or hormone deficiency because of the displacement of the regular anterior pituitary structure [11]. The prevalence of the different cellular origins of tumors for all PA patients is displayed in Figure 2a. Each of these tumors lead to very specific set of symptoms related to the physiological role of the corresponding hormone.

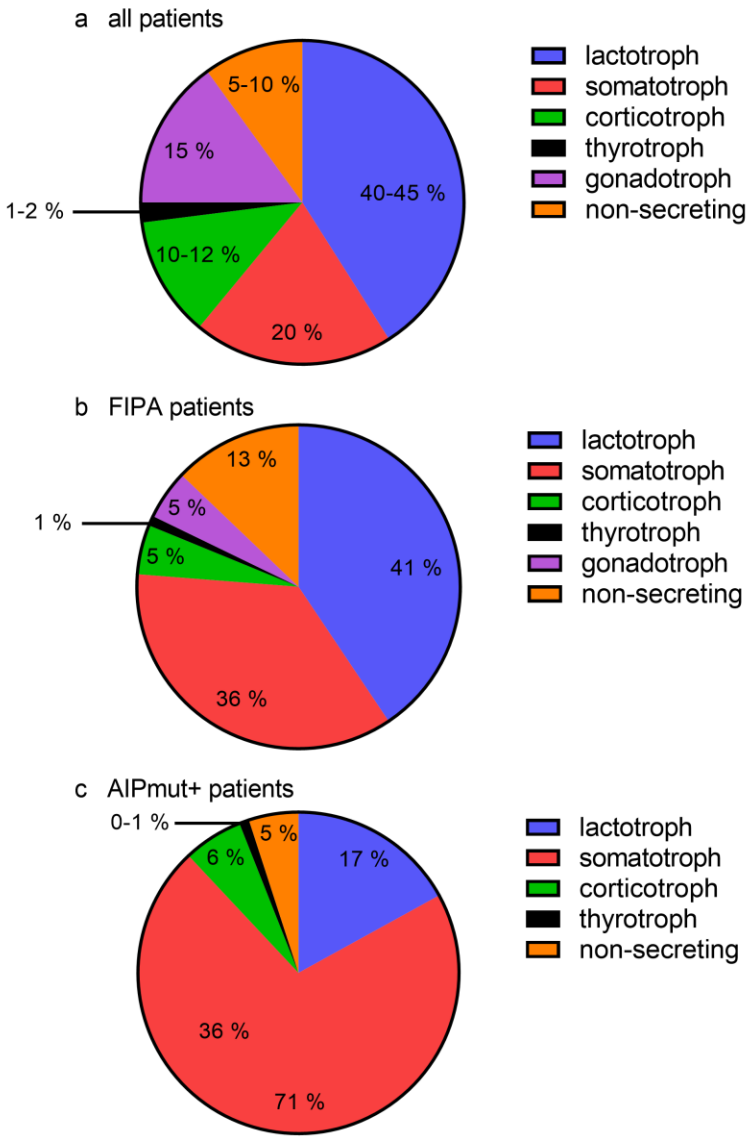

Figure 2: Prevalence of PA tumor types. (a) in all patients [12], (b) in Familial Isolated Pituitary adenoma syndrome (FIPA) [13, 14] and (c) in patients bearing AIP mutations (*AIP*mut+) [14-23].

Somatotropinomas, the main tumor type used in this study, are characterized by an increased secretion of growth hormone (GH) and Insulin-like growth factor-1 (IGF-1). They cause different phenotypes in patients dependent on ages. Children and adolescents, before epiphyseal fusion, develop gigantism in response to the excess of secreted GH. As the epiphyseal plates are fused in adults, immoderate growth of the long bones is not possible. Adults suffering from somatotropinomas present with acromegaly leading to disproportionate growth of some organs, tissues and bones. The acromegalic syndrome was already described in the 19th century and the connection with enlargement of the pituitary was made, but experimental proof was delivered in the early 20th century by surgical intervention to partially remove the pituitary [24]. Typical signs

and symptoms of acromegaly are soft tissue swelling, leading on the one hand to an enlargement of hands, feet and nose, and on the other to an enlargement and dysfunction of internal organs, like heart and kidneys. Pronounced protrusion of the brow and jaw, leading to jaw spacing can typically be observed in patients with acromegaly. Amongst the severe complications are diabetes mellitus, hypertension and failure of the heart or kidneys. These symptoms and complications can also be accompanied by hypopituitarism and mass effect symptoms (e.g. visual impairment, headaches) [12, 24, 25].

1.1.3. Treatment of PAs and their symptoms

The goals of PA therapy for any kind of treatment are improved quality of life, improved survival, normalizing hormonal hypersecretion, reversing the symptoms of mass effect, preserving or recovering the function of the normal pituitary and preservation of adenoma recurrence [26].

Surgical intervention

The first-line of treatment in all PAs, with the exception of prolactimomas, is transphenoidal surgery or craniotomy. For the majority (95 %) of PA patients that undergo surgery transphenoidal surgery can be used, which is less invasive. Craniotomy is usually chosen when transphenoidal surgery is not possible due to size, invasion or location of the tumor. Surgery often results in immediate remission of some of the signs and symptoms, like symptoms of the mass effect and normalization of hormone levels [26].

Radiotherapy

Radiation therapy is usually used as an adjunctive treatment to surgery and pharmaceutical treatment. This includes patients in which surgery and medical treatment have not been successful in controlling growth and, in case of secreting PAs, secretion of the tumors. Radiotherapy can be applied as conventional external beam radiation, which has the disadvantages that the therapy effect takes a long time to develop an effect and a higher risk of side effects, such as hypopituitarism, chiasmal damage and brain lesions [27]. On the other hand stereotactic radiosurgery enables the application of precisely focused, high-dose radiation, which reduces the risks of side effects [28].

Chemotherapy

Systemic medical treatment is required in patients without successful surgery, radiation therapy or tumor specific medical treatment. This is the case in aggressive PAs and pituitary carcinomas (with metastases), which are rare and often respond poorly to standard treatment. A

chemotherapeutic, which has been widely used in aggressive PAs and pituitary carcinomas is Temozolomide [29, 30]. In a systematic review, Temozolomide has been shown to be provoke a response (complete or partial response or stable disease) in approx. 80 % of treated patients with aggressive PAs or pituitary carcinomas [29].

Targeted therapy for the different PA histotypes

The choice of targeted therapy for the treatment of PAs depends on the PA histotype. In general, these drugs aim to subdue hormonal hypersecretion, which improves the patients' quality of life and reduce morbidity and mortality, but is no curative treatment of the PA since it is not cytotoxic to the tumor cells [26].

Somatotropinomas generally have a weaker response towards pharmacological treatment than other PA histotypes. The gold standard for drug treatment of somatotropinomas are somatostatin analogs (SSAs) such as octreotide, lanreotide or pasireotide which normalize GH and IGF-1 levels in approximately 50 % of patients [31]. These drugs target one or several somatostatin receptors (SSTRs) to mimic the effects of somatostatin, which is a hypothalamic hormone leading to a reduction of the synthesis and secretion of GH (Table 2). Variations in expression of the different SSTRs in PAs explain the heterogeneity of the response of patients towards SSAs. Somatotropinoma symptoms may also be treated by GH receptor antagonists, like pegvisomant or dopamine agonists [32, 33].

Prolactinomas are usually treated by dopamine agonists (DAs), such as cabergoline or bromocriptine. With these drugs, hormone levels can be normalized and in case of macroadenomas tumor shrinkage has been observed [34]. For PRL secreting microadenomas, restoring gonadal function and fertility with the treatment is a priority. In these cases, surgery is very often not necessary [34, 35].

NFPAs are often large at the time of the diagnosis, since they lack the signs and symptoms of hormonal hypersecretion that facilitate an early diagnosis [36]. Therefore, surgery and adjunctive radiation therapy is sometimes unsuccessful in removing all tumor tissue. In order to achieve further tumor shrinkage, somatostatin analogs and dopamine agonists can be used [37].

A variety of pharmacological treatment is available for ACTH-secreting PAs. SSAs (pasireotide) [38], glucocorticoid receptor antagonists [39], steroidogenesis inhibitors, and DAs [40] can be used as therapy, but SSAs and DAs usually work less well in ACTH-secreting PAs than in other PAs. Besides drug treatment, patients with no successful pituitary surgery can also undergo adrenalectomy, which however causes severe and life-long complications [41].

Patients suffering from TSH-secreting PAs usually undergo antithyroid therapy followed by surgery. SSAs (octreotide, lanreotide) can inhibit TSH secretion and, to a lesser extent, lead to tumor shrinkage. Due to the presence of dopamine type 2 receptors on most TSH-secreting PAs, DAs have been administered on affected patients, but TSH secretion and tumor growth have not been persistently blocked [42].

1.1.4. Genetics of PAs

The majority of PAs occur sporadically. Several genes have been described as being mutated in sporadic tumorigenesis in the pituitary. These mutated genes often lead to one specific tumor type and therefore cause the syndromes associated with the respective tumor (e.g. acromegaly in somatotropinomas).

The most prevalent oncogene, found mutated in about 40 % of somatotroph tumors is the gsp oncogene. Gsp is the product of the *GNAS* gene that encodes a stimulatory subunit of a guanine nucleotide binding protein (G Protein) resulting in a constitutively active receptor linked adenylate cyclase (AC) and therefore autonomous production of cyclic adenosine monophosphate (cAMP) in these cells [43]. In somatotroph cells of the pituitary, activation of AC is physiologically triggered by growth hormone-releasing hormone (GHRH) (Table 2) binding the growth-hormone-releasing hormone receptor (GHRHR), a G-protein coupled receptor that activates AC. This explains the specificity of the *gsp* oncogene for somatotropinomas. Somatic mutation of *GNAS* give rise to the McCune-Albright syndrome which is characterized by fibrous dysplasia, café-au-lait macules and overactivity of endocrine tissues [44].

In addition to *gsp*, mutations of the cell cycle regulator Cyclin D1 or the cyclin-dependent kinase (CDK) inhibitors (p16, p18, p53) have been reported to be involved in pituitary tumorigenesis [45-49]. ZAC (PLAG1) is a tumor suppressor that has been shown to be less expressed or even lost in PAs [50]. This protein is of special interest for somatotropinomas since octreotide (Oct), a SSA, which is the standard therapy for GH secreting PAs, has been shown to induce ZAC expression and therefore exerting its anti-proliferative effects in somatotroph cells [51].

About 5 % of PAs are associated with familial cancer syndromes [52-54]. These are mainly multitumor syndromes such as multiple endocrine neoplasia type 1 (MEN1), where PAs are a component of the tumor spectrum. MEN1 has been described by Wermer in 1954 as a syndrome comprising of adenomas of several endocrine glands (pituitary, parathyroids, pancreatic islets, gonads and gastrointestinal tract) in one family [55]. The causative MEN1 gene was mapped to a locus on chromosome 11q13 in the 1990s [56, 57]. Pituitary tumors occur in about 40 % of MEN1

patients [58, 59] and the predominant tumor type is PRL-secreting. In fact, the prevalence of the different tumor types in MEN1 patients is comparable to sporadic patients of all tumor types (Figure 2) [54, 55]. A second MEN-like syndrome involving the pituitary that does not harbor mutations in the MEN1 gene was described in rats and named the MENX syndrome [60]. The MENX locus was mapped to the distal part of rat chromosome 4 [61] and subsequently a mutation of the *Cdkn1b* gene was identified as being responsible for the MENX syndrome in rats, and for a related MEN1-like syndrome (MEN4) in humans. The human *CDKN1B* gene is located on chromosome 12 and encodes for $p27^{Kip1}$, a cyclin dependent kinase inhibitor [62]. Since MEN4 cases are extremely rare in man it is hard to make a statement about the predominant type of PA. So far, somatotropinomas, corticotropinomas and NFPAs have all been described in conjunction with germline *CDKN1B* mutations [62-65]. Another syndrome including PAs is the Carney Complex (CNC). CNC was initially described in a family presenting with cardiac and cutaneous myxomas, lentigines and endocrine overactivity. Due to hormonal hypersecretion, both Cushing syndrome, resulting from ACTH excess and acromegaly were present in members of the family [66]. In about 70% of CNC cases, mutation of the *PRKAR1A* gene occurs. *PRKAR1A* encodes the regulatory subunit Iα of protein kinase A and is located on chromosome 17q22-24 [67-69]. A putative second CNC gene was mapped to chromosome 2p16 but is not identified as yet [70].

In contrast to the multitumor syndromes described above, PAs can also be observed in a familial setting without additional endocrine malignancies. Thus, rare familial cases of acromegaly not associated to a MEN1 or CNC genotype have been observed [71-73]. These rare cases were initially described as isolated familial somatotropinomas (IFS) and were defined by the presence of two or more family members with somatotropinomas and no connection to MEN1 or CNC [74]. In the late 20^{th} century isolated cases of corticotropinomas [75, 76], prolactinomas [73, 77] as well as NFPAs [78] were reported to occur in familial settings. The occurence of two or more pituitary adenomas of any type, where mutations of *MEN1* and *PRKAR1A* were excluded, has been termed familial isolated pituitary adenoma (FIPA) [79]. The FIPA syndrome revealed a slightly different distribution of tumor types compared to other PAs (Figure 2b). Prolactinomas and somatotropinomas represent more than 2/3 of the FIPA cohort but the proportion of somatotroph adenomas is increased compared to all PA types (Figure 2a). PAs in FIPA patients are in general larger and more aggressive, leading patients to be typically diagnosed at a younger age [14, 19].

Unlike the MEN1 and MEN4 syndromes there appears to be no single causative gene mutation for FIPA, since the syndrome groups together all familial PA cases lacking *MEN1* or *PRKAR1A* mutations. However, a proportion of IFS cases could be linked to a tumor suppressor locus on chromosome 11q13.1-13.3 and a potential second locus on chromosome 2p16-12 [80].

Independently, the occurrence of familial PAs with a low penetrance in a Finnish cohort was described as pituitary adenoma predisposition (PAP) by Vierimaa and colleagues [81]. They identified germline inactivating mutations in the aryl hydrocarbon receptor interacting protein (AIP) in their patients. The patients were significantly younger than patients without AIP mutations and both somatotropinomas and prolactinomas were observed [81]. After the initial identification of AIP as a tumor susceptibility gene in FIPA cases, AIP mutations have been found to be present in up to 15 % - 30 % of patients with the FIPA phenotype [14, 16, 81, 82]. The impact of AIP mutations in sporadic PAs has been studied extensively. Although no involvement of AIP mutations (germline or somatic) was already reported [16, 23, 83-85], many studies found germline AIP mutations in apparently sporadic PAs [20, 22, 86-96]. In these cases, no family history of PAs is known, either because of the low penetrance of the disease [82] or due to the occurrence of *de-novo* mutations. However, somatic AIP mutations have not been identified in PAs so far [16, 22, 84, 87, 88, 96, 97].

A second gene mutation in FIPA was identified. Microduplications of the *GPR101* gene located on chromosome Xq26.3 cause X-linked acrogigantism (X-LAG), leading to abnormal growth already in infancy due to GH- or mixed GH/PRL-secreting PAs [98]. *GPR101* encodes an orphan G-protein–coupled receptor that is predicted to interact with the stimulatory alpha G-protein subunit to activate AC [98]. The physiological function of GPR101 is still unknown [99]. X-LAG accounts for 10 % of patients in a cohort of 208 patients suffering from pituitary gigantism, whereas AIP mutations were found in 29 % of the patients of this cohort [100]. Therefore, *AIP* and *GPR101* mutations represent the two most common causes for PAs in FIPA. However, for the remaining majority of FIPA cases the underlying genetic mechanisms are still unknown.

1.2. Aryl hydrocarbon receptor interacting protein (AIP)

Over 10 years ago, mutations in the aryl hydrocarbon receptor interacting protein (*AIP*) gene have been identified as a genetic cause of pituitary adenomas (see above) [81]. Nevertheless, the encoded protein has been initially described in a different context. Three groups independently identified AIP [101], also known as hepatitis B virus X-associated protein 2 (XAP2) [102, 103] or aryl hydrocarbon receptor activated protein 9 (ARA9) [104] as a component of the aryl hydrocarbon receptor (AhR) core complex. AIP is localized in the cytoplasm, is composed of 330 amino acids in an evolutionarily conserved sequence and has a molecular mass of 37 kDa [103]. The protein contains an immunophilin-like domain (peptidyl-prolyl *cis-trans* isomerase (PPIase)-like domain) on the N-terminus [105], nevertheless the domain is unable to bind immunosuppressive drugs (e.g. FK506) and was proven to be enzymatically inactive [106]. C-

terminal AIP contains three tetratricopeptide repeat (TPR) domains [107]. This domain is known to be able to mediate protein-protein interaction [108], which has been shown to be an important feature of AIP since a multitude of interaction partners of AIP have been identified so far [109]. Of note is the interaction with AhR and heat shock protein 90 (HSP90) in the context of the AhR core complex [101, 103, 104, 110, 111] which will be discussed in detail in paragraph 1.2.1. AIP has been also shown to interact with several members of the cAMP signaling pathway, such as two different phosphodiesterases (PDEs), PDE4A5 [112] and PDE2A3 [113], which hydrolyze cAMP and/or cGMP, as well as two members of the G-protein family [114].

1.2.1. Physiological functions of AIP

Besides AhR and AIP, the tetrameric AhR core complex contains a homodimer of Hsp90 and a single p23 in the unliganded state (Figure 3) [110, 111, 115]. The AhR core complex is part of the detoxification process in response to xenobiotics, which are chemical substances that are not naturally produced. Within the xenobiotic signaling pathway in which AIP is involved via the interaction with AhR, AIP mediates the retention of AhR in the cytoplasm, therefore increasing intracellular AhR levels [116, 117]. This stabilization was shown to be caused by impairment of proteasomal degradation due to protection from ubiquitination [118]. The complex dissociates upon binding of the ligand (e.g. environmental contaminants like 2,3,7,8-tetrachlorodibenzo-p-dioxin (TCDD)) to the receptor and AhR translocates into the nucleus. In the nucleus, AhR interacts with the aryl hydrocarbon receptor nuclear translocator (ARNT). The AhR-ARNT complex binds to xenobiotic response elements (XREs) mediating the transcription of detoxifying enzymes (Figure 3) [119].

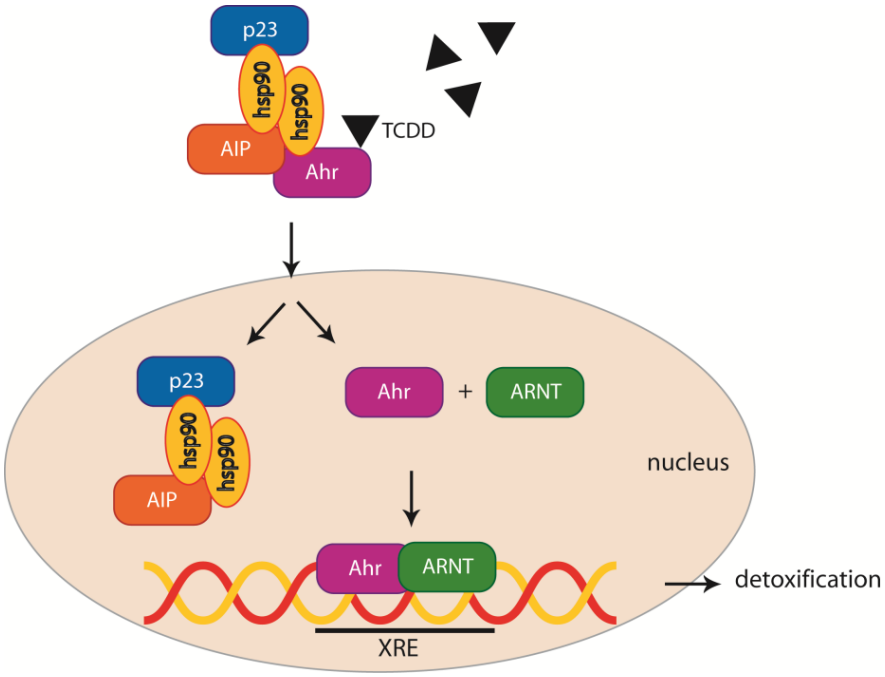

Figure 3: Canonical role of AIP in the context of detoxification. Ahr: aryl hydrocarbon receptor; AIP: Aryl hydrocarbon receptor interacting protein ARNT: aryl hydrocarbon receptor nuclear translocator 1; hsp90: heat shock protein 90; TCDD: Dioxin (2,3,7,8-tetrachloro-dibenzo-p-dioxin); XRE: xenobiotic response elements.
Figure: Eva-Maria Bogner

Apart from its role in detoxification, AIP is involved in cAMP signaling by interacting with both phosphodiesterases (PDEs) and G-proteins. PDEs are enzymes that catalyze the hydrolysis of cAMP and cGMP to 5'AMP and 5'GMP respectively [120, 121]. A huge variety of PDE isoforms are known, which allow a complex compartmentalization of cyclic monophosphates in cells and tissues [122]. Two PDE isoforms have been shown to interact directly with AIP, PDE4A5 [112] and PDE2A3 [113]. PDE4A5 hydrolyses specifically cAMP and in a yeast-2-hybrid assay it was shown that it interacts with AIP. This interaction occurs via the C-terminus of AIP, containing the TPR domains, and inhibits the catalytic activity of PDE4A5 by approximately 60 %. More specifically the Arg271 residue was vital for the interaction of AIP and PDE4A5 and therefore for the inhibition of the latter, since mutation of the residue to alanine attenuated both interaction and inhibition [112]. An interaction of PDE2A3 and AIP has also been revealed by a yeast-2-hybrid screening [113]. PDE2A3 is able to hydrolyse both cAMP and cGMP, thereby mediating the crosstalk of both signaling pathways [122]. Unlike the PDE4A5-AIP interaction, no effect on the enzymatic activity of PDE2A3 has been reported upon binding of AIP. Nevertheless, nuclear translocation of AhR was impaired after binding of AIP to PDE2A3, suggesting that this interaction might target PDE2A3 to AhR in order to cause its cytosolic retention [113]. Interaction of AIP with Gα13 inhibits the interaction of AIP and AhR, which in turn leads to increased ubiquitination of

AhR and reduced stability. Gαq is another G-protein subunit that directly interacts with AIP, whereas Gαs and Gαi did not [114]. Taken together, AIP is involved in the modulation of cytosolic cAMP levels by interacting with multiple different proteins.

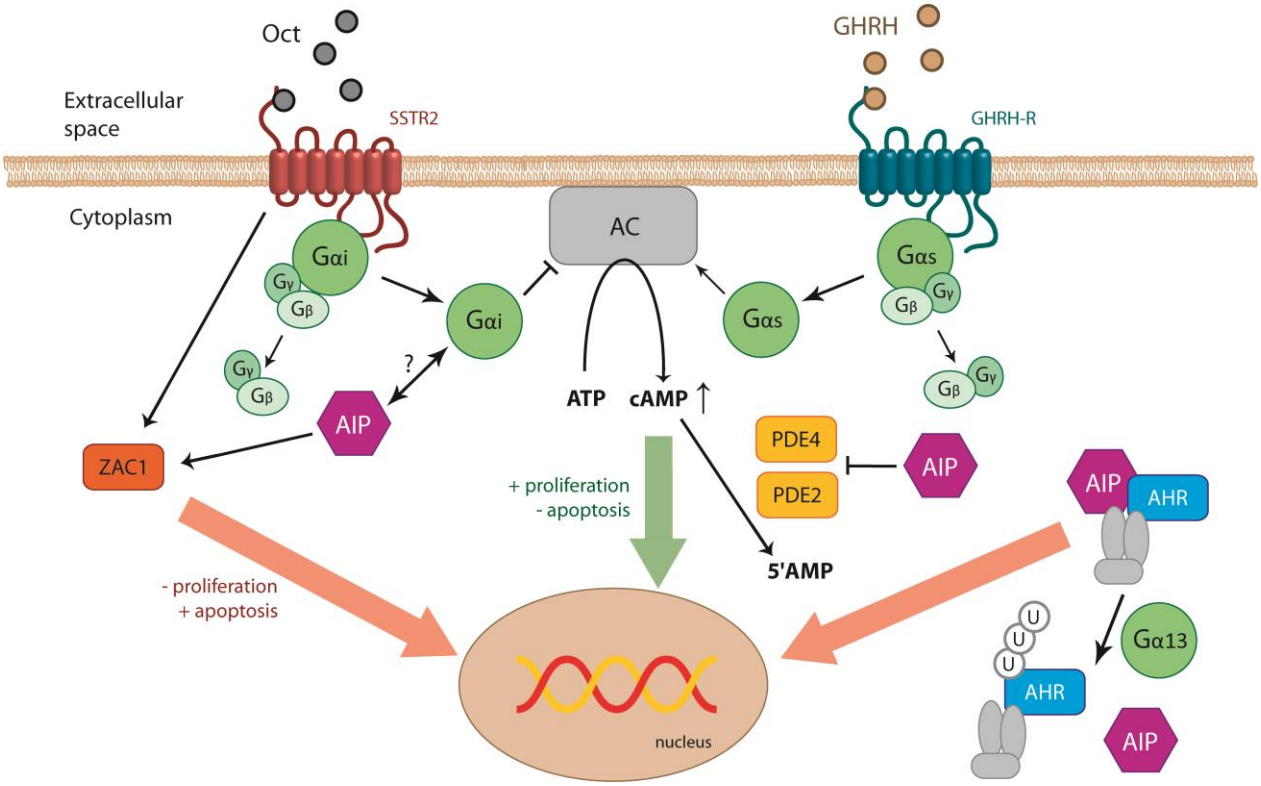

Figure 4: Summary of the AIP interaction partners that might be involved in PA development. AC: Adenylate cyclase; AHR: aryl hydrocarbon receptor; AIP: Aryl hydrocarbon receptor interacting protein; AMP: Adenosine monophosphate; ATP: Adenosine triphosphate; cAMP: Cyclic adenosine monophosphate; Gα13: Guanine nucleotide binding protein subunit alpha 13; Gαi: Guanine nucleotide binding protein, alpha inhibiting activity; Gαs: Guanine nucleotide binding protein, alpha stimulating activity; Gβ: Guanine nucleotide binding protein subunit beta; Gγ: Guanine nucleotide binding protein subunit gamma; GHRH: Growth hormone releasing hormone; GHRH-R: Growth hormone releasing hormone receptor; Oct: Octreotide; PDE: phosphodiesterase; SSTR2: Somatostatin receptor type 2; U: Ubiquitin; ZAC1 (=PLAG1): Pleiomorphic Adenoma Gene-Like 1
Figure: Eva-Maria Bogner

1.2.2. Role of AIP in PAs

AIP mutation positive PA patients (*AIP*mut+) display a very specific profile of clinical manifestations. Unlike in *AIP* mutation negative (*AIP*mut-) PA patients, the vast majority of *AIP*mut+ cases are somatotropinomas (about 70 %, Figure 2c). This may indicate that mutations in AIP might be involved in molecular pathways that are specific for somatotroph cell regulation. *AIP*mut+ PAs are diagnosed on average 2 decades earlier than unselected PA patients (23 yrs vs. 42yrs, depending on the study cohort [14, 18-20, 95, 96, 123]). Especially amongst children, adolescents and young adults presenting with PAs, the frequency of AIP mutations is high (12 –

20 %) [124]. The combination of the young age at onset with the preponderance of GH secreting adenomas leads to a frequent occurrence of gigantism in AIP mutated cases. In fact, *AIP* mutations together with *GPR101* mutations comprise a large proportion of all diagnosed cases of gigantism [100]. Increased aggressiveness with respect to size and invasion of surrounding tissues has been reported in tumors with *AIP* mutations [14, 16, 19, 81].

The role of AIP in therapy response is still unclear. *AIP*mut+ patients achieve disease control upon neurosurgery much less frequently than patients without *AIP* mutations. Therefore, these patients require secondary surgery more often. It has been shown that decrease of GH as well as IGF-1 and tumor shrinkage upon SSA therapy is more difficult to obtain than in PAs without mutations in *AIP* [19]. The reasons for these differences are not clear, but the involvement of Gαi proteins or ZAC1 has been proposed [125-127]. Defective Gαi signaling in *AIP*mut+ PAs might cause a constitutively active AC leading to constant cAMP production and therefore constant mitogenic signaling in somatotroph pituitary cells leading to PA development [125]. ZAC1 has been reported to be expressed at higher levels in PA patients after SSA treatment and this in increase in expression correlated with tumor shrinkage [126, 127]. In addition, Zac1 expression was induced after AIP-wt overexpression *in vitro*, while overexpression of mutant AIP had no effect on ZAC1 expression levels. Conversely, siRNA mediated knockdown of AIP reduces ZAC1 expression and increased both metabolic activity and clonogenicity of GH3 cells [126].

Among the various *AIP* mutations that have been descried so far, the most common mutations will be characterized shortly in the following paragraphs and their location is depicted in Figure 5.

By mutation screening in 45 seemingly sporadic somatotropinoma cases, two different mutations in *AIP* were identified, p.Gln14X in 6 patients and IVS3-1G>A in one patient [81]. The p.Gln14X variant has been described as a founder mutation since it occurred with a high frequency in familial PA patients from northern Finland. The first appearance of the mutation cannot be elucidated, nevertheless the first reports on patients presenting with tall stature, presumably gigantism, in northern Finland date back to the late 17th and early 18th century [79].

The arginine at position 304 has been shown to be a mutational hotspot since the two mutations p.Arg304X and p.Arg304Gln are very frequent. p.Arg304X was initially reported in an Italian FIPA family in the study by Vierimaa *et al.* that also described the p.Gln14X variant [81]. Similar to the p.Gln14X mutation, p.Arg304X is also a nonsense mutation leading to a premature termination of the translation of the protein, and to a partial loss of the C-terminal TPR-domains that are vital for protein-protein interactions. Up to now, p.Arg304X is the most frequent *AIP* mutation found in PA

patients [13, 15-17, 19, 63, 64, 101, 110-118]. p.Arg304Gln is a missense mutation that appears to be very prevalent [15, 16, 18, 20, 22, 23, 82, 91, 92, 94, 95, 128, 129]. Since Arg304 is located in the AhR binding region, this amino acid exchange might disturb this interaction [130, 131]. Although evidence indicates the presence of a mutational hot spot at amino acid 304 it has been also hypothesized that a founder mutation originating in central Italy could have caused a regional increase in the occurrence of p.Arg304X [132].

The p.Arg271Trp variant has been the subject of diverse studies. The mutation has been identified in a number of patients [14, 82, 92, 133, 134]. The affected residue is located within the third TPR-domain and is vital for the binding to AhR and hsp-90 [130]. As reported earlier, AIP interacts and inhibits PDE4A5 enzymatic activity via its TPR domain Several conserved residues have been tested with respect to their importance for this interaction, but Arg271 was the only one that significantly weakened both the binding of AIP with PDE4A5 and the inhibition of the latter [112]. Arg271 is considered as a mutational hotspot since it recurred in several kindreds that have been shown to lack ancestral linkage [134].

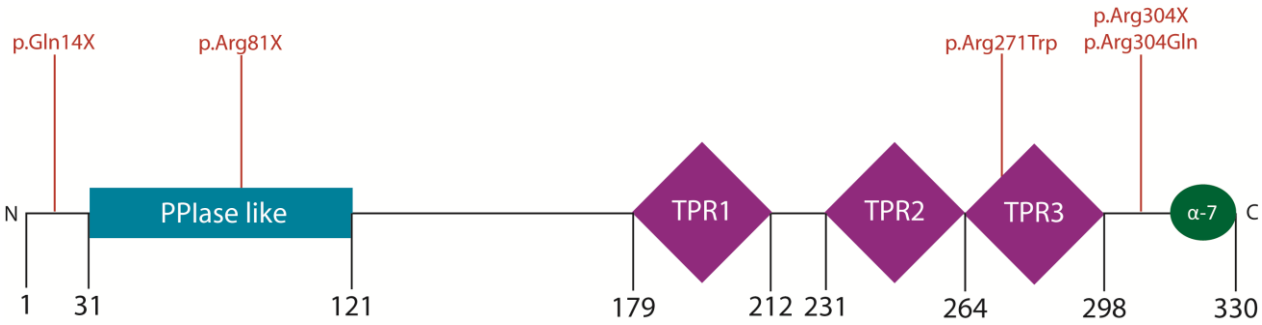

Figure 5: Schematic structure of the AIP protein. Location of most common AIP missense and nonsense mutations (n ≥ 10 patients), including the founder mutation and mutational hotspots, is marked. The terminal α-7 helix is crucial for protein–protein interaction, e.g. with hsp90 and AhR. AhR: Aryl hydrocarbon receptor; hsp90: heat shock protein 90; PPIase-like: peptidyl-prolyl cis–trans isomerase-like domain; TPR: tetratricopeptide repeat domain [14, 109]
Figure: Eva-Maria Bogner

1.3. microRNAs

microRNAs (miRNAs) are short, highly conserved RNAs which do not encode for proteins. miRNAs regulate gene expression at the post-transcriptional level via binding the 3' untranslated region (3'UTR) and subsequent cleavage of mRNAs that they target in a highly specific manner [135]. The seed region, a conserved sequence, which is located at the 5'-end of the miRNA, is essential for the binding of miRNA and 3'UTR of the mRNA. Since their first description, several

hundred miRNAs have been identified which play important roles in various physiological processes [136].

1.3.1. Biosynthesis, Transcriptional Regulation and cellular functions of miRNAs

The biogenesis of miRNAs is a two-step process involving sequential cleavages by RNase III-type endonucleases, which take place in different cellular compartments [137]. The primary transcript of the miRNA gene (pri-miRNA) is about 1kb long and forms a local stem-loop structure, which contains the sequence of the mature miRNA. The first processing event is the cleavage of the pri-miRNA into a precursor miRNA (pre-miRNA) of approximately 70 nts by the enzyme Droscha that takes place in the nucleus. This cleavage results in a hairpin-like structure [138]. After the initial step the pre-miRNA is transported from the nucleus to the cytoplasm by Exportin 5 (EXP5) [139, 140]. Subsequently, the pre-miRNA is cut by the RNase Dicer resulting in a double-stranded RNA duplex (mature and complementary strand (*)) of 21 – 25 nts [141-143]. The miRNA/miRNA* duplex, that is generated by the cleavage by Dicer then associates with a member of the Argonaute (AGO) protein family [144]. After the loading of the miRNA into AGO proteins, the strands dissociate and one of the two strands (the passenger strand) is discarded, whereas the other strand (the guide strand) remains in the complex [145, 146]. The selection of guide/passenger strand is achieved during AGO loading mainly due to thermodynamic stability of the termini of the miRNA duplex. Although one strand is usually favored for being the guide strand, also the other strand is occasionally picked as guide. This leads to a situation in which one strand is overrepresented in the pool of mature miRNAs compared to the complementary strand [145-147]. After dissociation of the mature from the complementary strand, the mature miRNA can be incorporated into the RNA-induced silencing complex (RISC) [145, 146]. The RISC is a multicomponent complex that works as the effector complex for the mRNA degradation mediated by miRNAs.

The pri-miRNA can be transcriptionally regulated in different ways. Apart from the localization of miRNA genes in intergenic regions, several clusters of miRNAs have been found to be co-expressed. Therefore, these miRNA gene clusters are considered as polycistronic transcription units [137, 148-151]. Additionally miRNA genes can also be located completely within the intron of a host gene and therefore be regulated by the promoter of the host gene, or they are transcribed by their own promoter [152-154]. The transcription of miRNA genes is carried out by RNA Polymerase II (Pol II) and is therefore controlled by transcription factors associated with RNA Pol II [155, 156].

Following loading into RISC, miRNAs can regulate their target genes by two mechanisms. The mechanism of posttranscriptional regulation depends mainly on the degree of complementarity of miRNA and mRNA seed match. Dependent on the degree of complementarity, the target mRNA will be cleaved after incorporation into RISC and thus degraded. Lower degrees of complementarity will lead to repression of translation of the mRNA without any cleavage [157-160].

1.3.2. miRNAs in health and disease

miRNAs are involved in a great variety of physiological processes, such as cell proliferation, apoptosis, cell cycle control and differentiation [136]. Approximately 60 % of the human genome has been estimated to be the target of one or several miRNAs [161]. miRNAs have been reported to have a multitude of mRNA targets in the genomes of different species [161-163]. Therefore, dysregulation of one or several miRNAs can cause dysfunctions of multiple cellular processes depending on the function of the genes that these miRNAs target.

Differential expression of miRNAs has been found in a variety of human diseases. Disorders that have been shown to be affected by miRNA dysregulation are neurological disorders, such as Alzheimer's disease [164], autoimmune diseases, like multiple sclerosis [165], and cancer. In tumor biology, miRNAs can be classified as oncogenic (oncomirs) or tumor suppressive depending on their target genes [166]. These two miRNA classes can affect one or several hallmarks of cancer [167], leading to the development of tumors. The initial report of miRNAs being dysregulated in cancer was provided by Croces group who showed that miR-15a and miR-16 were frequently deleted or down-regulated in chronic lymphocytic leukemia, therefore acting as a tumor suppressor miRNAs [168]. Subsequent studies revealed that miRNA can be involved in virtually all types of cancer and can be used as targets for therapy and markers for diagnosis and prognosis [169].

1.3.3. miRNAs in PAs

miRNA expression patterns have been studied in normal pituitary and PAs, either in general or of specific subtypes [170-174]. Mao et al. found a set of miRNAs differentially expressed between GH-secreting PAs and normal pituitary. Amongst these was a subset of miRNAs that was found to discriminate between micro- and macroadenomas as well as between Lanreotide treated and untreated patients. A subset of miRNAs was differentially expressed between responders and non-responders to SSAs [170]. Another group of miRNAs, including miR-34b (the letter suffix indicates a closely related mature sequence [175]), was downregulated in somatotropinomas versus normal pituitary with a possible role in targeting HMGA1 and HMGA2, which are known to

be important for pituitary tumorigenesis [176]. Down-regulation of miR-34b together with miR-34c could be confirmed in somatotropinomas, NFPAs and prolactinomas recently [177]. Another study compared the miRNA expression signature of a mixed set of PAs (GH-, PRL-, ACTH-secreting and NFPAs) with miRNA expression in normal pituitary. Again, macro- and microadenomas, as well as treated and untreated patients could be differentiated by miRNA expression. Within these PA samples miRNA expression could also predict the PA subtype [172]. miRNA expression in ACTH-secreting PAs was altered in comparison to normal pituitary. Nevertheless, this study could not show differential miRNA expression in respect to tumor size and remission after surgery [174]. Discrimination between ACTH-secreting adenomas and carcinomas was also performed. miR-122 and miR-493 were up-regulated in ACTH-secreting carcinomas versus adenomas indicating that these miRNA may be markers for increased aggressiveness in this PA histotype [178]. In NFPA, miRNA expression discriminated normal and tumor samples and showed a correlation with the tumor size. The profile of differentially regulated miRNA in this study indicated dysregulation of the TGFβ pathway via Smad3 [173].

Due to their importance in thyroid neoplasms, miR-130b and miR-23b expression has also been studied in PA development [179, 180]. Both miRNAs have been shown to be reduced in somatotropinomas, gonadotroph adenomas and NFPAs compared to normal pituitary. Via targeting HMGA2 and CCNA2 those miRNAs may affect the development of PA [181]. Bottoni and colleagues found miR-15a and miR-16-1 (the numbered suffix indicates identical mature sequences that arise from distinct genomic locations [175]) to be also downregulated in somatotropinomas and prolactinomas versus normal gland. Furthermore, patients with lower miR-15a and miR-16-1 () expression usually presented with larger tumor sizes [171] and miR-15a/miR-16 expression levels have been reported to have a negative correlation with cyclin D1 expression in MEN1 patients with PAs [182]. miR-15a and miR-16 together with miR-132 can target Sox5 directly, which may act as an oncogene in the pituitary [183]. Several other miRNAs have been described to act either as oncomiRs (e.g. miR-185 [184], miR-106b [185], miR-338-3p [186]) or tumor suppressor miRNAs (e.g. miR-133 [187], miR-153 [188], miR-524-5p [189]) in PAs (-3p and -5p indicate from which arm oft he precursor the mRNA is derived [175]).

miR-107 has been directly linked to AIP function in PAs. This miRNA was found to be overexpressed in both GH-secreting PAs and NFPAs and it could be shown that it directly targets AIP [190]. Another miRNA that has been reported to be directly linked to AIP is miR-34a. A correlation of low AIP expression with high levels of miR-34a has been observed in sporadic GH-secreting PAs without AIP mutations. Subsequently regulation and direct targeting of AIP by miR-

34a was shown *in vitro* [191]. Whether *AIP* mutation regulates the expression of miRNAs in PAs is currently unknown.

1.4. Hypothesis and aim of the thesis

AIP is a tumor susceptibility gene for hereditary PAs and a key gene in pituitary tumorigenesis. miRNAs were shown to be crucial for the development of a multitude of tumor types, including PAs. A connection of AIP and miRNAs has also been made in two studies [190, 191]. An indication that AIP deficiency might lead to dysregulated miRNA expression levels was that AhR has been found to regulate the expression of miRNA in various settings. AhR activation has been shown to upregulate the expression of miR-132/212 cluster in T-helper cell differentiation [192] as well as in two different breast cancer cell lines (MDA-MB-231 and T47D) where they have an anti-metastatic effect [193]. The expression of pulmonary miRNAs was regulated by AhR after chronic miRNA exposure [194].

As already discussed above, AhR is stabilized when in complex with AIP, since this interaction protects AhR from ubiquitination [116-118]. Impaired interaction of AhR with AIP can be caused by AIP mutations in the C-terminal TRP domains [16, 107, 131]. Loss of AhR-AIP interaction and subsequent proteasomal degradation of AhR might alter subsets of miRNA, which are regulated by AhR signaling.

We hypothesize that mutations in *AIP* cause differential expression of miRNAs, which in turn promotes oncogenic features in the pituitary, especially in somatotroph cells. These changes may lead to the characteristic clinical profile of patients with *AIP* mutations.

2. Material and Methods

2.1 Material

2.1.1 Instruments

4D-Nucleofector™ System (core and X-unit)	Lonza, Basel, Switzerland
7300 Real-Time PCR System	Applied Biosystems, Darmstadt, Germany
accu-jet®, pipettor	Brand, Weetheim, Germany
Adhesive seal Applicator	3M Deutschland, Neuss, Germany
Automated immunostainer, Discovery XT	Ventana Medical System, Inc., Tucson, AZ, USA
Axiovert 135, Microscope	Carl Zeiss, Jena, Germany
Biofuge fresco, centrifuge (Rotor:75003328 1.5/2mL)	Heraeus Instruments, Osterode, Germany Thermo Fischer Scientific, Waltham, MA, USA
Biofuge pico, centrifuge (Rotor:75003328 1.5/2mL)	Heraeus Instruments, Osterode, Germany Thermo Fischer Scientific, Waltham, MA, USA
BX 43, microscope	Olympus, Hamburg, Germany
CLSM FluoView FV1200, microscope	Olympus, Hamburg, Germany
Dispenser Multipette® plus	Eppendorf, Hamburg, Germany
E4 XLS+ Multichannel pipette, 20-200µl	Mettler Toledo, Gießen, Germany
Eppendorf 5415D, centrifuge (Rotor: F45-24-11 1.5mL)	Eppendorf, Hamburg, Germany Eppendorf, Hamburg, Germany
EVOS xl, microscope	Thermo Fischer Scientific, Langenselbold, Germany
Finnpipette™ Multichannel pipette 50-300µl	Thermo Fischer Scientific, Langenselbold, Germany
Fischerbrand Mini, centrifuge (Rotors:0.2, 1.5mL)	Fischer Scientific, Schwerte, Germany Fischer Scientific, Schwerte, Germany
Freezer -20°C Liebherr Comfort	Liebherr, Biberach an der Riss, Germany
Freezer -80°C HFC86-360	Heraeus Instruments, Osterode, Germany
Fridge +4°C Liebherr Premium	Liebherr, Biberach an der Riss, Germany
Fuego SCS basic gas burner	WLD-TEC, Göttingen, Germany
Gel Documentation System	Vilber Lourmat, Eberhardzell, Germany
GeneAmp™ PCR System 9700, PCR cycler	Applied Biosystems, Darmstadt, Germany
GFL Shaking Water Bath 1083	G. f. Labortechnik, Burgwedel, Germany
Ice Machine	Ziegra, Isernhagen, Germany
Incubator shaker Model G25	New Brunswick Sci., Edison, NJ, USA

Incubator Innova CO-170	New Brunswick Sci., Edison, NJ, USA
Infinite M200 plate reader	Tecan, Crailsheim, Germany
inoLab pH Level 1, pH-meter	WTW, Weilheim, Germany
L29, test-tube rotator	A. Hartenstein, Würzburg, Germany
LUNA™ Automated Cell Counter	Logos Biosystems, Waltham, MA, USA
Magnetic stir bars, various sizes	NeoLab, Heidelberg, Germany
Magnetic stirrer MR2000	Heidolph Instr., Schwabach, Germany
Maxwell 16	Promega, Mannheim, Germany
Microplate Reader Model 680	BioRad Lab., Munich, Germany
Microplate Reader Varioscan™ LUX	Thermo Fischer Scientific, Langenselbold, Germany
MilliQ water purification system	Sigma-Aldrich, Steinheim, Germany
Mini-Sub® Cell GT System	BioRad Lab., Munich, Germany
Mini Trans-Blot® Electrophoretic Transfer Cell	BioRad Lab., Munich, Germany
Model 200/2.0 Electrophoresis Power Supply	BioRad Lab., Munich, Germany
MSC-Advantage™ Class II Biological Safety Cabinet	Thermo Fischer Scientific, Waltham, MA, USA
Nalgene® Mr. Frosty® Cryo 1°C Freezing Container	Thermo Fischer Scientific, Rosklide, Denmark
NanoDrop™ 2000,spektrophotometer	Thermo Fischer Scientific, Langenselbold, Germany
Nano-Drop™ ND-1000, spektrophotometer	Thermo Fischer Scientific, Langenselbold, Germany
PIPETBOY acu, pipettor	Integra Biosciences, Fernwald, Germany
Pipetman Classic P2, 0,2-2 µl, pipette	Gilson, Limburg-Offheim, Germany
Pipetman Classic P10, 1-10 µl, pipette	Gilson, Limburg-Offheim, Germany
Pipetman Classic P20, 2-20 µl, pipette	Gilson, Limburg-Offheim, Germany
Pipetman Classic P100, 20-100 µl, pipette	Gilson, Limburg-Offheim, Germany
Pipetman Classic P200, 50-200 µl, pipette	Gilson, Limburg-Offheim, Germany
Pipetman Classic P1000, 200-1000 µl, pipette	Gilson, Limburg-Offheim, Germany
Pipetus®-akku, pipettor	Hirschmann Laborg., Eberstadt, Germany
PowerPac™ 300, Power Supply	BioRad Lab., Munich, Germany
Pressure cooking pot tender cooker	Nordic Ware, Frankfurt, Germny
Privileg 1034 HGD, Microwave	Otto, Hamburg, Germany
Rainin Pipet-Lite XLS+ Multichanel pipette	Mettler Toledo, Gießen, Germany
Research plus Single-Channel Pipette, Gray; 0.5-10 µL	Eppendorf, Hamburg, Germany

Research plus Single-Channel Pipette, Yellow; 2-20 µL	Eppendorf, Hamburg, Germany
Research plus Single-Channel Pipette, Yellow; 10-100 µL	Eppendorf, Hamburg, Germany
Research plus Single-Channel Pipette, Yellow; 20-200 µL	Eppendorf, Hamburg, Germany
Research plus Single-Channel Pipette, Blue; 100-1000 µL	Eppendorf, Hamburg, Germany
Rotana 460r, centrifuge (Rotor:5642 15/50mL)	Andreas Hettich, Tuttlingen, Germany Andreas Hettich, Tuttlingen, Germany
Rotina 420r, centrifuge (Rotor:4790 1.5mL)	Andreas Hettich, Tuttlingen, Germany Andreas Hettich, Tuttlingen, Germany
Rotor-Gene Q, real-time PCR cycler	Qiagen, Hilde, Germany
Sartorius Universal U3100D, scale	Sartorius, Götttingen, Germany
SensoQuest Labcycler, PCR cycler	SensoQuest, Göttingen, Germnay
SW21, water bath shaker	Julabo Labortechnik, Burgwedel, Germany
T-Personal Thermocycler, PCR cycler	Biometra, Göttingen, Germany
Thermomixer® comfort 1.5mL, heating block	Eppendorf, Hamburg, Germany
Thermomixer® compact 1.5mL, heating block	Eppendorf, Hamburg, Germany
ThermoStat™ plus 1,5mL, heating block	Eppendorf, Hamburg, Germany
Tweezers No.5	A. Dumont&Fils, Montignez, Switzerland
UM 300, universal oven	Memmert, Schwabach, Germany
Uniflow UVUB 1800, hood	UniEquip, Planegg, Germany
Unitwist RT, rocking table shaker	UniEquip, Planegg, Germany
Variofuge 3.0R, centrifuge (Rotor: 8074, inserts 8078, 15mL, 50mL)	Heraeus Sepatech, Osterode, Germany Heraeus Sepatech, Osterode, Germany
Vortex-Genie 2, vortexer	Scientific Industries, Bohemia, NY, USA
Whirlpool ProMicro 825, microwave	Bauknecht Hausg., Stuttgart, Germany
XCell SureLock™ Mini-Cell Electrophoresis System	Invitrogen, Darmstadt, Germany
X-ray cassette	Carl Roth, Karlsruhe, Germany

2.1.2 Consumable Materials

Adhesive seal films MicroAMPTM	Applied Biosystems, Darmstadt, Germany
Amersham™ Hybond™-ECL, Membrane for western blotting	GE Healthcare, Munich, Germany

Amersham™ Hyperfilm™-ECL, photographic film	GE Healthcare, Munich, Germany
Blotting paper grade 3m/N 65g/m^2	Munktell&Filtrak, Bärenstein, Germany
Cell counting slides for LUNA™ Automated Cell Counter	Biozym Sci Hessisch Oldendorf, Germany
Cell culture inserts for 24-well plates, 8.0µm pores, transparent PET membrane, BD BioCoat™	BD Biosciences, Heidelberg, Germany
CELLSTAR®, serological pipettes 5mL	Greiner BioOne, Frickenhausen, Germany
CELLSTAR®, serological pipettes 10mL	Greiner BioOne, Frickenhausen, Germany
CELLSTAR®, serological pipettes 25mL	Greiner BioOne, Frickenhausen, Germany
Combitips® for Multipette® 12.5mL	Eppendorf, Hamburg, Germany
Corning® syringe filters, Nylon membrane, pore size 0.45 µm	Sigma-Aldrich, Steinheim, Germany
Coverslips 12mm round	Carl Roth, Karlsruhe, Germany
Cryogenic vials sterile 2mL freestanding Falcon™	BD Biosciences, Heidelberg, Germany
Falcon® 6-well Clear Flat Bottom TC-treated Multiwell Cell Culture Plate, sterile	Corning, Corning, NY, USA
Falcon® 12-well Clear Flat Bottom TC-treated Multiwell Cell Culture Plate, sterile	Corning, Corning, NY, USA
Falcon® 24-well Clear Flat Bottom TC-treated Multiwell Cell Culture Plate, sterile	Corning, Corning, NY, USA
Falcon® 96-well Clear Flat Bottom TC-treated Multiwell Cell Culture Plate, sterile	Corning, Corning, NY, USA
Falcon™ Cell Culture Inserts PET track-etched membrane (8 µm pore size)	BD Biosciences, Heidelberg, Germany
Falcon® reaction tubes Blue Max 15mL	BD Biosciences, Heidelberg, Germany
Falcon® reaction tubes Blue Max 50mL	BD Biosciences, Heidelberg, Germany
Gel cassettes 1.5mm	Life Technologies, Carlsbad, Germany
Glass slides SuperFrost® 76x26mm	Carl Roth, Karlsruhe, Germany
Millex® syringe-driven filter unit 0.22µm	Merck, Darmstadt, Germany
Microplates, TC well, clear bottomed, white walled	Lonza, Basel, Switzerland
Omnifix® syringe, single-use 50mL	B. Braun, Melsungen, Germany
Parafilm®	Carl Roth, Karlsruhe, Germany
Pasteur pipettes glass 3.2mL	Carl Roth, Karlsruhe, Germany
PCR tube stripes 0,2mL	Eppendorf, Hamburg, Germany
Petri dishes 100 * 15, 56.7cm^2 Nunclon™ Δ	Nunc, Rosklide, Germany
pH indicator stripes	Merck, Darmstadt, Germany
Rainin Bioclean-Tips, Pipette tips	Mettler Toledo, Gießen, Germany

Reaction tubes 1.5mL	Eppendorf, Hamburg, Germany
Reaction tubes 2mL	Eppendorf, Hamburg, Germany
Reaction tubes, RNase free 1.5mL	Zymo Research, Freiburg, Germany
Scalpel, sterile, disposable	Aesulap, Tuttlingen, Germany
Sterican® cannulas Ø0.60*0.60mm, 23G * 2 3/8''	B. Braun, Melsungen, Germany
Sterican® cannulas Ø0.80*0.50mm, 21G * 2''	B. Braun, Melsungen, Germany
Strip Tubes and Caps, 0.1 ml	Qiagen, Hilde, Germany
Thermo-Fast® PCR plates (0,2mL), 96-well, non-skirted	Abgene/Thermo Scientific, Rockford, IL, USA
TipOne® graduated filter tips, pipette tips, 0,1-10µl	Starlab, Ahrensburg, Germany
TipOne® graduated filter tips, pipette tips, 1-20µl	Starlab, Ahrensburg, Germany
TipOne® graduated filter tips, pipette tips, 1-100µl	Starlab, Ahrensburg, Germany
TipOne® graduated filter tips, pipette tips, 1-200µl	Starlab, Ahrensburg, Germany
TipOne® graduated filter tips, pipette tips, 101-1000µl	Starlab, Ahrensburg, Germany
Tissue culture flask 25cm^2, filter cap	Greiner BioOne, Frickenhausen, Germany
Tissue culture flask 75cm^2, filter cap	Greiner BioOne, Frickenhausen, Germany
Tissue culture flask 175cm^2, filter cap	Greiner BioOne, Frickenhausen, Germany
Tissue culture plates 6-well Nunclon™ Δ	Nunc, Rosklide, Germany

2.1.3 Chemicals and reagents

β-mercaptoethanol >99%	Sigma-Aldrich, Steinheim, Germany
Agarose LE for gel electrophoresis	Biozym, Hessisch-Oldendorf, Germany
Ampicilin sodium salt	Sigma-Aldrich, Steinheim, Germany
Ampuwa® water	Fresenuis KABI, Bad Homburg, Germany
Ammonium Persulfate (APS) >98%	Sigma-Aldrich, Steinheim, Germany
Antibody Dilutent	Dako/Agilent, Santa Clara, CA, USA
Bis-acrylamide ProtoGel® 30% (w/v)	National Diagnistics, Nottingham, UK
Blotting-Grade Blocker	BioRad Lab., Munich, Germany
Bovine serum albumine (BSA) >98%	Sigma-Aldrich, Steinheim, Germany
Butane Campinggaz® CV360	CampingGaz, Hungen-Inheiden, Germany
Chloroform, min. 99% p.a.	Merck, Darmstadt, Germany
Citrate Buffer 10x	DCS, Hamburg, Germany
Citrate buffer, pH 6, 10x	Sigma-Aldrich, Steinheim, Germany
Cycloheximide 98 %	Sigma-Aldrich, Steinheim, Germany
DCS LabLine antibody dilutent	DCS, Hamburg, Germany
DMEM + GlutaMAX™, 4.5g/L D-glucose, pyruvate	Fischer Scientific, Schwerte, Germany

DMSO	Sigma-Aldrich, Steinheim, Germany
dNTP Mix 10mM each	Fermentas, St. Leon-Rot, Germany
DTT 0.1M	Fischer Scientific, Schwerte, Germany
EDTA >99% p.a.	Carl Roth, Karlsruhe, Germany
Eosin Y alcoholic solution	Bio-Optica, Milano, Italy
Epoxomicin	Enzo Life Sciences GmbH, Lörrach, Germany
Ethanol, ASC, ISO	Merck, Darmstadt, Germany
Ethidium bromide	Sigma-Aldrich, Steinheim, Germany
Fetal bovine serum (FBS)	Fischer Scientific, Schwerte, Germany
First strand buffer 5x	Fischer Scientific, Schwerte, Germany
Formaldehyde 35 wt. % in H_2O	Sigma-Aldrich, Steinheim, Germany
Fungizone™	Fischer Scientific, Schwerte, Germany
G153 A and B, photographic developer	Agfa Healthcare, Mortsel, Belgium
G354, photographic fixer	Agfa Healthcare, Mortsel, Belgium
Gel loading dye, 6x	New England Biolabs, Frankfurt, Germany
GeneChip miRNA 1.0 Array	Affymetrix, High Wycombe, UK
Glycerol >99%	Sigma-Aldrich, Steinheim, Germany
Goat Serum	PAA, Pasching, Germany
Ham's F-10 Nutrient Mix	Fischer Scientific, Schwerte, Germany
Ham's F-12K (Kaighn's) Medium	Fischer Scientific, Schwerte, Germany
HBSS 1x without $CaCl_2/MgCl_2$	Fischer Scientific, Schwerte, Germany
Hydrochloric acid 5M	Neo-Lab, Heidelberg, Germany
Hematoxilin (Carazzi's)	Bio-Optica, Milano, Italy
HiPerFect transfection reagent	Qiagen, Hilde, Germany
Hoechst 33258 bisBenzimide	Sigma-Aldrich, Steinheim, Germany
Horse Serum (HS)	Fischer Scientific, Schwerte, Germany
Hydrochloric acid 1M	Sigma-Aldrich, Steinheim, Germany
Hydrogen peroxide 30%	Merck, Darmstadt, Germany
Isopropanol, ACS, ISO	Merck, Darmstadt, Germany
Kanamycin A monosulfate	Sigma-Aldrich, Steinheim, Germany
Laemmli sample buffer 1x	BioRad Lab., Munich, Germany
LB broth base	Fischer Scientific, Schwerte, Germany
Lipofectamine™ 2000 transfection reagent	Invitrogen, Darmstadt, Germany
Lipofectamine™ 3000 transfection reagent	Invitrogen, Darmstadt, Germany
Methanol, ACS, ISO	Merck, Darmstadt, Germany
NP-40 Tergitol®	Sigma-Aldrich, Steinheim, Germany
Opti-MEM® reduced serum media	Fischer Scientific, Schwerte, Germany

Paraformaldehyde (PFA)	Merck, Darmstadt, Germany
PBS powder pH 7.4	Sigma-Aldrich, Steinheim, Germany
Penicilin-Streptomycin, liquid	Fischer Scientific, Schwerte, Germany
Ponceau S, practical grade	Sigma-Aldrich, Steinheim, Germany
Protease inhibitor cocktail tablets complete mini	Roche Diagnostics, Mannheim, Germany
Restore™ PLUS, stripping buffer for western blot	Fischer Scientific, Schwerte, Germany
RIPA buffer	Sigma-Aldrich, Steinheim, Germany
RNaseZAP®	Sigma-Aldrich, Steinheim, Germany
Roti®-Stock 10x TBS	Carl Roth, Karlsruhe, Germany
RPMI 1640 + GlutaMAX™	Fischer Scientific, Schwerte, Germany
SDS 10% (w/v) solution	BioRad Lab., Munich, Germany
SDS-PAGE running buffer Rotiphorese®, 10x	Carl Roth, Karlsruhe, Germany
SOC Medium	Sigma-Aldrich, Steinheim, Germany
Sodium Azide >99%	Sigma-Aldrich, Steinheim, Germany
Sodium chloride >99.5%	Merck, Darmstadt, Germany
SuperSignal® West Femto, chemiluminescent substrate	Thermo Fischer Scientific, Darmstadt, Germany
SuperSignal® West Pico PLUS, chemiluminescent substrate	Thermo Fischer Scientific, Darmstadt, Germany
TaqMan® Universal PCR Master Mix (2x)	Thermo Fischer Scientific, Waltham, MA, USA
TBE Tris/Boric Acid/EDTA, 10x	BioRad Lab., Munich, Germany
TBS-T, 10x	Carl Roth, Karlsruhe, Germany
TEMED 99%	Amresco, Solon, OH, USA
Toluidine blue O (C.I. 52040) Certistain®	Merck, Darmstadt, Germany
Triton X-100, >10% in H_2O	Sigma-Aldrich, Steinheim, Germany
Trizma® base	Sigma-Aldrich, Steinheim, Germany
TRIzol® reagent	Fischer Scientific, Schwerte, Germany
Trypan Blue solution 0.4%	Sigma-Aldrich, Steinheim, Germany
Trypsin, 0.05% with EDTA	Fischer Scientific, Schwerte, Germany
Tween 20	Carl Roth, Karlsruhe, Germany
VECTASHIELD® mounting medium	BIOZOL Diagnostica, Eching, Germany
Xylol >99%	Merck, Darmstadt, Germany

2.1.4 Buffers and Solutions

All listed buffers and solution were prepared in MilliQ-H_2O, unless stated differently.

Agarose gel	1 % (w/v) agarose LE in 1x TBE Boil until dissolved cool to approx. 60°C add 0,005 % (v/v) ethidium bromide
Antibody dilution solution for Western Blot	3 % (w/v) BSA in TBS-T Sterile filtration with syringe filter Add 20 µl NaOAc
Paraformaldehyde	2 % (w/v) paraformaldehyde in PBS 15 µL phenol red Add 10 M NaOH until dissolved (color change from pink to colorless) adjust pH to 7.4 with HCl
PCR master mix	6 % (w/v) sucrose 200 µM dATP 200 µM dCTP 200 µM dGTP 200 µM dTTP 10 % (v/v) 10x buffer (Biotherm, no $MgCl_2$)
Ponceau dye	0.1 % (w/v) Ponceau 5 % (v/v) acetic acid
Separating gel (10%) for SDS-PAGE (10mL)	3.33 ml 30 % (w/v) acrylamide/bis 4 ml H_2O bidest. 2.5 ml 1.5M Tris (pH 8.8) 100 µl 10 % (w/v) SDS 50 µl 10 % APS 5 µl TEMED
Stacking gel (4%) for SDS-PAGE (5mL)	670 µl 30 % (w/v) acrylamide/bis 3 ml H_2O bidest. 1.26 ml 0.5M Tris (pH 6.8) 50 µl 10 % (w/v) SDS 25 µl 10 % APS 5 µl TEMED
TBS-T 10x (pH 7.6)	0.2 M Trizma® base 1.5 M NaCl 1 % (v/v) Tween-20

	For 1x, dilute 1/10 in H_2O bidest.
TE buffer	10 mM Tris-HCl (pH 8.0) 1 mM EDTA 50 mM NaCl
Toluidine Blue (2%)	2 % (w/v) Toluidine Blue in 50 ml H_2O

2.1.5 Commercially available Kits

Avidin/Biotin Blocking Kit	Vector Laboratories, Burlingame, CA, USA	# SP-2001
BCA Protein Assay Pierce®	Fischer Scientific, Schwerte, Germany	#23225
Caspase-Glo® 3/7 Assay	Promega, Mannheim, Germany	#G8091
Direct cAMP ELISA kit	Enzo Life Sciences GmbH, Lörrach, Germany	#ADI-900-066
DNeasy Blood & Tissue Kit	Qiagen, Hilde, Germany	#69504
Dual-Luciferase® Reporter Assay System	Promega, Mannheim, Germany	#E1910
FlashTag™ Biotin HSR RNA Labeling Kit	Genisphere, Hatfield, PA, USA	#901910
HistoMark Biotin Streptavidin-HRP	SeraCare, Wedel Germany	#5520-0023
Mycoplasma detection Kit	PromoKine, Heidelberg, Germany	#PK-CA20-700-20
Maxwell® 16 Simply RNA Cells Kit	Promega, Mannheim, Germany	#AS1270
miRNeasy FFPE Kit	Qiagen, Hilde, Germany	#217504
miRNeasy Mini Kit	Qiagen, Hilde, Germany	#217004
P4 Primary Cell 4D-Nucleofector X Kit	Lonza, Basel, Switzerland	#V4SP-4960
Peroxidase Substrate Kit DAB	Vector Laboratories, Burlingame, CA, USA	#SK-4100
QIAprep® Spin Miniprep Kit	Qiagen, Hilde, Germany	#27106
QIAquick PCR Purification Kit	Qiagen, Hilde, Germany	#28104
QuikChange II Site-Directed Mutagenesis Kit	Agilent Technologies, Santa Clara, CA, USA	#200523
Quick Ligation™ Kit	New England Biolabs, Frankfurt, Germany	#M2200S
Rat/Mouse Growth Hormone ELISA	Merck, Merck, Darmstadt, Germany	#EZRMGH-45K
RNeasy Mini Kit	Qiagen, Hilde, Germany	#74104
SF Cell Line 4D-Nucleofector X Kit	Lonza, Basel, Switzerland	#V4XC-1024
TaqMan™ MicroRNA Reverse Transcription Kit	Thermo Fischer Scientific, Waltham, MA, USA	#4366596
WST-1, cell proliferation reagent	Roche Diagnostics, Mannheim, Germany	#05015944001

ZymoPURE II Plasmid Maxiprep Kits	Zymo Research, Irvine, CA, USA	#D4202

2.1.6 Constructs

pCMV-Myc

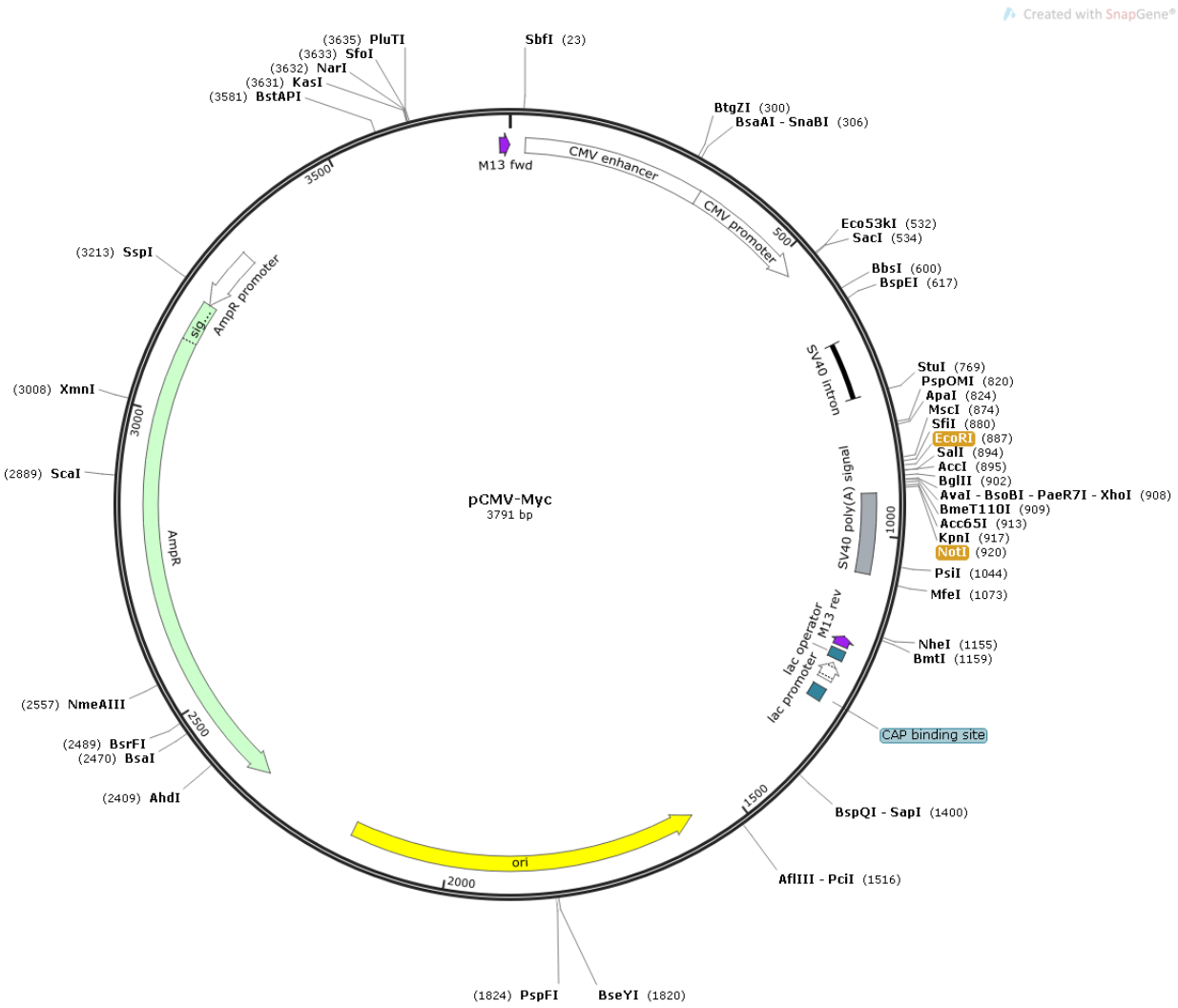

Figure 6: Map and features of the pCMV-myc vector. The vector was used to clone the wild-type human AIP cDNA. (sequence derived from https://www.addgene.org/42192/sequences/, map was created by SnapGene. The restriction enzyme sites that were used for cloning are highlighted in yellow.

psiCHECK™-2

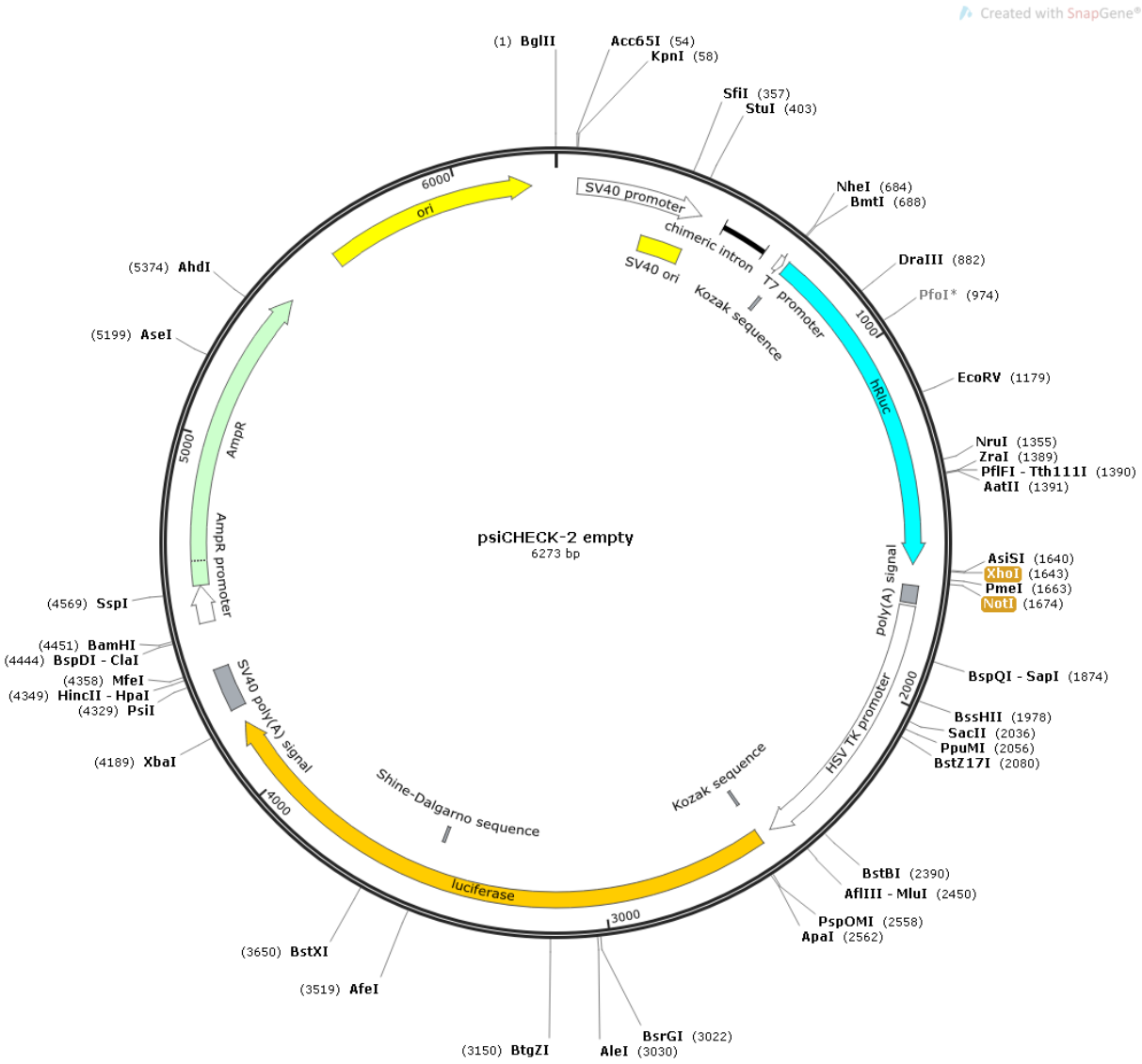

Figure 7: Map and features of the psiCHECK™-2 vector. The vector was used to clone the miR-34a predicted seed match in GNAI2 3'UTR. The multiple cloning site is located directly downstream of hRluc (sequence derived from https://www.addgene.org/42192/sequences/, map created by SnapGene. The restriction enzyme sites that were used for cloning are highlighted in yellow.

2.1.7 Antibodies

Antibodies for Immunhitochemistry (IHC) of formalin-fixed paraffin embedded (FFPE) tissue sections

All antibodies were diluted in DCS antibody dilution buffer as indicated in Table 3.

Table 3: Antibodies for IHC on FFPE tissue sections

Type	Antibody	Company	ID	Species	Dilution
First AB	anti-AIP/ARA9 (35/2)	Novus Biologicals Bio-Techne GmbH, Wiesbaden, Germany	NB100-127	mouse	1:1000
First AB	anti-Gαi-2	Abcam, Cambridge, UK	EPR9469	rabbit	1:200
Second AB	Histomark Biotin Streptavidin HRP- system Goat anti rabbit IgG	Kirkegaard&Perry Laboratories Inc., MA, USA	710018	mouse	undiluted
Second AB	Histomark Biotin Streptavidin HRP- system Goat anti rabbit IgG	Kirkegaard&Perry Laboratories Inc., MA, USA	710019	rabbit	undiluted

Antibodies for Immunfluorescence (IF) on cells

Table 4: Antibodies for IF on PFA-fixed cells

Type	Antibody	Company	ID	Species	Dilution
First AB	anti-Ki-67 (SP6)	Abcam, Cambridge, UK	ab 16667	rabbit	1:250
Second AB	Alexa fluor 555	Cell Signaling Technology (CST), Cambridge, UK	4413	rabbit	1:100

Primary Antibodies for Western Blotting

Table 5: Primary antibodies for Western Blotting

Antibody	Company	ID	Host	Dilution	Clonality	Band Size
anti-α-Tubulin	Sigma-Aldrich, Steinheim, Germany	B-5-1-2	mouse	1:1000	monoclonal	approx. 50 kDa
anti-AIP/ARA9 (35/2)	Novus Biologicals Bio-Techne GmbH, Wiesbaden, Germany	NB100-127	mouse	1:750	monoclonal	approx. 37 kDa
anti-ARNT/HIF-1β	Novus Biologicals Bio-Techne GmbH, Wiesbaden, Germany	NB100-110	rabbit	1:2000	polyclonal	approx. 92 kDa
anti-Erk1/2	Cell Signaling Technology (CST), Cambridge, UK	9107	rabbit	1:1000	monoclonal	approx. 42/44 kDa
anti-Gαi-2	Abcam, Cambridge, UK	EPR9469	rabbit	1:10000	monoclonal	approx. 40 kDa
anti-p-Erk1/2	Cell Signaling Technology (CST), Cambridge, UK	9101	rabbit	1:1000	polyclonal	approx. 42/44 kDa

Secondary Antibodies for Western Blotting

Table 6: Secondary antibodies for Western Blotting

Antibody	Company	ID	Host	Dilution
anti-mouse IgG HRB-linked	GE Healthcare, Little Chalfont, UK	NA934-1ML	Sheep	1:2000
anti-rabbit IgG HRB-linked	GE Healthcare, Little Chalfont, UK	NA934-1ML	donkey	1:3000

2.1.7 Primers and Oligos

Random Primers for reverse transcription were purchased from Promega (Mannheim, Germany). For (q)RT-PCR, pre-designed primers were ordered from Thermo Fischer Scientific (Waltham, MA, USA) for each gene of interest (Table 7). Cycle threshold (Ct) values were calculated after quantifying PCR reaction products for each sample and subsequently the relative miRNA amount

of each sample was calculated by linear regression. Values were normalized against a reference control gene (see Ref. in Table 7 and Table 8).

Table 7: TaqMan™ assays for gene expression analysis by qRT-PCR (has: homo sapiens, mmu: mus musculus, rno: rattus norvegicus)

Gene Symbol	Assay ID	Context Sequence
AIP (hsa)	Hs04935271_m1	TCCTCTGTGACATCAAGCATGTGGT
Aip (mmu)	Mm00479315_m1	GGATGGCACTAAGGCCACGTTCCAC
Aip (rno)	Rn00597273_m1	AGGATGGCACTAAGGCCACCTTCCA
Gnai2 (rno)	Rn01447850_m1	AATGACTCAGCCGCTTACTACCTGA
Gnai3 (rno)	Rn00565387_m1	CCAGAGCGGATGATGCCCGACAGTT
B2m (mmu) (Ref)	Mm00437762_m1	CGGCCTGTATGCTATCCAGAAAACC
B2m (rno) (Ref.)	Rn00560865_m1	GCTTGCCATTCAGAAAACTCCCCAA
TBP (has) (Ref.)	Hs.00427620_m1	GAGCCAAGAGTGAAGAACAGTCCAG

Table 8: TaqMan™ assays for miRNA expression analysis by qRT-PCR (has: homo sapiens, rno: rattus norvegicus)

Gene Symbol	Assay ID	Mature miRNA Sequence
rno-miR-145-5p	rno480938_mir	GUCCAGUUUUCCCAGGAAUCCCU
rno-miR-187-3p	rno477941_mir	UCGUGUCUUGUGUUGCAGCCGG
rno-miR-195-5p	rno480882_mir	CCAAUAUUGGCUGUGCUGCUCCA
rno-miR-34a-5p	rno481304_mir	UGGCAGUGUCUUAGCUGGUUGU
hsa-miR-383-3p	478868_mir	ACAGCACUGCCUGGUCAGA
U6 snRNA (Ref.)	001973	GTGCTCGCTTCGGCAGCACATAT ACTAAAATTGGAACGATACAGAGA AGATTAGCATGGCCCCTGCGCAA GGATGACACGCAAATTCGTGAAG CGTTCCATATTTT

Table 9: Primer for cloning and mutagenesis

Primer name	sequence
AIP-EcoRI-Fw	GAGGCCCGAATTCGGATGGCGGATATCATCGCA
AIP-NotI-Rev	CCCCGCGGCCGCTCAATGGGAGAAGATCCCCCG
R271W-27nt-Fw	GGCCTACTTCAAGTGGGGCAAGGCCAA
R271W-27nt-Fw	TGGGCCTTGCCCCACTTGAAGTAGGCC

Table 10: Oligos for cloning (oligos were ordered from Sigma-Aldrich)

Oligo name	**sequence**
Oligo GNAI2 top	TCGAGATATAAGCTTTGTTCCAGACAACTGCCAATGTCACTGAGGGAAAGC
Oligo GNAI2 bottom	CTATATTCGAAACAAGGTCTGTTGACGGTTACAGTGACTCCCTTTCGCCGG
Oligo GNAI2 mut top	TCGAGATATAAGCTTTGTTCCCTGAGGGAAAGC
Oligo GNAI2 mut bottom	CTATATTCGAAACAAGGGACTCCCTTTCGCCGG

2.1.8 Enzymes

HindIII	New England Biolabs, Frankfurt, Germany
NcoI	New England Biolabs, Frankfurt, Germany
NheI	New England Biolabs, Frankfurt, Germany
Phusion® High Fidelity DNA Polymerase	New England Biolabs, Frankfurt, Germany
PmeI	New England Biolabs, Frankfurt, Germany
SuperScript® II Reverse Transcriptase	Life Technologies, Carlsbad, Germany
T4 DNA Ligase	New England Biolabs, Frankfurt, Germany
Taq® DNA Polymerase	Fermentas, St. Leon-Rot, Germany
XhoI	New England Biolabs, Frankfurt, Germany

2.1.9 Bacteria

OneShot® TOP10 *E. coli* competent cells	Invitrogen, Grand Island, NY, USA

2.1.10 Cell lines

The human cell line HEK293 was authenticated by the Leibniz Institute DSMZ - German Collection of Microorganisms and Cell Cultures GmbH (Braunschweig, Germany).

GH3	ATCC
GH4C1	Courtesy of Dr. Chiara Maria Zatelli (Department of Medical Science, University of Ferrara, Italy)
MEF *Aip* -/- (Primary mouse embryonic fibroblasts from *Aip*-/-mouse embryos)	Courtesy of Dr Auli Kahru (Department of Medical Genetics, University of Helsinki, Finland)

HEK293	CRL-11268™, Courtesy of Dr Natasa Anastasov (ISB, HMGU, Munich Germany)

2.1.11 Human pituitary adenoma tissue

The human pituitary adenoma tissues with and without AIP mutations that was used for miRNA array analysis, qRT-PCR and immunhistochemical stainings and the clinical data on the patients of the cohort listed in Table 11 were kindly provided by Dr. Adrian Daly (Department of Endocrinology, University of Liége, Belgium). Fifteen paraffin-fixed, formalin-embedded (FFPE) tissue blocks of PAs with *AIP* germline mutations (*AIP*mut+) and 27 block without AIP germline mutations (*AIP*mut-) were collected. For miRNA array analysis, 20 PAs were used (10 *AI*Pmut- and 10 *AIP*mut+). Amongst these samples there were 12 somatotropinomas (5 *AIP*mut- and 7 *AIP*mut). The p.R271W mutation was the most prevalent mutation among the AIP mutation positive samples (n=4). Additionally the mutations p.R128H (n=1), p.L115W (n=1) and a previously undescribed p. C238W mutation (n=1) were present in these samples.

Table 11: List of patient samples and clinical parameters. Abbreviations: GH: growth hormone; PRL: prolactin; SSA. Somatostatin analog; DA: Dopamine analog.

Patient ID	Genotype	tumor type	score AIP	score Gal2	Array (GH)	Array (PRL)	sex	largest diameter (mm))	Invasion	age at diagnosis	SSA/DA/type	SSA/DA dose (mg/month)	Timing of SSA (preop/postop)
AIP1	wt	GH	3				f	14 (macro)	no	36	OctSC	0,1 3x daily	preop
AIP2	wt	GH	3	0			f	20 (macro)	yes	61	OctSC	0,1 3x daily	preop
AIP3	wt	GH	3		+		f	9 (micro)	no	40	OctLAR	30 mg/month	preop
AIP4	wt	GH	3		+		m	16 (macro)	no	53	Lan AG	30mg/month	preop
AIP5	wt	GH	2	2			m	15 (macro)	yes	19	OctSC	0,1 3x daily	postop
AIP6	wt	GH	3				f	8 (micro)	no	51	Lan AG	30	preop
AIP7	wt	GH	3	2	+		f	14 (macro)	yes	52	OctSC then LAN AG	0,1 mcg 3x daily; 30 mg/mo LAN AG	postop
AIP8	wt	GH	3		+		f	20 (macro)	yes	62	Lan AG	30	postop
AIP9	wt	GH	1				m	30 (macro)	yes	33	Lan AG	20	postop
AIP10	wt	GH	3	2			m	12 (macro)	no	48	Lan AG	60-120	preop
AIP11	wt	GH	3	3	+		m	14 (macro)	no	35	Lan AG	N/A	preop
AIP12	wt	GH	3	2			f	12 (macro)	no	50	Lan AG	N/A	preop
AIP13	R271W	GH	3	1	+		f	60 (macro)	yes	22	none	none	none
AIP14	R271W	PRL	2	1		excluded	m	40 (macro)	no	12	Bromocriptine	N/A	postop
AIP15	R271W	GH	2		+		m	15 (macro)	yes	15,5	none	none	none
AIP16	R56C	PRL	2	1		+	m	70 (macro)	yes	25	Cabergoline	2 mg/week	postop
AIP17	F269F	PRL	2	0		+	m	20 (macro)	yes	10	Cabergoline	40mg/month	postop
AIP18	Q146S	GH	2	0	+		m	15 (macro)	yes	18	Oct LAR	30	postop
AIP19	wt	PRL				+	m	50 (macro)	yes		Quinagolide then Cabergoline	150/day and 0,5x2/week	preop/postop
AIP20	wt	PRL				+	f	35 (macro)	yes	27	Cabergoline	0,5-1x2-3/week	preop/postop
AIP21	R271W	GH	2	2	+		m	20 (macro)	yes	20	none	none	N/A
AIP22	L115W	GH			+		f	37 (macro)	yes	19	OCT sc /Pasi	100 mcg s.c. t.i.d / pasi 20mg/week	postop
AIP23	R128H	GH	2	1	+		m	20 (macro)	no	28	Cabergoline and Octreotide SC	0,5/w and 0,1x2/d	preop
AIP24	M1I	GH	3	1			m	14 (macro)	no	19	none	none	none
AIP25	wt	PRL	0	0		+	f	44 (macro)	yes	63	Cabergoline	0.5/2days	preop/postop
AIP26	wt	PRL	1	1		+	f	5 (micro)	no	27	No	0.5x2/week / 0.25/week	preop
AIP27	wt	PRL	1	0			f	5 (micro)	no	37	Cabergoline	0.5 x 1/week, then 0.5 x2/week preop, then 0.25mg/week postop for ?long	preop/postop
AIP28	wt	PRL	2	2		+	f	9 (micro)	no	31	Cabergoline	N/A	postop
AIP29	wt	PRL	1	0			f	8 (micro)	yes	27	Cabergoline	0.5mg/week	preop
AIP30	Q146S	GH					f	20 (macro)	yes	24	Sandostatin LAR/Pegvisomant	40mg/month	postop
AIP31	R271W	GH	1	1			m	39 (macro)	yes	30	Sandostatin LAR	40mg/month	postop
AIP32	R271W	GH	0	0			m	12 (macro)	no	27	Sandostatin LAR	40mg/month	postop
AIP33	R271W	GH	2	1			m	25 (macro)	yes	20	Oct LAR	40mg/month	postop
AIP34	C238W	GH	3	2			m	40 (macro)	yes	14	Lan AG	120mg/month	postop
AIP35	wt	GH	1	2			m	25 (macro)	yes	55	Somatuline, then+ Cabergoline preop, Somatuline + Pegvisomant postop	Somatuline 120mg/3weeks; then +Cabergoline 0.5mg x2/week preop; Somatuline 120mg/4weeks, then +Pegvisomant 15mg/2days	preop/postop
AIP36	wt	GH	3	2			m	21 (macro)	no	40	Dopastatine (I think), then Sandostatine, then + Cabergoline preop; Sandostatine, then + Cabergoline post	Sandostatine 30mg/3 weeks; then + Cabergoline 0.5mg x 2/week preop, Sandostatine 30mg/4weeks, then + Cabergoline 0.5mgx2/week postop	preop/postop
AIP37	wt	GH	3	3			f	9 (micro)	no	62	Somatuline	Somatuline 90mg/mo	preop
AIP38	wt	GH	3	2			m	17 (macro)	no	27	Somatuline, then + Cabergoline	120mg/4, then every 3 weeks + Cabergoline up to 0.5 x2/week	preop
AIP39	wt	GH	3	2			f	11 (macro)	no	38	Somatuline	up to 120mg/3weeks	preop
AIP40	wt	GH	2				m	macro	no	40	Lan AG	N/A	preop
AIP41	wt	GH	2	2			f	micro	no	37	Oct LAR	N/A	preop
AIP42	wt	GH	2	3			f	28 (macro)	no	28	Somatuline + Cabergoline preop	Somatuline 120mg/3weeks + Cabergoline 0.5mg x 2/week	preop

2.1.12 Standards

Quick-Load® 100bp DNA ladder	New England Biolabs, Frankfurt, Germany
Quick-Load® 1 kb DNA ladder	New England Biolabs, Frankfurt, Germany
PageRuler™ prestained protein ladder	Fermentas, St. Leon-Rot, Germany

2.1.13 Desinfections

Antifect®FD10	Schülke & Mayr, Norderstedt, Germany
Pursept®-A Classic Fresh Merz	Frankfurt a.M., Germany
Ethanol 70 % (v/v) in water for bacteriology	
Ethanol 80 % (v/v) in water for cell culture	

2.1.14 Software

Adobe Illustrator CS2	Adobe, San José, CA, USA
Adobe Photoshop CS2	Adobe, San José, CA, USA
AimImageBrowser 3.5	Carl Zeiss, Jena, Germany
AxioVision 4.6	Carl Zeiss, Jena, Germany
GraphPad Prism 8	https://www.graphpad.com/scientific-software/prism/
GNU Image Manipulation Programm 2.10.14	https://www.gimp.org/
ImageJ 1.52e	https://imagej.nih.gov/ij/
Integrative Genome Viewer 2.8.x	https://www.broadinstitute.org/igv/home [195]
LabSens V2.3	Olympus Soft Imaging Solutions, Münster, Germany
Microplate Manager 5.2.1	BioRad Laboratories, Munich, Germany
MS Office 2010	Microsoft, Unterschleißheim, Germany
Rotor-Gene Q 2.3.1.49	Qiagen, Hilde, Germany
SigmaPlot 7.0	Sigma-Aldrich, Steinheim, Germany
SnapGene 5.0	http://www.snapgene.com/
SkanIT™ Software for microplate reader	Thermo Fischer Scientific, Waltham, MA, USA

2.1.15 Online tools

DIANA tools	miRNA target prediction	http://diana.imis.athena-innovation.gr/DianaTools/index.php
miRANDA-mirSVR	miRNA target prediction	http://www.microrna.org/microrna/home.do
PlasMapper Version 2.0	Generation and annotation of plasmid maps	http://wishart.biology.ualberta.ca/PlasMapper/
PITA	miRNA target prediction	https://genie.weizmann.ac.il/pubs/mir07/mir07_prediction.html
TargetScan 7.0	miRNA target prediction	http://www.targetscan.org/vert_70/

2.2 Methods

2.2.1 Molecular biology methods

DNA and RNA isolation

Extraction of miRNA from patient formalin-fixed paraffin embedded (FFPE) tissue sections (20 µm) was performed with the miRNeasy FFPE Kit (#217504, Qiagen, Hilde, Germany) according to the manufacturer's protocol. miRNA from cell pellets was extracted with the miRNeasy Mini Kit (#217004, Qiagen, Hilde, Germany) also following the manufacturer's instructions.

Plasmid DNA extraction from bacterial suspensions was performed either by QIAprep® Spin Miniprep Kit (#27106, Qiagen, Hilde, Germany) or the ZymoPURE II Plasmid Maxiprep Kits (#D4202, Zymo Research, Irvine, CA, USA).

For RNA and DNA extraction from cells the Maxwell® 16 (Promega, Mannheim, Germany) was used. The cell pellets were treated according to the protocol and applied to a Maxwell® 16 LEV Cartridge. The extraction process was performed automatically by the Maxwell® 16 device. In addition, the RNeasy Mini Kit (#74104, Qiagen, Hilde, Germany) was used for RNA extraction, and the DNeasy Blood & Tissue Kit (#69504, Qiagen, Hilde, Germany) was used for extraction of genomic DNA from cell pellets.

DNA, RNA and miRNA content was quantified by measuring the absorbance of the samples at a wavelength of 260 nm by the NanoDrop™ 2000 spectrophotometer. DNA and RNA purity was assessed by calculating the 260 nm/280 nm and the 260 nm/230 nm ratios of absorbance. A 260 nm/280 nm ratio of 1.8 was considered as pure DNA, while a ratio of 2.0 was accepted as pure

RNA. In case lower ratios were calculated, contamination of the sample, e.g. with proteins or phenol might have occurred. As a secondary measure the 260 nm/230 nm ratio was assessed as a secondary measure of DNA/RNA purity. These values were expected to be in the range of 2.0 – 2.2. Lower ratios might indicate contamination with carbohydrates or phenol.

miRNA profiling

miRNA profiling was performed by Dr. Nikolai Falk (PATH, HMGU Munich) in cooperation with Dr. Martin Irmler (IEG, HMGU, Munich).

Before submitting the RNA samples to a miRNA array, samples had to be labelled in order to be detected after hybridization to the array. According to the manufacturer's protocol, the RNA samples were labelled with the FlashTag™ Biotin HSR RNA Labeling Kit (#901910, Genisphere, Hatfield, PA, USA).

In a first step, a poly(A) tail is added to the RNA with a poly(A) polymerase. Subsequently, Biotin-labelled 3DNA® is ligated to the poly(A) tail. The Biotin-labelled RNA can afterwards be detected by streptavidin-tagged fluorescent dyes.

Table 12: Poly(A) tailing reaction setup

Component	**Volume [µl]**
10x reaction buffer	1.5
25 mM $MnCl_2$	1.5
ATP Mix	1
Poly(A) Polymerase	1
RNA (250 ng/µl)	8
RNA Spike Control Oligos	2
Σ	**15**

Volume of the RNA samples was adjusted to 8 µl with RNase-free water. The reaction mix was incubated for 15 min.

Table 13: FlashTag™ Biotin HSR Ligation reaction setup

Component	**Volume [µl]**
Poly(A) tailed RNA	15
5x FlashTag™ Biotin HSR Ligation Mix	4
T4 DNA Ligase	2
Σ	**21**

After gently mixing and centrifuging the reaction mix, it was incubated at RT for 25 min. The reaction was stopped by the addition of 2.5 µl of HSR stop solution.

From the ligation mix, 21.5 µl were used for hybridization with a GeneChip miRNA 1.0 Array (Affymetrix, High Wycombe, UK), which is based on the Sangre miRBase miRNA database v11 (April 15, 2008).

Agarose gel electrophoresis

PCR products were analyzed on a 1% agarose gel containing 0.005% ethidium bromide. 1 µl of the PCR sample was mixed with 5 µl Gel loading dye, 6x (New England Biolabs, Frankfurt, Germany). The PCR samples were separated within the electrical field alongside a DNA standart (Quick-Load® 100bp DNA ladder and/or Quick-Load® 1 kb DNA ladder (New England Biolabs, Frankfurt, Germany)) at 80 – 100 V. Intercalation of ethidium bromide into the sample DNA allows visualization of DNA bands under UV light after the separation.

Quantitative reverse transcription PCR (qRT-PCR) at mRNA levels

For qRT-PCR RNA samples were transcribed into cDNA by reverse transcription. For each sample 250 - 500 ng RNA was adjusted to 9 µl with RNase free water and 1 µg random primers (Promega, Mannheim, Germany) were added. The master mix prepared according to Table 14 is added to the RNA/primer mix and incubated at 42 °C for 1h. The reaction was terminated by 5 min incubation at 95 °C. The resulting cDNA was either directly subjected to qPCR or stored at -20 °C until further use.

Table 14: Reverse Transcription reaction setup per sample

Component	**Volume [µl]**
5x first strand buffer	4
DTT (0.1 M)	2
dNTP Mix (10 mM each)	1
RNaseOUT	1
SuperScript® II Reverse Transcriptase	1
Σ	**9**

After reverse transcription mRNA levels of specific genes of interest were analyzed by TaqMan™ PCR (Thermo Scientific™). Therefore, 10 µl TaqMan® Universal PCR Master Mix (2x) is mixed with 1 µl of the TaqMan™ gene expression assay (see Table 7) and 9µl cDNA template plus Nuclease-free water. The samples were pipetted into 0.1 ml Strip Tubes for the Rotor-Gene Q device (72-well rotor) in duplicates. Non-specific binding controls without cDNA template were

pipetted alongside the samples. Species-dependent reference genes were also loaded to allow normalization of the cDNA input. Step 3 and 4 of the qPCR program (Table 15) was performed for 40 cycles.

Table 15: Set-up for Rotor-Gene Q qPCR

Step	Temp [°C]	Duration [sec]
1	50	120
2	95	600
3	94	15
4	60	60
5	4	∞

Quantitative reverse transcription PCR (qRT-PCR) at miRNA levels

Reverse Transcription of miRNA-enriched RNA for miRNA expression studies was conducted by the TaqMan® MicroRNA Reverse Transcription Kit (#4366596, Thermo Fischer Scientific, Waltham, MA, USA) and a specific miRNA primer for Reverse Transcription that are included in the miRNA TaqMan® assays. Initially, RNA samples were diluted to a concentration of 2 ng/µl with RNase-free water. The Master Mix was prepared and the PCR was performed following the manufacturer's instructions. cDNA was either directly subjected to miRNA qPCR or stored at -20 °C until further use.

After reverse transcription miRNA levels of specific genes of interest were analyzed by miRNA TaqMan™ PCR (Thermo Scientific™). Therefore, 5 µl TaqMan® Universal PCR Master Mix (2x) is mixed with 0,5 µl of the TaqMan™ gene expression assay (see Table 7), 2µl cDNA template and 2.5 µl nuclease-free water. The samples were pipetted into 0.1 ml Strip Tubes for the Rotor-Gene Q device (72-well rotor) in duplicates. Non-specific binding controls without cDNA template were pipetted alongside the samples. U6 snRNA was used as a reference gene (Table 8) for normalization. The same program of the Rotor-Gene Q was used for miRNA qPCR as for mRNA qPCR.

2.2.2 Cloning

Cloning procedure and mutagenisis

Wild-type human AIP cDNA was cloned into the pCMV-Myc vector using the primer AIP-EcoRI-Fw and AIP-NotI-Rev listed in Table 9. Subsequently the R271W mutation was introduced by site-directed mutagenesis with the primer R271W-27nt-Fw and R271W-27nt-Fw (Table 9) and the

Quickchange II Site-directed mutagenesis Kit following the manufacturer's instructions. The mutagenesis was verified by sequencing. Cloning, mutagenesis and sequencing were performed by Dr. Sara Molatore.

The predicted seed match (Figure 39) for miR-34 in the 3'UTR of GNAI2 was cloned into the psiCHECK™-2 vector (#C8021, Promega, Mannheim, Germany). Therefore, two single stranded DNA oligonucleotides (oligos) representing top and bottom strand of the seed match were designed, with additionally XhoI and NotI restriction sites at the ends of the fragment that results after hybridization. A HindIII restriction site was added to the fragment as well in order to allow identification of insert containing vectors after cloning. The oligos were phosphorylated and annealed following the reaction setup in Table 16. The annealing was conducted in a thermocycler for 30 min at 37 °C followed by heat inactivation for 5 min at 95 °C. Subsequently, the temperature was dereased for 5 °C per minute to a final temperature of 25 °C.

Table 16: Reaction setup for oligo annealing

Component	**Volume [µl]**
Oligo 1 (100 µM)	1
Oligo 2 (100 µM)	1
10x T4 ligation buffer	1
Nuclease-free H_2O	6.5
T4 ligase	0.5
Σ	**10**

The empty psiCHECK-2 vector (2 µg) was double digested with XhoI and NhoI according to the manufacturers recommendations. Subsequently, the digested vector was subjected to purification using the QIAquick PCR purification kit. The ligation of the digested vector and the insert was performed according to Table 17. After gently mixing and microfuging the reaction mix was incubated at room temperature for 5 min. Afterwards, the reaction was chilled on ice and directly proceeded with transformation.

Table 17: Reaction setup for ligation of digested vector and insert

Component	Volume [µl]
psiCHECK-2 [100 ng]	X
Annealed oligos [2391 ng]	X
Quick Ligase Reaction Buffer (2X)	10
Quick Ligase	1
Nuclease-free H_2O	ad. 20
Σ	**20**

Heat shock transformation and plasmid isolation

One Shot® TOP 10 chemically competent *E.coli* were used for transformation of the cloned construct. Bacteria were thawed on ice and 50 µl of bacterial suspension was mixed with 50 – 100 µg of ligated plasmid DNA. After mixing gently, the bacteria were incubated on ice for 30 min followed by a heat shock of 45 sec at 42 °C. The bacteria were placed on ice for 2 min for cooling and subsequently recovered in 1 ml pre-warmed SOC medium for 45 min at 37 °C and 300 rpm shaking. A dilution streak of 50 – 100 µl of the bacterial suspension was done on agar plates containing 100 µg/ml Ampicillin. The agar plates were incubated overnight at 37 °C in order to allow the growth of bacterial colonies. Single colonies were picked and inoculated into 10 ml of LB medium containing the respective antibiotic. After incubation of the suspension shaking at 37 °C overnight, plasmid DNA was isolated as described above. Glycerol stocks were generated for long term storage of the bacteria containing the plasmid.

2.2.3 Cell culture methods

Subculturing of adherent and semi-adherent cell lines

Cells were cultured at 37 °C and 5 % CO_2. All cell culture work was performed under sterile conditions (sterile hood with controlled air flow). All solutions that were used for maintenance of cells in culture were pre-warmed to 37 °C before use. Cells were subcultured on a regular basis (frequency depending on the growth rate of each cell line) in order to avoid confluency and cell death. Therefore, cells were washed with PBS to remove serum containing media from the cells. For semi-adherent cell lines both, the removed culture media and PBS for washing was centrifuged for 5 min at 1000 rpm to collect floating cells. Subsequently, cells were detached from the surface of the cell culture vessel either mechanically by scraping them off or enzymatically by incubation with 0.05 % trypsin/EDTA for 3 – 5 min at 37 °C. The enzymatic activity of trypsin was quenched by adding media with serum to the cells. A splitting ration between 1:3 and 1:9 was

used and cells were subcultured every 2 - 3 days depending on cell type. All cell lines were used for 30 passages (20 passages for MEFs) at most to avoid phenotypic variations of the cells.

Table 18: Composition of cell culture media [FBS: fetal bovine serum; HS: horse serum; P/S: Penicillin/Streptomycin (5000 u/mL each); A: Amphotericin B (antimycotic, 250 µg/ml)]

Cell line	Medium	Supplements
AtT20	DMEM	10 % FBS 1 % P/S
GH3	Ham's F-12K	15 % HS 2.5 % FBS 1 % P/S
GH4C1	Ham's F10	15 % HS 2.5 % FBS 1 % P/S
HEK293	DMEM	10 % FBS 1 % P/S
MEF *Aip*-/-	DMEM	10 % FBS 1 % P/S 1 % A

Cryoconservation of cell lines

For establishing a sufficient stock of cells with low passage number, several vials of cells were frozen each time after thawing cells. For thawing, cryoconserved cells were put into a water bath with 37 °C directly after taking it out of liquid nitrogen. The cell lines were frozen in DMSO, which needs to be removed from the thawed cells quickly due to its cytotoxicity. Therefore, as soon as the vial was completely thawed it was inoculated into 10 ml pre-warmed medium (containing serum) of the respective cell line. Cells were centrifuged at 100 rpm for 5 min at RT and the supernatant containing DMSO was removed. The cell pellet was resuspended in cell line specific medium (containing serum) and transferred into an adequate cell culture flask.

After thawing the cells were expanded for 1 – 3 passages. At 70 – 80 % confluency the cells were detached from the flask by scraping or trypsinization, depending on the downstream analysis, and centrifuged (1000 rpm, 5 min; RT). The cell pellet was resuspended in 1.5 ml serum (FBS or HS depending on the cell line) with 10 % (v/v) DMSO. The cell suspension was transferred into cryogenic vials and stored overnight at -80 °C in a freezing container filled with isopropanol. Due

to the circumfluent isopropanol layer, the temperature of the cells was decreased slowly at approximately 1 °C/min. Subsequently the cells were stored at -196 °C in liquid nitrogen.

Mycoplasma test

Mycoplasma contamination can have drastic effects on cultured cells and is unaffected by most antibiotics. Therefore, to detect contaminated cells and avoid contamination of other cell lines all new cells were routinely tested with the mycoplasma test kit. Supernatant from the cultured cells was centrifuged (250 x g, 5 min, RT) and supernatant was transferred into a sterile tube and again centrifuged (20000 x g, 10 min, RT) to accumulate mycoplasma. The pellet was resuspended in 50 µl buffer. For PCR, 5 µl were heated to 95 °C for 3 min. and mixed with 35 µl H_2O and 10 µl reaction mix. The PCR was conducted following the steps described in Table 19. Steps 2 – 4 were repeated for 35 cycles. Subsequently the samples were analyzed by agarose gel electrophoresis.

Table 19: Set-up for Mycoplasma PCR

Step	Temperature [°C]	Duration [sec]
1	94	30
2	94	30
3	60	120
4	72	60
5	94	30
6	60	120
7	72	300

Automated cell counting

For cell counting, 10 µl of cell suspension was applied on a LUNA™ disposable counting slide and counted by the LUNA™ Automated Cell Counter. A high resolution brightfield image of the cells was captured and analyzed to provide total cell counts. Live and dead were distinguished by dye exclusion with Trypan Blue. The cell counter was able to quantify cells between 5 x 10^4 and 1 x 10^7 cells with a cellular diameter between 3 – 60 µm.

Transient transfections

MEF AIP -/- at approx.. 70 % confluency were transiently transfected with AIP plasmids [AIP wt (1 µg + 3 µg empty vector) and AIP-R271W (4 µg)] or co-transfected with the AIP plasmids and miRNA hairpin inhibitor (25 nM, anti-miR-34a, anti-miR-145 with the 4D-Nucleofector System X unit and the P4 Primary Cell 4D-Nucleofector® X Kit. Cell pellets were re-suspended with the P4 buffer containing Supplement 1 solution at a concentration of 0.5 – 2 x 10^6 cells per 100 µl buffer. Electroporation was conducted using the pulse code CZ-167 and the cells were allowed to sit at room temperature for 10 min following the reaction. Subsequently, cells were re-suspended with 400 µl pre-warmed complete medium and plated in 6-, 24- or 96-well plates according to the subsequent analysis.

GH3 and GH4C1 cells at approx.. 70 % confluency were transiently transfected with 150 nM miRNA mimics (unspecific control mimic, miRIDIAN microRNA rno-miR-34a mimic, miRIDIAN microRNA rno-miR-145 mimic) or hairpin inhibitor (neg. Control inhibitor or anti-miR-34a (miRIDIAN microRNA Rat rno-miR-34a inhibitor) using the 4D-Nucleofector System X unit and the SF Cell Line 4D-Nucleofector® X Kit. Cell pellets were re-suspended with the SF buffer containing Supplement 1 solution at a concentration of 0.5 – 2 x 10^6 cells per 100 µl buffer. Electroporation was conducted using the pulse code DS-131 and the cells were allowed to sit at room temperature for 10 min following the reaction. After re-suspension with 400 µl pre-warmed growth medium cell were seeded for further downstream functional analysis.

HEK293 cells were plated 24h before transfection in 24-well-plates at a density of 0.05 x 10^6 cells per well. The cells were transiently transfected with Lipofectamine™ 3000 Transfection Reagent. Therefore, 1 µg of the vector and 150 nM of either neg. Control inhibitor or anti-miR-34a was diluted in 25 µl Opti-MEM™ Reduced Serum Medium and 2 µl P3000 reagent (Lipofectamine™ 3000 Kit) was added. In parallel 1,5 µl Lipofectamine™ 3000 was diluted in 25 µl Opti-MEM™. The two mixtures were combined and the transfection complexes could form during 15 min incubation at room temperature. Subsequently, the transfection complexes were added to the cells (50 µl per 24-well). After 24 h downstream analysis of the transfected cells was performed.

Functional characterization of transfected cells

Cell viability assay

Cell viability was assessed by a colorimetric assay using WST-1 reagent. Transfected cells were plated in a 96-well plate at a density of 1.5x 10^5 cells per well and 6 wells per group. WST-1 was added 1:10 to the cells 24, 48 or 72 h after transfection and absorbance at 450 nm was measured 60 min after WST-1 addition.

Transwell assay

In order to assess migration behavior of transfected cells a transwell assay was performed. Therefore, transfected cells were plated in 24-well plates with adequate cell culture inserts. The wells of the 24-well plate contained the normal growth medium of the respective cells whereas the inserts hold the respective medium containing antibiotics with reduced serum content (0.1 % FBS, 0.02 % HS). Cells were allowed to migrate for 24 h. Afterwards, the membranes of the cell culture inserts were stained with Toluidin Blue after fixation of the cells with Methanol. Membranes were mounted on glass slides with Pertex® mounting medium and capped with coverslips. Images were recorded using an Olympus BX43 microscope.

Colony formation assay

Clonogenic potential of the cells was monitored by seeding cells at a low density of 1 x 10^3 cells per well in 6-well plates. After eight days, colonies were washed with PBS and subsequently stained with 0,3 % (w/v) Crystal Violet in 30 % (v/v) Ethanol. The colonies were washed again and counted. Only colonies with a diameter of more than 100 µm were taken into consideration

Apoptosis

Cells were plated in 96-well plate at a density of 1.5 x 10^5 cells per well and 6 wells per group. For assessment of apoptosis in the cells, Caspase-Glo® 3/7 Assay was performed according to the manufacturer's instructions.

Drug treatment

Cells were treated with 25 µg/ml cycloheximide (CHX) and/or 10 µM epoxomicin (EPOX) in complete medium for the indicated times.

For therapy response, cells were treated with 10 nM or 100 nM Octreotide (kindly provided by Italfarmaco SpA, Milan, Italy) in serum-free medium for the indicated times.

2.2.4 Biochemical methods

Protein extraction and quantification

Cells were collected at the indicated time points and lysed in radio-immunoprecipitation assay (RIPA) buffer supplemented with protease and phosphatase inhibitors. The lysates were incubated on ice for 20 min and subsequently centrifuged at 13000 x g at 4 °C for 10 min in order to remove cellular debris. Extracted proteins were stored at -20 °C.

Protein concentrations were determined by the Pierce™ bicinchoninic acid (BCA) Protein Assay Kit. 2 µl of protein samples were mixed with 98 µl Ampuwa® water. In parallel a standard curve with six solutions containing BSA concentrations in ascending order *ad* 100 µl was made. Reagent A and B of the Pierce™ bicinchoninic acid (BCA) Protein Assay Kit were mixed 1:1 and 1 ml of the mixture was added to both protein samples and standards. Samples and standards were incubated at 60 °C shaking and subsequently absorbance at 650 nm was assessed by a spectrophotometer. Finally, the protein concentration could be calculated with the values from the standard curve.

SDS-PAGE

Discontinuous sodium dodecyl sulphate polyacrylamide gel electrophoresis (SDS-PAGE) was used to separate proteins according to their size. 2x or 4x Laemmli buffer was mixed with 5 % (v/v) β-mercaptoethanol and added to 30 – 50 µg of protein (1:1 for 2x Laemmli, 3:1 for 4x Laemmli). Samples were heated up to 95 °C for 5 min and afterwards separated in 1x SDS running buffer on discontinuous polyacrylamide gels (4 %stacking gel, 10 % separating gel, see 2.1.4 Buffers and Solutions) next to a pre-stained protein ladder. A voltage of 90 V was applied until all samples moved beyond the stacking gel. Afterwards the voltage was increased to 120 V.

Western blot transfer

Proteins in the SDS-PAGE gel were blotted in a wet blot system onto a nitrocellulose membrane that is non-specifically protein-binging. The SDS-PAGE gel and the nitrocellulose membrane were stacked on whatman filter paper and sponges and placed in the blotting chamber that was filled with transfer buffer. The transfer was performed at 100 V for 2 h at 4 °C. Ponceau S staining was performed for 5 min at RT for the rapid and reversible detection of the proteins trapped on the nitrocellulose membrane in order to determine the quality of the transfer and the separation of the proteins. Rigorous washing of the membrane in TBS-T removed the staining completely from the membrane.

Protein detection

For detection of specific proteins on the nitrocellulose membrane they were hybridized with the relevant antibodies and detection systems. Initially the membrane was blocked for 1 h at RT on a rocking table in 5 % (w/v) nonfat milk (Blotting-Grade Blocker) in order to reduce unspecific binding of the antibody. After blocking the membrane was washed 3 times for 5 min with TBS-T. The primary antibody was diluted in antibody dilution solution for Western Blot in concentrations depending on the antibody (reported in Table 5). The blocked membrane was incubated with the antibody overnight at 4 °C or for 1 – 2 h at RT. After washing three times for 5 min with TBS-T to remove unbound primary antibody, a species-specific secondary antibody coupled to horseradish peroxidase diluted in 5 % (w/v) nonfat milk was applied on the membrane for 1 h at RT. After incubation with the secondary antibody the membrane was washed again three times for 5 min with TBS-T. Subsequently, the chemoluminescent substrate for the horseradish peroxidase (SuperSignal® West Pico/Femto chemoluminescent substrate, mixed 1:1) was applied on the membrane for 5 minutes in the dark. The membrane was then exposed on a photographic film in a X-ray cassette to protect it from light. For additional probing of the membranes with another antibody, the membrane was treated with Restore™ PLUS, stripping buffer for 15 min at RT. The membrane was washed 3 times for 5 min with TBS-T and afterwards the detection process, as was described above, was repeated starting with blocking of the membrane.

Enzyme linked immunosorbent assay (ELISA)

In order to measure the levels GH that was secreted from GH3 cells into the culture medium after treatment with Octreotide the Rat/Mouse Growth Hormone ELISA was used. Transfected, serum-starved GH3 cells were incubated with 100 nM Octreotide or vehicle for 48 h. Subsequently, the cell culture supernatants (diluted 1:50 in assay buffer (provided by the kit), were collected and centrifuged at 1000 rpm for 5 min to remove cellular debris. The supernatants were then passed through the Growth Hormone ELISA following the manufacturer's protocol. In short, all samples were applied to the Microtiter Assay Plate that was pre-coated with a polyclonal antibody specific for GH (washed one time with wash buffer (provided by the kit)) along with the prepared standards, quality controls and assay buffer for the blank wells. The plate was covered with a plate sealer and incubated for 1.5 h on an orbital microtiter plate shaker (400 – 500 rpm). The plate was then inverted and decanted onto absorbent towels and washed three times with wash buffer (plate was tapped after each washing). 100 µl of the labelled detection antibody (provided by the kit) was added to all wells and the covered plate was incubated for 1 h shaking. After washing as described before, 100 µl Enzyme solution (provided by the kit) was added and the sealed plate was incubated for 30 min on the plate shaker. The plate was washed again, and 100 µl substrate solution (3,3',5,5'- tetramethylbenzidine, provided by the kit) was applied on all wells. The plate

was covered and incubated for 5 – 20 min until the blue color for the standard wells (proportional to increasing GH concentrations) was well established. The enzymatic reaction was stopped by adding 100 µl stop solutions (provided by the kit) to all wells, which caused a color change to yellow. Absorbance was read at 450 nm and 590 nm(for correction) in a plate reader within 5 min. The final GH concentrations were calculated with the standard curve.

Intracellular cAMP levels were assessed in transfected cells by the Direct cAMP ELISA kit. 24h after transfection, growth medium was removed and cells were covered by 0.1 M HCl in order to stop the activity of endogenous phosphodiesterases and lyse the cells. After 10 – 20 min of incubation with HCl the cells were scraped and pelleted by centrifugation (1000 rpm, 5 min, RT). All samples and the prepared standards were acetylated by adding10 µl of a 1:2 mix of acetic anhydride and trimethylamine to increase the sensitivity of the assay. A total volume of standards, controls and samples were applied on the microtiter plate (provided by the kit). 50 µl cAMP conjugate and 50 µl cAMP ELISA antibody (both provided by the kit) were added to the respective wells. The plate was sealed and incubated for 2 h on an orbital plate shaker (500 rpm). The plate was tapped and washed three times and 200 µl of the substrate solution (provided by the kit) was added to each well. The plate was incubated for 1 h at RT (without shaking) before 50 µl stop solution (provided by the kit) was added to terminate the reaction. Optical density was read at 405 nm and final cAMP concentrations were calculated with the standard curve.

2.2.5 Immunhistological stainings

Haematoxylin and eosin (H&E) staining

FFPE tissue sections were cut with a thickness of 2 µm and immersed into haematoxilin for 4 min. Subsequently the slides were washed for 5 min under running water to remove excess haematoxilin and cause a color change to blue/purple due to the increase of the pH. Eosin staining was performed by 20 sec incubation in eosin which stains cytoplasmatic components in a red color. The sections were washed again under running water for 5 min and dehydrated by an ascending alcohol series (50 %, 70 %, 96 %, 100 %,) and xylol. The slides were finally mounted with coverslips.

Immunhistochemistry (IHC) on tissue sections

Immunhistochemical stainings of FFPE tissue sections (2 µm) were performed using either an automated immunostainer, as previously described [196] or manually according to the following procedure. First, paraffin sections were deparaffinized (two washes in xylol for 10 min) and hydrated in a descending alcohol series (100 % (2x), 96 %, 70 % ethanol; 5 min each). Afterwards,

the slides were washed in distilled water and TBS-T (pH 7.0) for 5 min each. To block endogenous peroxidase activity and minimized nonspecific background staining, the samples were incubated in hydrogen peroxide (H_2O_2) solution (0.3 % (v/v) H_2O_2 in methanol) for 10 min. After washing twice for 5 min in TBS-T, antigen retrieval was performed to enable antibody-binding and improve staining intensity. Therefore, the sections were cooked for 30 min at 1000 W in citrate acid monohydrate buffer (pH 6.0) in a microwave. Afterwards, the slides were washed in TBS-T for 5 min to cool them down. To avoid unspecific antibody-binding, the slides were blocked with normal goat serum (NGS) for 30 min at room temperature and washed once with TBS-T. Primary antibodies against the specific protein of interest were diluted in Dako REAL™ antibody dilutent in concentrations specific for each antibody. The slides were incubated with the primary antibody overnight at 4 °C in a humidified chamber. The next day, the samples were washed 3 times in TBS-T for 5 min and incubated with biotinylated secondary antibodies for 45 min. The secondary antibody is conjugated to biotin beads, which can subsequently capture an avidin-enzyme detection complex. After the incubation time, the slides were washed 3 times for 5 min in TBS-T to remove the antibody and incubated in streptavidin-horseradish peroxidase for 30 min at RT. The slides were washed 3 times for 5 min in TBS-T and treated with DAB staining solution to enable visualization. The slides were counterstained with haematoxylin for 10 sec and washed under running water for 4 min. Therafter, slides were dehydrated in an ascending alcohol series (70 %, 96 % and 100 % ethanol) with 2 min incubation at each concentration. Subsequently, the sections were incubated in xylol twice for 10 min and mounted with cover slips. Images were recorded using an Olympus BX43 microscope.

For Guanine Nucleotide Binding Protein (G Protein), Alpha Inhibiting Activity Polypeptide 2 (Gαi-2-) IHC an Avidin-Biotin block (AB-block) was used to decrease unspecific background staining. High levels of endogenous biotin can cause high backround levels with biotin-based IHC detection. Therefore, an excess of avidin is added to the sample to bind endogenous biotin, which is in turn blocked by adding an excess of biotin. Finally, biotin an avidin in washed away For AIP-IHC the AB-block was not necessary.

IHC results were evaluated using a semi-quantitative method taking into account the staining intensity: − (negative), + (mild positive), ++ (moderate positive), and +++ (strong positive). Slides were scored using a double-blind method by two independent observers; the percentage of discrepancies was below 3 %. Images were recorded using a Hitachi camera HW/C20 installed in a Zeiss Axioplan microscope with Intellicam software (Carl Zeiss MicroImaging, Göttingen, Germany).

Immunfluorescence (IF) on cells

In order to perform IF staining of cells, the cells were plated and cultured on cover slips in 24-well plates. The cells were washed 3 times with PBS and subsequently fixed with 2 % (w/v) PFA for 30 min at RT. Cells were then washed again 3 times in PBS. Incubation for 3 min at RT in 0.1 % (v/v) Triton X-100 (in PBS) was performed to increase permeability of the cell membrane. The cells were washed 5x for 5 min and blocked in 5 % (v/v) NGS for 30 min at RT. The primary antibodies were diluted in 5 % (v/v) NGS and applied in the cells overnight at 4 °C. On the next day the cells were washed 3 times with warm PBS and the secondary antibody conjugated with Alexa fluor 555 (diluted 1:300 in 5 % (v/v) NGS) was added for 1 h at 4 °C. After washing 3x with warm PBS the cells were counterstained with DAPI (diluted 1:1000 in H_2O) for 3 min t RT. Following 3 washes with PBS the cover slips were mounted on glass slides with vectasield and stored at -20 °C. The signal form the fluorophore was recorded with a Axiovert 135 microscope.

2.2.6 Statistical Analysis

Results of the cell assays are shown as the mean of values obtained in independent experiments ± SEM and $p<0.05$ was considered statistically significant.

All statistical analyses were performed in GraphPad Prism 8 (https://www.graphpad.com/scientific-software/prism/). If applicable, data was tested for normal distribution by Shapiro-Wilk test and variances were tested to be equal by F-test.

Significance tests for comparison of two datasets were selected according to the results of the above mentioned tests. Normally distributed datasets with equal variances were tested by unpaired t-test. Welch's t-test was applied on normally distributed data without equal variances. If the data was not equally distributed significance was tested by Mann-Whitney test. Three or more data sets were analyzed by one-way ANOVA for normally distributed data with either Tukey's, Sidak's or Dunnett's correction for multiple comparisons. Kruskal-Wallis test was applied on not normally distributed data. For analysis of grouped data sets two-way ANOVA was calculated.

Correlations were generated by calculating the Pearson correlation coefficient and two-tailed p-value. Linear regression was performed on the correlation.

Analysis of the array data was performed by Dr. Martin Irmler (IEG, HMGU, Munich). Array data was processed and annotated with the miRNA OC tool (Affymetrix, version 1.0.33.0) using settings recommended by Genisphere. Briefly, background was detected and removed by RMA global background correction, followed by quantile normalization and summarization using median

polishing. Statistical analysis of the resulting dataset was performed by utilizing the statistical programming environment R (R Development Core Team 2011 R: A Language and Environment for Statistical Computing. Vienna, Austria: The R Foundation for Statistical Computing) implemented in CARMAweb [197]. Genewise testing for differential expression was done employing the limma t-test and Benjamini-Hochberg multiple testing correction. All gene sets were filtered for true detection in at least half of the samples in at least one group per comparison. For technical replicates, the average was used foe calculations. Functional annotations were generated using QIAGEN's Ingenuity Pathway Analysis (IPA®, QIAGEN Redwood City, www.qiagen.com/ingenuity) using Fisher's Exact Test p-values. Input were regulated eight miRNAs from somatropinomas (FC>1.5x, p<0,002; miR-383 was excluded). Heat maps were generated in R. The array data are openly available in GEO (GSE140604).

3. Results

3.1 Literature review of pathogenic and likely pathogenic AIP mutations in PA patients

Ever since Vierimaa *et al.* were able to identify germline mutations in *AIP* in a Finish cohort with young age at onset, low penetrance PAs, it has been hypothesized that AIP mutations lead to tumor development by loss of tumor-suppressive function of wild-type AIP [81]. Accordingly, many mutations in AIP are truncating mutations, including nonsense and frameshift mutations that lead to a premature stop, as well as missense mutations that lead to a decreased stability of the protein [198]. More than 100 AIP mutations have been described since the initial discovery of AIP as a tumor suppressor in PAs. In order to get a comprehensive view of the AIP mutations that have been described so far, the literature was reviewed and results were recorded in Table 20.

Table 20: AIP pathogenic and likely pathogenic mutations in PA patients.

mutation	predicted AA change	Type of mutation	tumor type (secreted hormone)	number of patients	reference
c.40C>T	p.Gln14X	nonsense	GH, GH/PRL, PRL	13, 2, 2, 3, 3	[15, 81, 82, 125, 199]
c.910C>T‡	p.Arg304X	nonsense	GH, PRL, GH/PRL, NFPA	2, 3, 1, 10, 8, 1, 2, 5, 2, 1, 1, ?, 7, 2, 16, 13, 1	[14, 16-18, 20, 81, 82, 92, 123, 128, 132, 133, 200-204]
IVS3-1G>C		splice site	GH/PRL	1	[14]
c.424C>T	p.Gln142X	nonsense	GH, PRL	4	[14]
c.649C>T	p.Gln217X	nonsense	GH	2, 3	[14, 21]
c.715C>T	p.Gln239X	nonsense	GH	2	[14]
c.811C>T	p.Arg271Trp	missense	GH, PRL	4, 1, 1, 1, 3	[14, 82, 92, 133, 134]
c.721A>G	p.Lys241Glu	missense	PRL, NFPA, GH	2, 2, 1, 1	[14, 17, 205]
c.138_161del24	p.Gly47_Arg54del	in-frame deletion	GH	2	[14]
c.517_521delGAAGA	p.Glu174fsX21	frameshift	GH, PRL	3, 3	[14, 17, 206]
c.854_857delAGGC	p. Gln285fsX17	frameshift	GH	2, 3	[14, 17]

mutation	predicted AA change	Type of mutation	tumor type (secreted hormone)	number of patients	reference
c.804A>C	p.Tyr268X	nonsense	GH, NFPA	4, 1, 3	[22, 82, 207]
c.286_187delGT	p.Val96ProfsX32	frameshift	GH	3	[87]
c.145G>A	p.Val49Met	missense	GH	1	[87]
c.911G>A	p.Arg304Gln	missense	ACTH, GH, NFPA, PRL	1, 2, 2, 2, 1, 1, 2, 2, 1, 1, ?, 1, 1	[15, 16, 18, 20, 22, 23, 82, 91, 92, 94, 95, 128, 129]
IVS2-1G>C		splice site	GH	1	[15]
c.824_825insA	p.His275Gln.fsX12	frameshift	GH	1	[15]
c.66_71delAGGAGA	p.Gly23_Glu24del	in-frame deletion	GH	1	[15]
c.878_879AG>GT*	p.Glu293Gly	missense	GH	1	[15]
c.880_891delCTGGACCCAGCC*	p.Leu194_Ala297	large deletion	GH	1	[15]
c.542delT	p.Ile182Ser.fs12X	frameshift	GH	1	[15]
c.404delA	p.His135Leu.fs21X	frameshift	GH	1, 1	[123], [18]
c.601A>T	p.Lys201X	nonsense	GH	2	[123]
c.64C>T	p.Arg22X	nonsense	GH	1, 1	[86, 92]
c.807C>T	p.Phe269Phe	splice site	GH, NFPA, PRL	2, 1, 1, 1, 1, 4	[16, 82, 89, 92, 94, 133, 208]
c.70G>T	p.Glu24X	nonsense	GH, GH/PRL	7, 5, 2	[16, 82, 209]
c.241C>T	p.Arg81X	nonsense	GH/PRL, GH	2, 1, 2, 12, 1	[16, 82, 96, 210, 211]
c.713G>A	p.Cys238Tyr	missense	GH	3, 4	[16, 82]
c.-270-269CG>AA†		promoter mutation	GH, GH/PRL	2	[16]
c.-220G>A†		promoter mutation	GH, GH/PRL	2	[16]
c.794_823dup		In-frame insertion	GH	3	[16]

mutation	predicted AA change	Type of mutation	tumor type (secreted hormone)	number of patients	reference
c.100-1025_279+357del	p.Ala34_Lys93del (Ex2del)	large deletion	NFPA	1	[212]
c.1104-1109_279+578	Ex1_2del	large deletion	GH, NFPA, GH/PRL	4, 2	[18, 212]
la176c.742_744delTAC	p.Tyr248del	in-frame deletion	GH	1	[89]
c.500delC	p.Pro167His.fsX3	frameshift	GH	4	[213]
c.871G>A	p.Val291Met	missense	GH/PRL	1	[91]
IVS3+1G>A		splice site	GH	1, 1	[91, 128]
c.584T>C	p.Val195Ala	missense	PRL	1, 1, 1	[17, 92, 214]
c.829G>C	p.Ala277Pro	missense	GH	1, 1	[17, 92]
c.468+16G>T		intronic	GH	1	[17]
+15C>T		intronic	GH/PRL	1	[17]
	p.Gln82fsX7	frameshift	GH	1	[17]
	p.Arg128His	missense	GH	1	[17]
c.279+23C>T		intronic	PRL/GH	1	[17]
c.646G>T	p.Glu216X	nonsense	NFPA, GH/PRL	2, 1	[95, 215]
c.490C>T	p.Gln164X	nonsense	GH	2, 3, 1	[18, 82, 129]
c.662dupC	p.Glu222X	nonsense	GH	2, 3	[18, 82]
c.249G>T	p.Gly83Ala.fsX15	frameshift	PRL, GH	3, 4	[18, 82]
c.74_81delins7	p.Leu25Pro.fsX130	frameshift	GH, PRL, GH/PRL	5, 10	[18, 82]
c.308A>G	p.Lys103Arg	missense	ACTH	1	[205]
c.919dupC	p.Gln307Pro.fsX104insC	frameshift	NFPA	1	[205]
	p.Pro114fsX	frameshift	GH	1	[205]

mutation	predicted AA change	Type of mutation	tumor type (secreted hormone)	number of patients	reference
c.244_248delGAAGG	p.Glu82fsX7	frameshift	GH	1	[92]
c.250G>A	p.Glu84Lys	missense	GH	1	[92]
c.350delG	p.Gly117Ala.fsX39	frameshift	GH, PRL	1, 1	[20, 92]
c.550C>T	p.Gln184X	nonsense	GH	1	[92]
c.591G>A	p.Glu197Glu	synonymous	GH	1, 1	[92, 95]
c.783C>G	p.Tyr261X	nonsense	GH	1, 2, 4	[20, 82, 92, 96]
c.166C>A	p.Arg56Cys	missense	PRL	1	[92]
c.174G>C	p.Lys58Asn	missense	PRL, LH/FSH	2, 1	[20, 92]
c.803A>G	p.Tyr268Cys	missense	PRL	1	[92]
c.88_89delGA	p.Asp30Trp.fsX14	frameshift	NFPA	1	[92]
c.2C>T	p.Met1?	initiator codon	GH/PRL	1	[95, 216]
c.805-825dup	p.Phe269_His275dup	in-frame duplication	GH/PRL, GH, NFPA	2, 1, 2, 16	[16, 20, 82, 217]
c.469-2A>G	p.Glu158_Gln184del	Splice site	PRL, GH/PRL, GH	2, 1, 1	[20, 82, 123, 208]
c.974G>A[304]	p.Arg325Gln	missense	PRL, GH, NFPA	1, 1, 2	[20, 200, 218]
c.872T>A	p.Val291Glu	missense	GH/PRL	1	[20]
c.563G>A	p.Arg188Gln	missense	PRL	1	[20]
c.752delT	p.Leu251Arg.fsX52	frameshift	ACTH	1	[20]
c.509T>C	p.Met170Thr	missense	GH	1	[20]
c.825_845delCGCGGCCGTGTGGAATGCCCA[o]	p.His275Gln.fsX49	frameshift	GH	1	[219]
c.4delG	p.Ala2Arg.fsX16	frameshift	GH	1	[220]
c.355C>T	p.ARG119Trp	missense	GH	1	[21]

mutation	predicted AA change	Type of mutation	tumor type (secreted hormone)	number of patients	reference
c.90T>G	p.Asp30Glu	missense	GH	1	[21]
c.955G>A	p.Glu319Lys	missense	GH	1	[21]
c.976G>A	p.Gly326Arg	missense	GH	1	[21]
c.784G>A	p.Asp262Asn	missense	GH	1	[21]
c.967G>A	p.Arg323Trp	missense	NFPA	1	[21]
c.645+41dupG		duplication	NFPA	1	[21]
c.685C>T	p.Gln229X	nonsense	GH	1	[221]
c.38T>A	p.Ile13Asn	missense	GH	1	[222]
c.943C>T	p.Gln315X	nonsense	GH	3	[223]
c.844C>T		nonsense	GH	1	[129]
c.3G>A		promoter	GH	3, 2	[82, 204]
c.427C>T	p.Gln143X	nonsense	GH	1	[82]
c.570C>G	p.Tyr190X	nonsense	GH	9	[82]
c.816delC	p.Lys273Arg.fsX30	frameshift	GH	1, 1	[22, 82]
c.868A>T	p.Lys290X	nonsense	GH	1, 1	[82, 202]
c.872_877delTGCTGG	p.Val291_Leu292del	in-frame deletion	GH	1, 1	[82, 202]
c.967delC	p.Arg323Gly.fsX39	frameshift	GH	4	[82]
c.976_977insC	p.Gly326Ala.fsX?	frameshift	GH	1, 1	[82, 202]
c.978dupG	p.Ile327Asp.fsX?	frameshift	GH	1	[82]
c.815G>A	p.Gly272Asp	missense	GH	1, 1	[204, 224]
c.733>735delGAG	p.Glu246del	deletion	GH/PRL, GH	1, 2	[125, 199]

mutation	predicted AA change	Type of mutation	tumor type (secreted hormone)	number of patients	reference
c.455T>G	p.Met152Arg	missense	GH	1	[225]
c.715_72delinsTCAACTAC		indel	GH	1	[225]
c.707_716delinsGGC		indel	GH	1	[225]
c.100-18C>T		intronic	PRL, GH	1, 3, 1	[94, 95, 204]
c.772C>T	p.Leu258Phe	missense	PRL	1	[95]
c.836G>A	p.Trp279X	nonsense	GH	2	[226]
c.70>89delGAGCTCCCGGACTTTCAAGA		deletion	GH	1	[199]
c.316C>T	p.Arg106Cys	missense	PRL	1	[133]
c.468G>A	p.Lys156Lys	synonymous	NFPA	1	[133]
c.969G>T	p.Arg323Arg	synonymous	GH	1	[200]
c.991T>C	p.X331Arg	stop loss	GH	1	[227]
c.512C>T	p.Thr171Ile	missense		3	[228]

*†‡ mutations were found in the same patient
º found in a MEN-1 context

3.2 Collection of pituitary adenoma samples and analysis of clinical parameters of the patients

We aimed to study the miRNA expression pattern of AIP mutation positive (*AIP*mut+) versus AIP mutation negative (*AIP*mut-) PAs in order to illuminate the molecular basis that underlies AIP-dependent tumorigenesis.

As a starting point a total of 42 primary PAs were collected in collaboration with Dr. Adrian Daly (Department of Endocrinology, University of Liége, Belgium), who also provided us with the clinical parameters of the patients listed in Table 11. The sample set comprised 10 prolactinomas and 32 somatotropinomas. Seven prolactinomas were *AIP*mut- and 3 carried a mutation in AIP (*AIP*mut+), whereas 20 somatotropinomas were *AIP*mut- and 12 were *AIP*mut+. Apart from the AIP mutation

status, no other mutations of genes often involved in PAs were tested. 20 of these samples were subjected to miRNA expression array analysis.

The patient cohort comprises 42 pituitary adenoma patients of which 20 (47.6 %) are female and 22 (52.4 %) are male. The median age at diagnosis is 30 years (10 – 63 years). 30 patients (71.4 %) had macroadenomas (largest diameter > 10 mm) and four (9.5 %) had giant ademonas (largest diameter >40 mm). Eight patients (19,0 %) carried microadenomas. In half of the patients (50,0 %) invasion of the tumor was observed (Table 21).

Table 21: Summary of the clinical characteristics of the PA patients that participated in the study.

		number of patients (n=42)		*AIP*mut- (n=27)		*AIP*mut+ (n=15)	
		number	%	number	%	number	%
sex	Female	20	48	17	63	3	20
	male	22	52	10	37	12	80
age at diagnosis	< 30 yrs	20	48	6	22	14	93
	≥ 30 yrs	22	52	21	78	1	7
tumor size	micro	8	19	8	30	0	0
	macro	30	71	17	63	13	87
	giant	4	10	2	7	2	13
invasion	no	21	50	17	63	4	27
	yes	21	50	10	37	11	73

The patients were diagnosed at a significantly younger age in the *AIP*mut+ group (median age at diagnosis 20 years, 10 – 30 years) compared to the *AIP*mut- group (median age at diagnosis 39 years, 19 – 63 years) (Figure 8a). When patients are stratified into two groups, below the age of 30 (< 30 yrs) and at the age of 30 and older (≥ 30 yrs), the distribution in almost even in all patients diagnosed. In *AIP*mut- patients 78 % are 30 years and older, while only 22 % are diagnosed at an age younger than 30 years. Strikingly 93 % of *AIP*mut+ patients have an age at diagnosis below 30, while 7 % were 30 years or older at diagnosis (Table 21). This is in line with previously published studies. Tumor size of *AIP*mut+ patients was higher than in the *AIP*mut- group (Figure 8b,Table 21). This has also been described before for patients carrying *AIP* mutations. Each group included two patients with giant adenomas (diameter > 40 mm) and all microadenomas (diameter < 10 mm) were in the *AIP*mut- patient group (Table 21). Invasive behavior was observed in 73.3 % of *AIP*mut+ PAs, while only 37.0 % of *AIP*mut- PAs were invasive (Table 21). The early age at onset, increased tumor size and enhanced frequency of invasiveness points to an overall higher aggressiveness in *AIP*mut+ PAs. The majority of *AIP*mut+ patients are male. This male predominance can also be observed in our patient cohort since 80.0 % of *AIP*mut+ patients are male. In the *AIP*mut- group only 38.0 % males can be found. All statements about clinical

parameters are in agreement with previously published data from clinical studies [14, 16, 18-20, 81, 95, 96, 123].

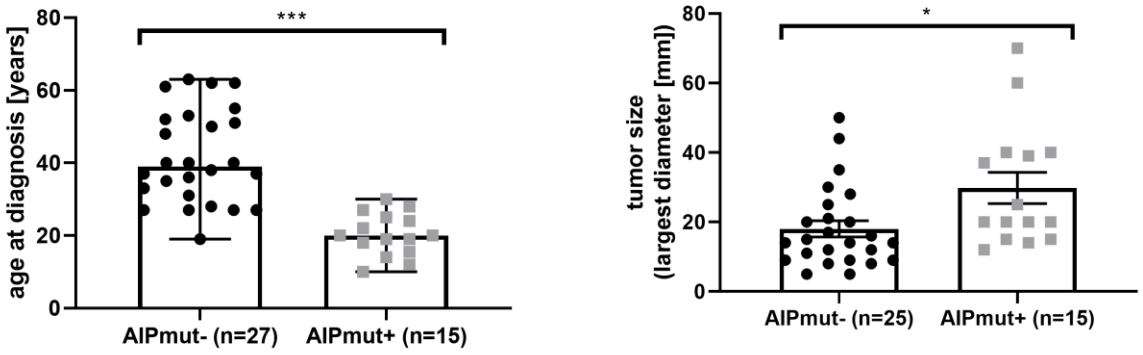

Figure 8: Clinical parameters of the patient cohort. (a) age at diagnosis [years]. ***, p<0.001; (by Welch's t-test; normality test (Shapiro-Wilk) passed; variances significantly different (F test)) (b) largest tumor diameter [mm]. *, p>0,05; ***, p<0.001; (by Mann-Whitney test; normality test (Shapiro-Wilk) failed).

For all patient samples the genotype was assessed. Besides 27 *AIP*mut- cases, 15 patient samples were found to carry AIP mutations. The most prevalent mutation in the sample set was the R271W mutation (n=7). Apart from this mutation, R56C (n=1), F269F (n=1), Q146S (n=2), L115W (n=1), R128H (n=1), M1I (n=1), C238W (n=1). In addition, when available, the sex of the patients, tumor size, invasion status, age at diagnosis, type and dosage of treatment and the timing of the treatment is reported in Table 11.

3.3 MiRNA expression in human pituitary adenomas

3.3.1 miRNA expression analysis in *AIP*mut+ *versus AIP*mut- PAs

Since PAs with AIP mutations are rare, the sampels were collected throughout the course of the study. The miRNA array analysis was performed after collection of 20 PAs, the remaining 22 sampes were obtained after the miRNA array was competed. Therefore, for miRNA profiling of *AIP*mut+ versus *AIP*mut- PAs, a total of 20 primary PAs were used. With the miRNA array we hope to identify miRNAs, which may be involved in the specific clinical phenotype that can be found in *AIP*mut+ PAs. We employed GeneChip miRNA 1.0 Arrays from Affymetrix which are designed to interrogate 848 human miRNAs, small RNAs and non-coding RNAs.

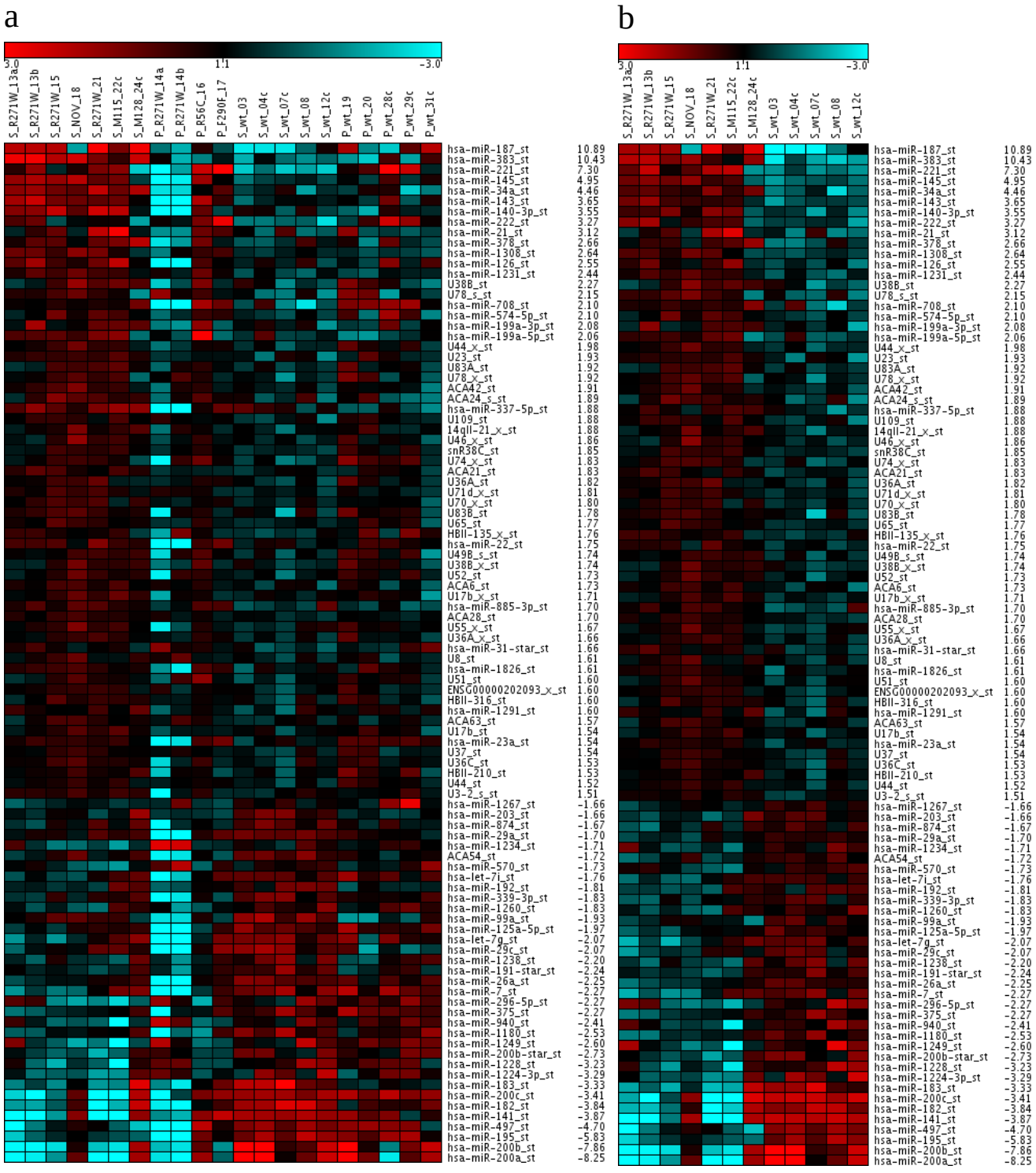

Figure 9: Unsupervised hierarchical clustering of miRNA expression profiles of *AIP*mut- pituitary adenomas versus PAs with AIP mutations. Heat Map of 98 human small RNAs differentially regulated with p<0.05, FC>1.5x, background-filtered. Red (blue) indicates higher (lower) lower expression level with respect to the median across all samples. The log2 scale is provided.

Table 22: Differentially expressed miRNAs in *AIP*mut+ *versus AIP*mut- PAs. Differentially expressed miRNAs are shown as fold changes ($p < 0.05$, FC > 1.5x; limma t-test)

miRNA	Fold change	miRNA	Fold change	miRNA	Fold change	miRNA	Fold change	miRNA	Fold change
miR-187	10.89	U83A	1.92	ACA6	1.73	miR-1267	-1.66	miR-940	-2.41
miR-383	10.43	U78_x	1.92	U17b_x	1.71	miR-203	-1.66	miR-1180	-2.53
miR-221	7.30	ACA42	1.91	miR-885-3p	1.70	miR-874	-1.67	miR-1249	-2.60
miR-145	4.95	ACA24_s	1.89	ACA28	1.70	miR-29a	-1.70	miR-200b*	-2.73
miR-34a	4.46	miR-337-5p	1.88	U55_x	1.67	miR-1234	-1.71	miR-1228	-3.23
miR-143	3.65	U109	1.88	U36A_x	1.66	ACA54	-1.72	miR-1244-3p	-3.29
miR-140-3p	3.55	14qII-21_x	1.88	miR-31*	1.66	miR-570	-1.73	miR-183	-3.33
miR-222	3.27	U46_x	1.86	U8	1.61	let-7i	-1.76	miR-200c	-3.41
miR-21	3.12	snR39C	1.85	miR-1826	1.61	miR-192	-1.81	miR-182	-3.84
miR-378	2.66	U74_x	1.83	U51	1.60	miR-339-3p	-1.83	miR-141	-3.87
miR-1308	2.64	ACA21	1.83	ENSG00000202093_x	1.60	miR-1260	-1.83	miR-497	-4.70
miR-126	2.55	U36A	1.82	HBII-316	1.60	miR-99a	-1.93	miR-195	-5.83
miR-1231	2.44	U71d_X	1.81	miR-1291	1.60	miR-125a-5p	-1.97	miR-200b	-7.86
U38B	2.27	U70_x	1.80	ACA63	1.57	let-7g	-2.07	miR-200a	-8.25
U78_s	2.15	U83B	1.78	U17b	1.54	miR-29c	-2.07		
miR-708	2.10	U65	1.77	miT-23a	1.54	miR-1238	-2.20		
miR-574-5p	2.10	HBII-135_X	1.76	U37	1.54	miR-191*	-2.24		
miR-199a-3p	2.08	miR-22	1.75	U36C	1.53	miR-26a	-2.25		
miR-199a-5p	2.06	U49B_s	1.74	HBII-210	1.53	miR-7	-2.27		
U44_x	1.98	U38B_x	1.74	U44	1.52	miR-296-5p	-2.27		
U23	1.93	U52	1.73	U3-2_s	1.51	miR-375	-2.27		

The analysis of the hierarchical clustering *AIP*mut- and *AIP*mut+ patient samples showed that no clear clustering is prevalent when all PA samples are analyzed (Figure 9a). Especially the P_R271W_14a and P_R271W_14b samples, two prolactinomas from the same patient, do not cluster with the rest of the *AIP*mut+ PAs. Instead they seem to display a global miRNA downregulation, which might be due to poor RNA quality. Therefore, these samples had to be excluded for the subsequent analysis. No further analysis was done for prolactinomas since the remaining sample number was too low to be statistically relevant. In contrast, concerning exclusively somatotropinoma samples, a clustering into the AIP mutation statuses (*AIP*mut- and

*AIP*mut+) is obvious (Figure 9b). 89 miRNAs, small RNAs and non-coding RNAs were detected to be differentially expressed between *AIP*mut+ and *AIP*mut- somatotropinomas with a fold change (FC) > 1.5x and p < 0.05 and are listed in Table 22.

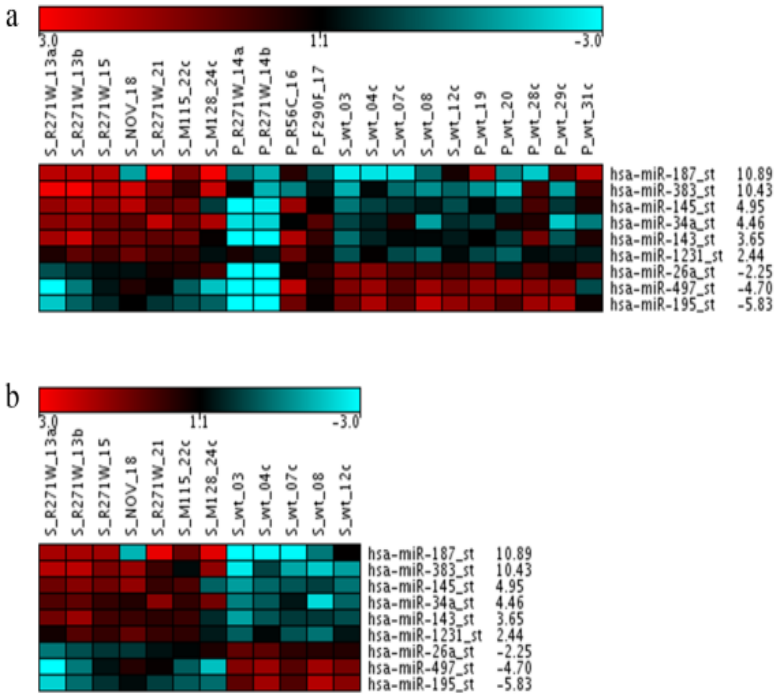

Figure 10: miRNA expression profiles of *AIP*mut- and *AIP*mut+ PAs. (a-b) Adenoma samples were ordered by hierarchical clustering. Heat map of 9 human small RNAs regulated with FDR<10%, FC>1.5x, background-filtered. Red (blue) indicates higher (lower) lower expression level with respect to the median across all samples. The log2 scale is provided. (a) Heat map shows the expression of selected miRNAs in both somatotropinomas (n=12) and prolactinomas (n=9). (b) Heat map shows the expression of selected miRNAs only in the somatotropinomas.

In addition, a false discovery rate (FDR) < 10 % was applied, which narrowed the set of miRNAs to 9 miRNAs that were differentially expressed in *AIP*mut+ samples compared to *AIP*mut- PAs (Table 23). Among them, six miRNAs (miR-187, -383, -145, -34a, -143, -1231) were significantly up-regulated whereas three miRNAs (miR-195, -197, -26a) were down-regulated in *AIP*mut+ versus *AIP*mut- (Figure 10).

The miRNA expression array was performed by Dr. Nikolai Falk (PATH, HMGU Munich) and statistical analysis was done by Dr. Martin Irmler (IEG, HMGU, Munich).

Table 23: Differentially expressed miRNAs in *AIP*mut+ *versus AIP*mut- PAs ranked based on fold change ($p < 0.05$ (), FC > 1.5x, FDR < 10 %: limma t-test)

miRNA	Fold change	miRNA	Fold change
miR-187	10.89	miR-26a	-2.25
miR-383	10.43	miR-497	-4.70
miR-145	4.95	miR-195	-5.83
miR-34a	4.46		
miR-143	3.65		
miR-1231	2.44		

3.3.2 Validation of differential miRNA expression in somatotropinomas

To validate the results of the miRNA arrays, we investigated the expression of the miRNAs with the highest differential expression (i.e. miR-187, miR-383, miR-145, miR-34a, miR-195) by quantitative (q)RT-PCR. The results show a significant up-regulation of miR-187, miR-145 and miR-34a, as well as a down-regulation of miR-195 in *AIP*mut+ versus *AIP*mut- somatotropinomas (Figure 11a, c, d, e). For miR-383 the increased expression observed by array analysis could not be validated by qRT-PCR (Figure 11b). Therefore, this miRNA was excluded from further studies.

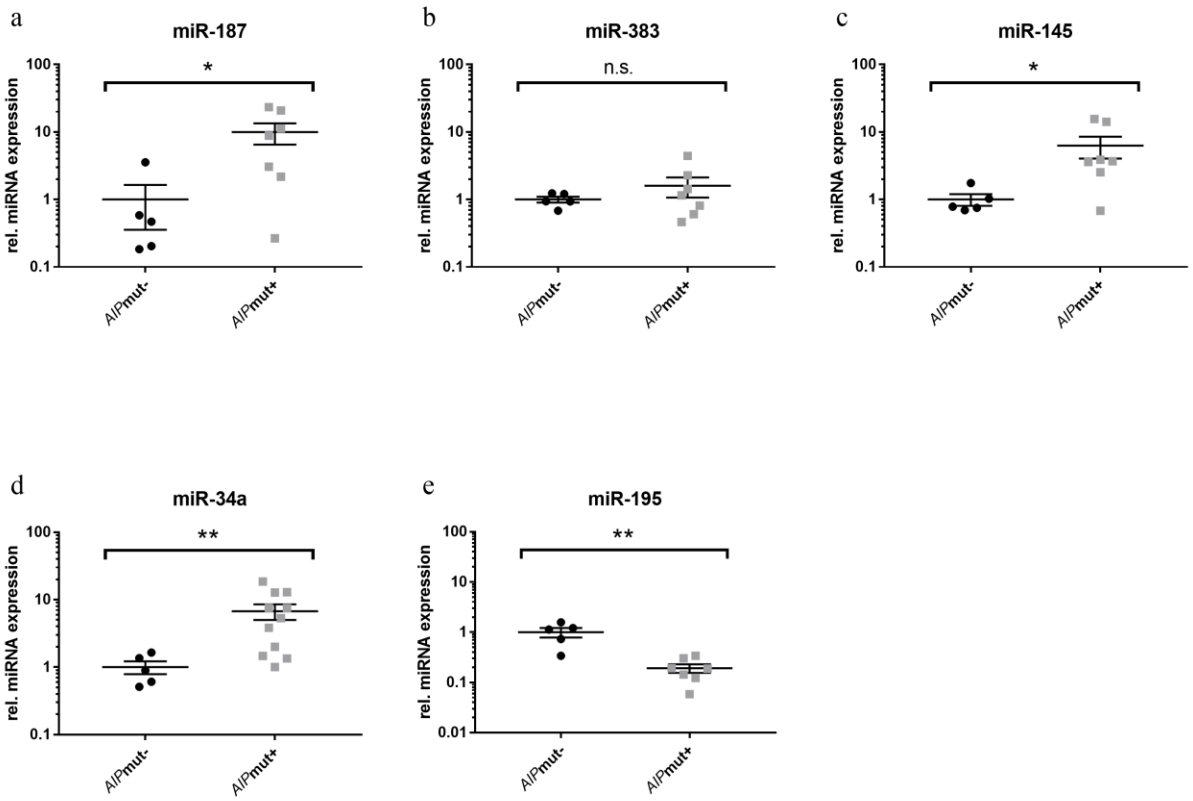

Figure 11: miRNA expression profiles of *AIP*mut- and *AIP*mut+ PAs by (q)RT-PCR. Validation of selected miRNAs in human somatotropinomas by qRT-PCR. The line represents the mean value and results are reported as the mean ±SEM. Each dot represents an *AIP*mut- PA, each filled square represents an *AIP*mut+ PA. *, p<0.05; **, p<0.01; n.s., not significant (by Mann-Whitney test; normality test (Shapiro-Wilk) failed).

3.4 miRNA expression depends on AIP mutation status

As already mentioned above the AIP-R271W mutation is the most frequent mutation in our sample series (n=7, Table 11), so it was assumed that this mutation has the biggest impact on the miRNA signature of the samples containing AIP mutations. Therefore, for further *in vitro* analysis AIP-R271W was used as a representative mutant AIP protein.

3.3.1 Mutant AIP increases cell proliferation of *AIP* -/- MEFs

The pCMV-Myc (Figure 6) vector was used as the backbone for cloning the human wild-type AIP cDNA. In a next step the wild-type sequence was mutated in order to achieve the construct for AIP-R271W. Cloning and mutagenesis of the plasmids was done by Dr. Sara Molatore (PATH, HMGU Munich).

As no cell line without endogenous AIP expression is available, mouse embryonic fibroblasts (MEFs) derived from *Aip*-/- mice were used as recipient cells in order to avoid interference from

endogenous wild-type AIP (*Aip*-/- MEFS were kindly provided by Auli Kahru, (Department of Medical and Clinical Genetics, University of Helsinki, Finland)). *Aip*-deficient (*Aip*-/-) MEFs were transfected with plasmids containing either AIP wild-type (wt) or AIP-R271W and cell proliferation was measured using the WST-1 assay 24h, 48h and 72h after transfection. Twenty-four hours after transfection cell proliferation was significantly increased in cells transfected with AIP-R271W compared to those transfected with AIP-wt. This effect was no longer present 48h or 72h after transfection (Figure 12). A possible accelerated degradation of AIP-R271W might explain, why the effect of mutant AIP on cell proliferation is lost already 48h after transfection.

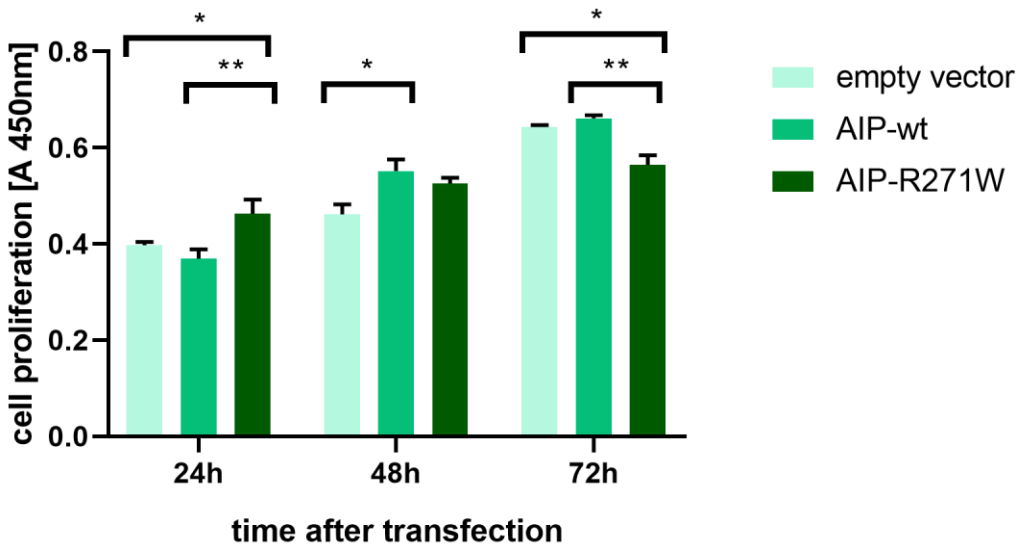

Figure 12: Effect of mutant AIP on cell proliferation. *Aip*-/- MEFs were transfected with empty vector, AIP-wt or AIP-R271W constructs. Cell proliferation was assessed 24h, 48h and 72h after transfection. The experiment was independently performed 3 times each with 6 technical replicates and values are reported as the mean±SEM. Only the statistically significant differences are indicated. *, p<0.05; **p<0,01; (by two-way ANOVA and Tukey's multiple comparisons test).

3.3.2 Mutant AIP is highly unstable *in vitro*

The effect of ectopic expression of the AIP-R271W variant on cell proliferation was determined. As expected, no signal from AIP protein was detected in cells transfected with the empty vector, since these cells do not express AIP endogenously. Unfortunately, AIP-R271W could not be detected 24h after transfection, while AIP-wt was detectable in the cells (Figure 13a). Thus, the transfection protocol was optimized in terms of the amount of transfected plasmid DNA. Transfection of a 4x higher amount of mutant AIP plasmid finally resulted in protein levels comparable to those of the AIP-wt protein (Figure 13b).

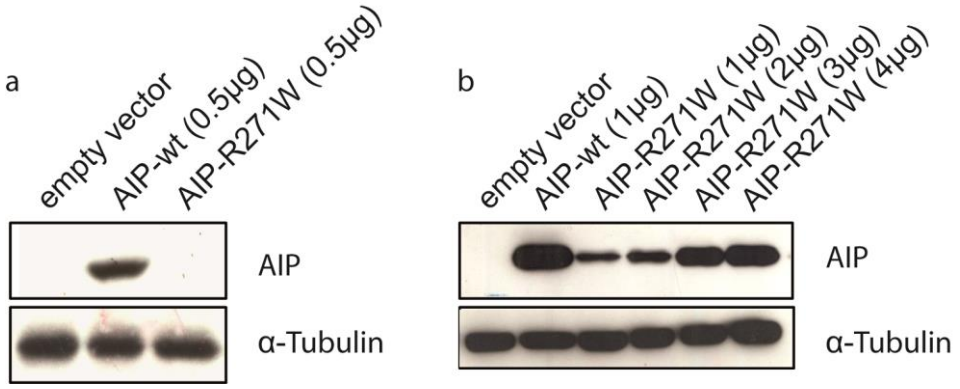

Figure 13: Protein levels of AIP in MEFs 24h after transfection. MEFs were transfected with empty vector, AIP-wt or AIP-R271W constructs and harvested 24h after transfection. Western blot was performed using an anti-AIP antibody. α-Tubulin was used as loading control. (a) same amount of plasmid DNA (0.5 µg) was transfected into MEFs. (b) Four times more mutant AIP construct (4 µg) was transfected compared to AIP-wt containing vector (1 µg).

To confirm that the different levels of wt or mutant AIP proteins in *Aip*-/- MEFs was indeed due to enhanced instability, transfected cells were treated with cycloheximide (CHX), in order to inhibit *de novo* protein synthesis. With the treatment, the approximate half-life of the wt and mutant AIP proteins was estimated. CHX has been shown to work effectively already after 45 min at a concentration of 50 µg/mL [229]. Therefore, for a lower concentration of 25 µg/mL the 4 h time point was used, in which it was expected to already see an effect in case of a reduced protein stability. AIP-wt showed no decrease in expression over the course of the experiment (0h–20h), indicating a protein half-life that exceeds this time frame. In contrast, the level of AIP-R271W was decreased already after 4h and were virtually undetectable 20h after transfection, indicating that this variant is indeed less stable than AIP-wt (Figure 14).

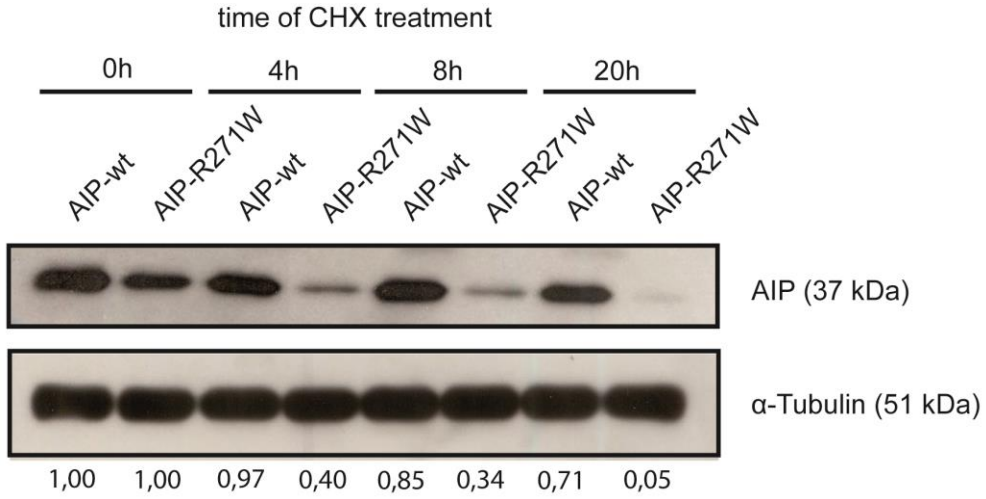

Figure 14: Protein stability of mutant and wild-type AIP *in vitro*. *Aip*-/- MEFs were transfected with AIP-wt or AIP-R271W constructs. Twenty-four h later they were treated with 25µg/mL Cycloheximide (CHX) for the indicated times and collected for protein extraction. Western blot was performed using an anti-AIP antibody. α-Tubulin was used as loading control.

We were further interested in the contribution of the proteasome to the accelerated degradation of AIP-R271W. Treatment of transfected MEFs with both CHX and the proteasome inhibitor epoxomicin (EPOX) established that the degradation of mutant AIP is mediated, at least in part, by the proteasome (Figure 15). Indeed, EPOX partially inhibited the degradation of AIP-R271W protein, albeit it did not restore the levels of the mutant protein to those of wt AIP (Figure 15). This is in agreement with previously reported in vitro data analyzing the half-life of several AIP variants, including AIP-R271W [198]. In this respect, the analyses of all subsequent experiments were conducted 24h after transfection and plasmid DNA amount was adjusted in order to reach equal protein levels of AIP-wt and AIP-R271W. Thus, ectopic AIP-R271W promotes the proliferation of Aip-/- MEFs although it is present at low levels, which indicates an induction of cell proliferation by the protein.

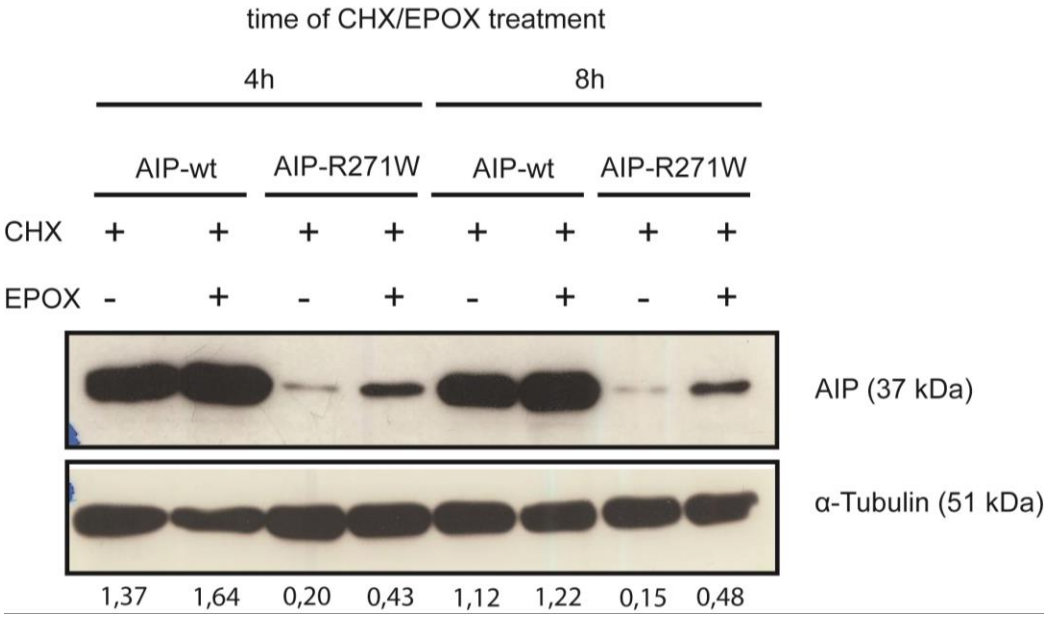

Figure 15: Protein stability of mutant and wild-type AIP in vitro. *Aip*-/- MEFs transfected as in Figure 15 were treated with 25µg/mL CHX alone or in combination with 10µM Epoxomicin (EPOX) for the indicated times. Western blot was performed using an anti-AIP antibody. α-Tubulin was used as loading control.

3.3.3. Mutant AIP affects the expression levels of miR-145 and miR-34a in MEF AIP -/- cells

Although it is not clear how an AIP mutation might affect miRNA expression, we wanted to compare miRNA levels to the AIP mutation status. To demonstrate a possible link between the presence of mutant AIP protein and miRNA expression, *Aip*-/- MEFs were transiently transfected with either AIP-wt or AIP-R271W plasmids and the levels of selected miRNAs were assessed by

qRT-PCR. Given the instability of the AIP-R271W protein, miRNA expression was determined 24h after transfection.

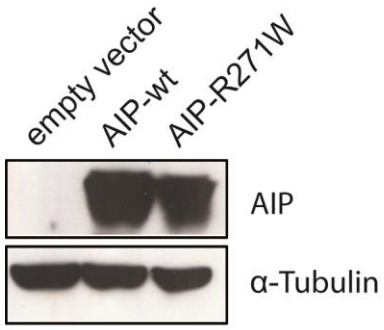

Figure 16: AIP protein levels after transfection of AIP plasmids in *AIP-/-* MEFs. *AIP-/-* MEFs were transfected with either the empty vector (4µg), AIP-wt (1µg+3µg empty vector) or AIP-R271W (4µg). Western blot was performed 24h after transfection using an anti-AIP antibody. α-Tubulin was used as loading control.

In order to assure comparable levels of AIP-wt and AIP-R271W Western Blot was performed using an anti-AIP antibody (Figure 16). Four times more mutant AIP (AIP-R271W) than AIP-wt was used for the transfection, as this was found to deliver similar protein levels in transfected cells (Figure 13).

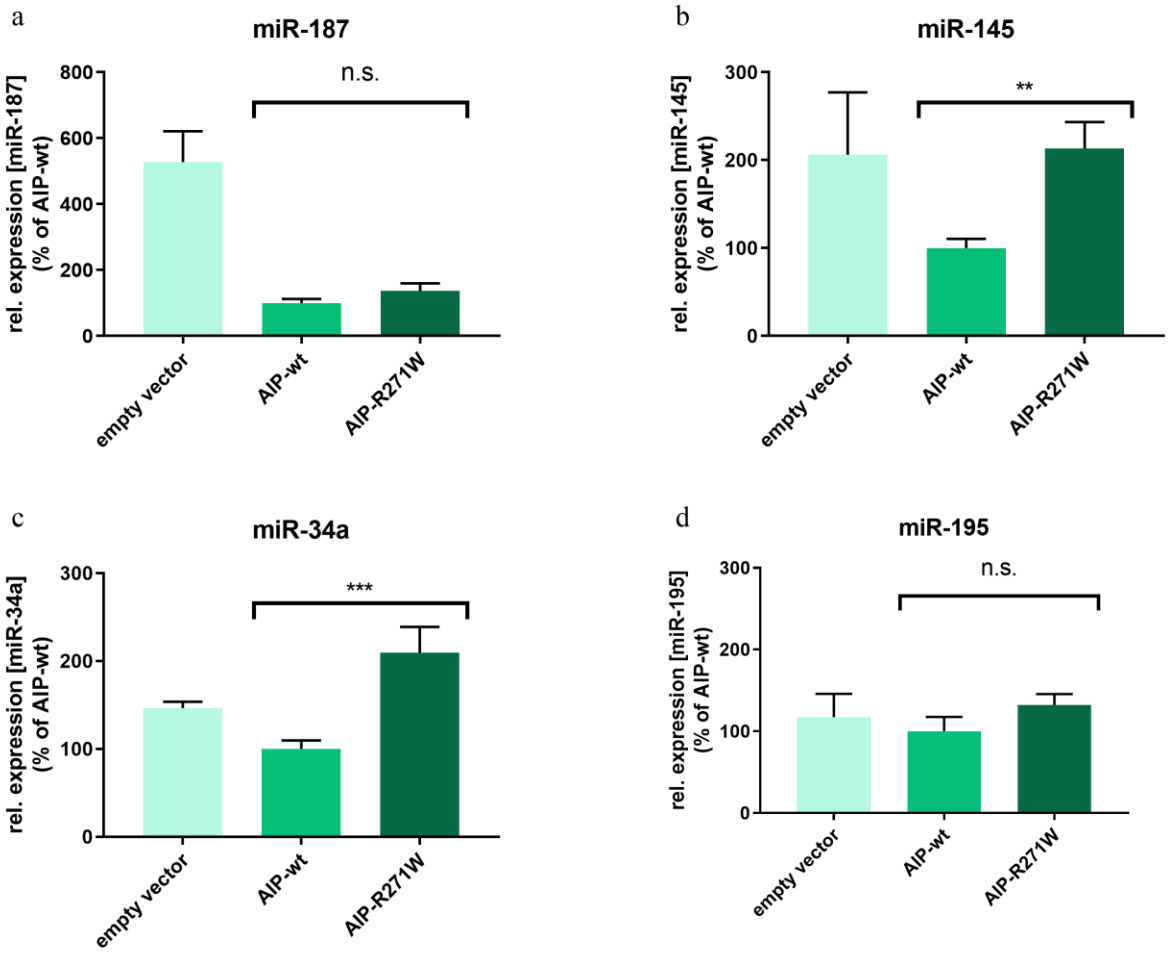

Figure 17: Effect of mutant AIP on miRNA expression. *Aip-/-* MEFs were transfected with empty vector, AIP-wt or AIP-R271W constructs. Expression levels of selected miRNAs were measured 24h post-transfection. (a) miR-187. The experiment was performed with 2 biological and 3 technical replicates and results are reported (±SEM); n.s., not significant (by unpaired t-test; normality test (Shapiro-Wilk) passed; variances not significantly different (F test)); (b) miR-145. The experiment was performed with 4 biological and 3 technical replicates and results are reported (±SEM); **p<0,01 (by Welch's t-test; normality test (Shapiro-Wilk) passed; variances significantly different (F test)); (c) miR-34a. The experiment was performed with 4 biological and 3 technical replicates and results are reported (±SEM); ***p<0,001 (by Mann-Whitney test; normality test (Shapiro-Wilk) failed); (d) miR-195. The experiment was performed with 3 biological and 3 technical replicates and results are reported (±SEM); n.s., not significant (by unpaired t-test; normality test (Shapiro-Wilk) passed; variances not significantly different (F test)).

In line with the results from the array analysis, miR-34a and miR-145 were significantly up-regulated upon transfection of AIP-R271W compared to AIP-wt (Figure 17b, c). In contrast, the level of expression of miR-195 and miR-187 was not changed in cells transfected with mutated AIP compared to wild-type AIP (Figure 17a, d). Altogether, the expression of both miR-34a and miR-145 was regulated by ectopic mutant AIP. These two miRNAs were chosen for further in vitro characterization.

3.3.4. Further characterization of mutant AIP in *Aip-/-* MEF cells

We could demonstrate that transfection of AIP-R271W in *Aip*-/- MEFs promotes proliferation and increases the expression of miR-145 and miR-34a. In addition, it was of interest if AIP mutation affects other features of the cells that would contribute to a tumorigenic phenotype, such as migration. Also to be considered is if the two candidate miRNAs, miR-145 and miR-34a, mediate the effect of mutant AIP on functional assays. Therefore, MEFs were either transfected with AIP-wt or AIP-R271W or co-transfected with the plasmids together with inhibitors of the selected miRNAs (Figure 18).

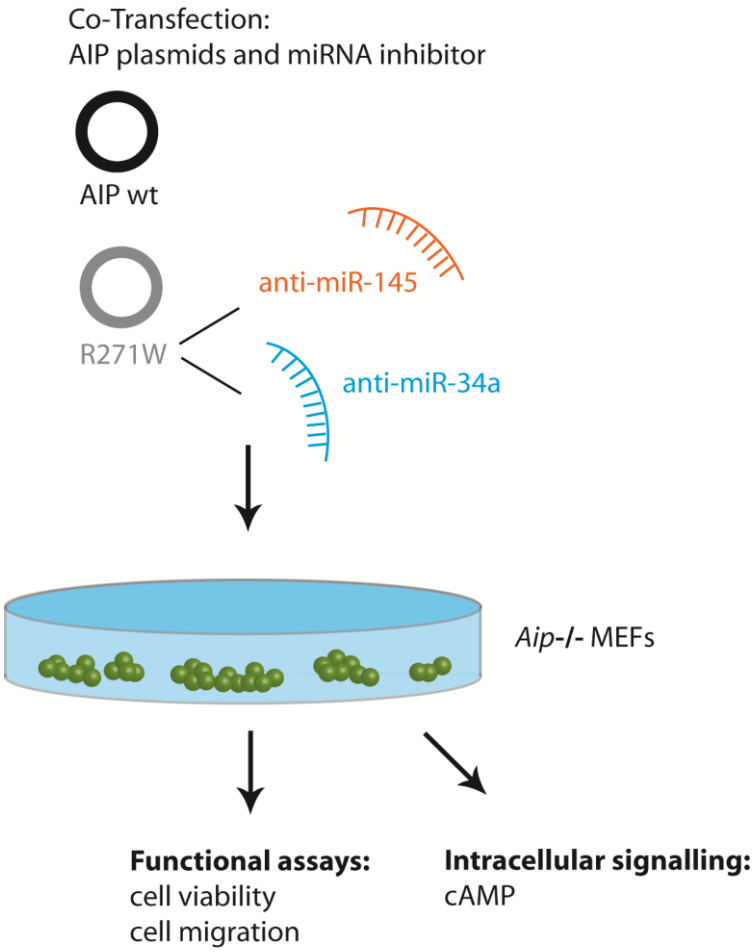

Figure 18: Outline of the workflow in *Aip-/-* MEFs: (Co-) Transfection of MEF *Aip* -/- with AIP plasmids and miRNA inhibitors
Figure: Eva-Maria Bogner

In addition to the proliferative behavior in response to transfection of mutant AIP, cell migration in transfected MEFs was assessed.

Comparable levels of wild-type and mutant AIP protein in transfected cells were verified by Western Blotting of samples of the transfected cells (Figure 19). The same amount of AIP plasmid DNA was used as described in the previous experiment.

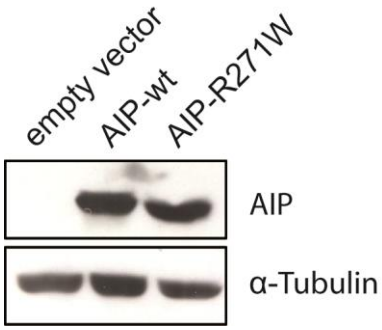

Figure 19: AIP protein levels after transfection of AIP plasmids in *AIP-/-* MEFs. *AIP-/-* MEFs were transfected with either the empty vector (4µg), AIP-wt (1µg+3µg empty vector) or AIP-R271W (4µg). Western blot was performed 24h after transfection using an anti-AIP antibody. α-Tubulin was used as loading control.

Transfection of mutant AIP-R271W caused a marked increase in the number of cells that migrated in a transwell assay (Boyden chamber assay) (Figure 20). The number of cells that migrated trough the membrane of the Boyden chamber was over two times higher in cells transfected with AIP-R271W than in AIP-wt transfected MEFs.

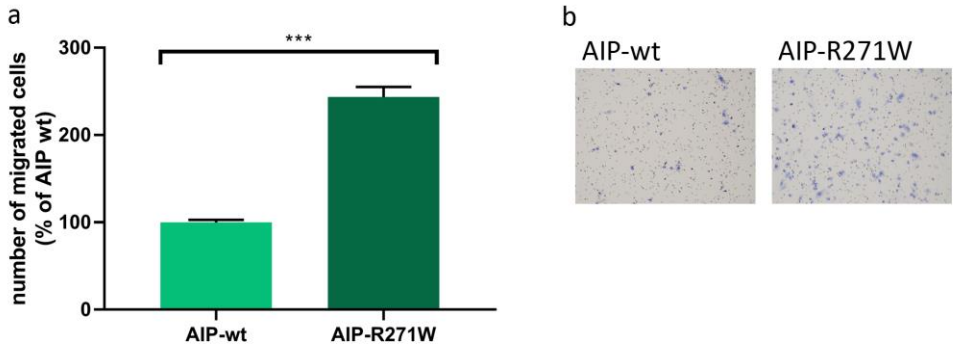

Figure 20: Effect of mutant AIP on oncogenic properties of MEF *Aip-/-*. MEFs were transfected with either with AIP-wt or AIP-R271W. The assay was performed 24h after transfection. (a) Results are reported as the mean ±SEM. Migration assays were conducted using the Boyden chamber and the migrated cells were counted. The experiment was independently performed twice each time with 2 technical replicates. ***, $p<0.001$; (by Welch's t-test; normality; variances significantly different (F test)).

A positive effect of mutant AIP on cell proliferation was observed before (Figure 12). However, co-transfection of AIP-R21W and either an unspecific control miRNA inhibitor, miR-34a-5p (miR-34a) or miR-145-5p (miR-145) inhibitors revealed no differences in cell proliferation (Figure 21), indicating that these two miRNAs do not mediate the effect of AIP-R271W in these cells.

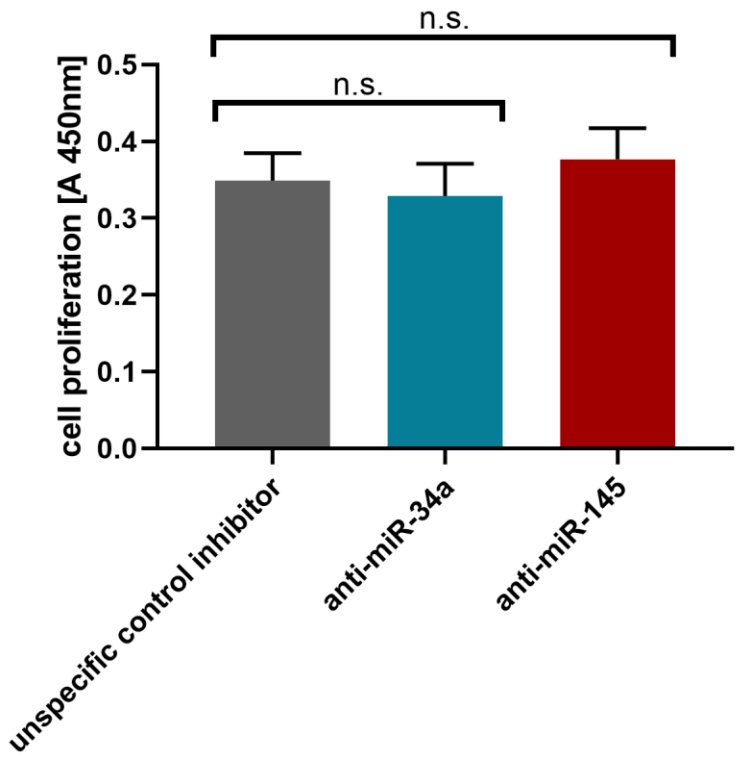

Figure 21: Co-transfection of miRNA inhibitors abrogate the positive effect of AIP-R271W on cell proliferation. MEFs were co-transfected with the AIP-R271W construct and either an unspecific control inhibitor, an inhibitor for miR-34a or an inhibitor for miR-145. Cell proliferation was assessed 24h after transfection using the WST-1 assay. The experiment was independently performed 2 times each with 6 technical replicates and values are reported as the mean±SEM; n.s., not significant (by one-way ANOVA and Sidak's multiple comparisons test).

Unlike the results of the proliferation assay, co-transfection of AIP-R271W with either an inhibitor for miR-34a or miR-145 lowered the number of migrated cells by 55% or 30%, respectively, compared an unspecific control inhibitor. This reduction leads to a migration phenotype *AIP*-/- MEFs co-transfected with AIP-R271W and one of the respective inhibitors, which is comparable to the transfection of AIP-wt alone (Figure 20b, Figure 22b).

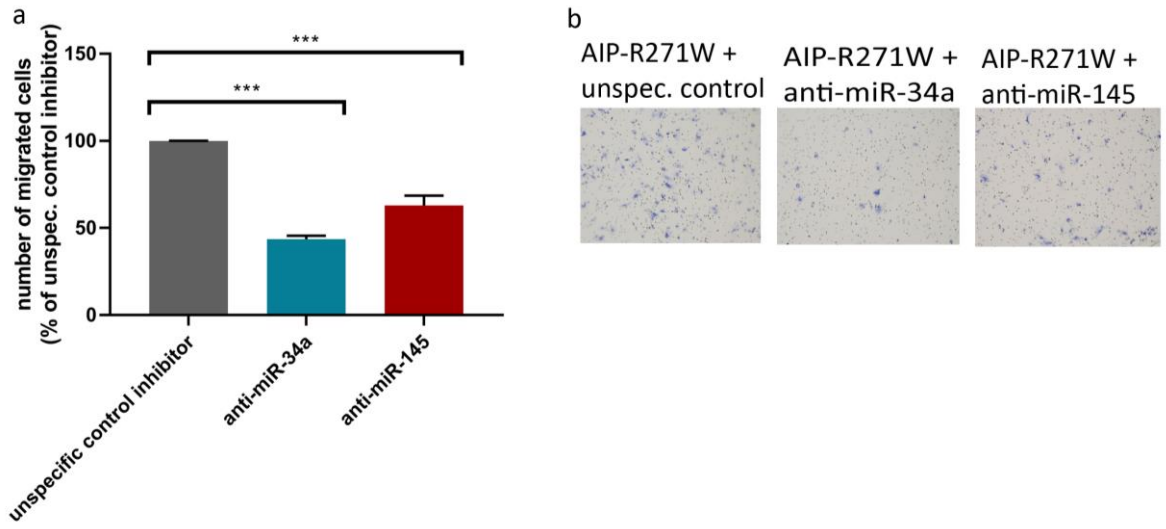

Figure 22: Co-transfection of miRNA inhibitors abrogate the positive effect of AIP-R271W on cell migration. MEFs were co-transfected with AIP-wt or AIP-R271W constructs and either an unspecific control inhibitor, an inhibitor for miR-34a or miR-145. The assay was performed 24h after transfection. Migration assays were conducted using the Boyden chamber and the migrated cells were counted. The experiment was independently performed twice each time with 2 technical replicates. Results are reported as the mean ±SEM. ***, $p<0.001$ (by one-way ANOVA and Dunnett's multiple comparisons test).

3.5 Tumorigenic behavior upon miRNA overexpression in GH3 cells

After assessing the effect of mutant AIP and co-transfection of AIP with inhibitors for the candidate miRNA, we wanted to investigate the effect miRNA modulation in a cellular model, which is more suitable for PAs. Since no human PA cell line is currently available, the rat GH3 cell line was used for further *in vitro* characterization since these are growth hormone (GH) and prolactin (PRL) producing pituitary tumor cells, thereby representing the most relevant cell culture model available for our study.

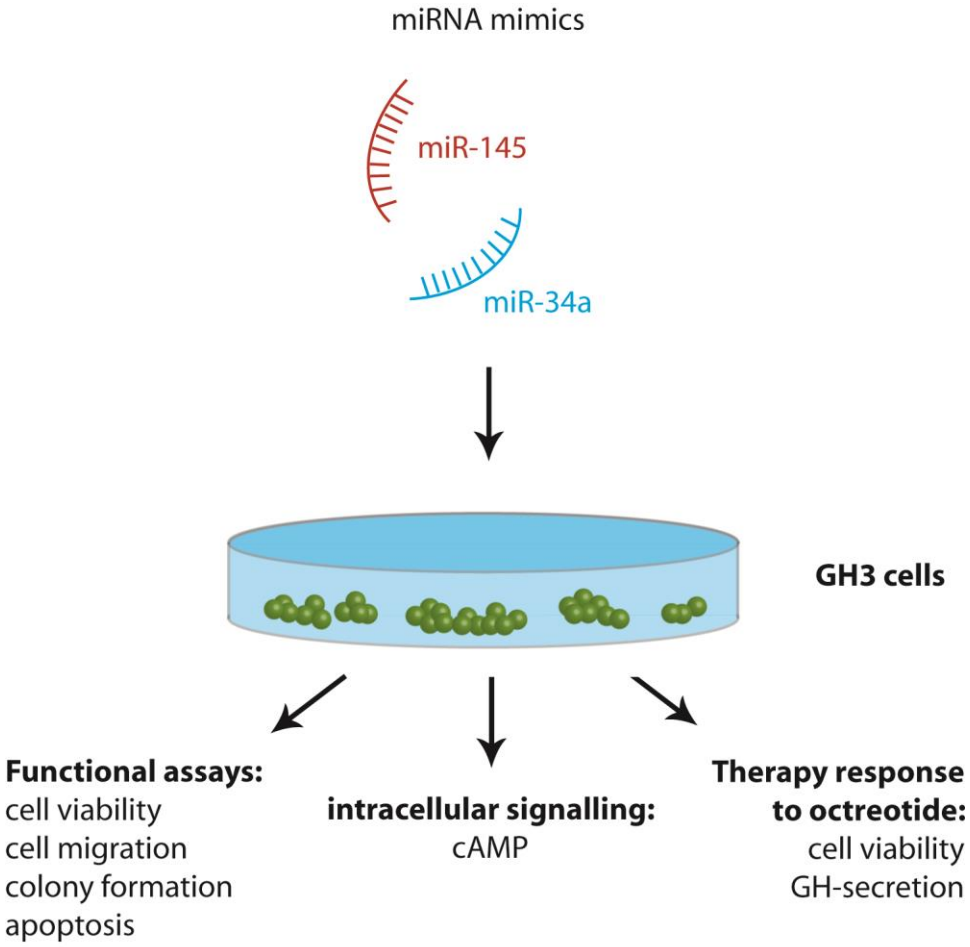

Figure 23: Outline of the workflow in GH3 cells: Transfection of GH3 cells with miRNA mimics and subsequent analysis of transfected cells.
Figure: Eva-Maria Bogner

The impact of miR-145 and miR-34a overexpression was studied *in vitro* on GH3 cells. GH3 cells were transfected with mature miRNA mimics of miR-34a-5p (miR-34a) and miR-145-5p (miR-145) and functional assays were performed addressing effects on proliferation, clonogenic potential, migration and apoptosis (Figure 23).

As a first step we wanted to assess cell proliferation. The proliferation of cells can be monitored in different ways. In order to get a comprehensive picture of the effects of miRNA overexpression on GH3 cells we chose to measure proliferation with two parameters: 1) The assessment of the metabolic activity of the cells by the WST-1 assay and 2) visualization of cell division by immunfluorescent staining of Ki-67 in transfected cells.

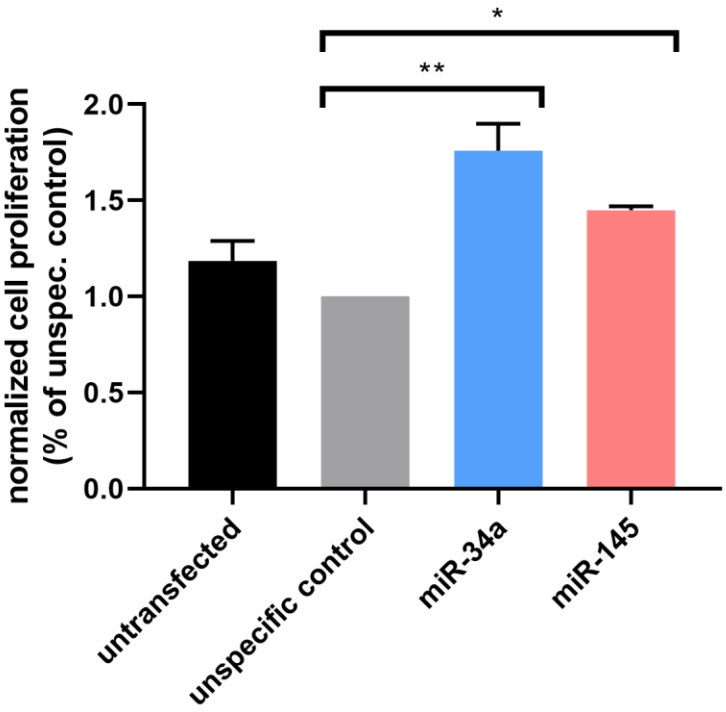

Figure 24: miR-34a and miR-145 increase cell viability of PA cells. GH3 cells were transfected with an unspecific miRNA (neg. control) or with specific mimics for mature miR-34a or miR-145. The assay was performed 24h after transfection. Results are reported as the mean ±SEM. Cell viability was assessed by the WST-1 assay. The experiment was independently performed 3 times each with 6 technical replicates. *, $p<0.05$; **, $p<0.01$; (by one-way ANOVA and Dunnett's multiple comparisons test).

Overexpression of either miRNA mimic, miR-34a and miR-145, increased GH3 cell proliferation when compared to cells transfected with an unspecific control miRNA mimic (Figure 24). Thereby we were able to show that miR-34a as well as miR-145 overexpressing GH3 cells proliferate more than cells that were transfected with an unspecific control miRNA, indicating a more oncogenic phenotype of miR-34a and miR-145 overexpressing GH3 cells.

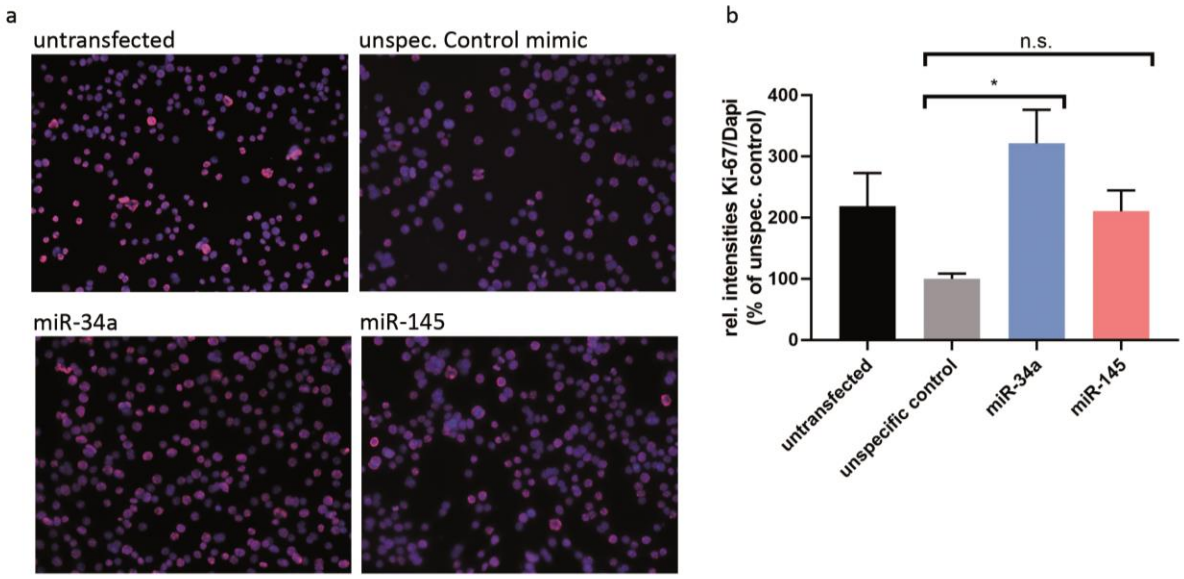

Figure 25: Immunfluorescent (IF) staining of Ki-67 in GH3 cells. (a) Ki-67 staining increased significantly with overexpression of miR-34a, a trend could also be observed with overexpression of miR-145. Representative pictures of 4 technical replicates for each condition. (b) Quantification of Ki-67 fluorescent intensity normalized to DAPI intensity. **, p<0.01; n.s., not significant (by one-way ANOVA and Dunnett's multiple comparisons test).

The positive effect of miR-34a overexpression on proliferative behavior of GH3 cells should be confirmed with a second method that does not rely on metabolic cell viability as the WST-1 assay. The cells were stained with an antibody against Ki-67, which is an established marker of cell proliferation. Staining intensity was used to quantify the effect of miR-34a on cell proliferation. In agreement with the WST-1 assay, miR-34a overexpression increased cell proliferation, since the intensity of Ki-67 expression in the miR-34a overexpressing group is significantly enhanced compared to transfection of an unspecific control mimic. In contrast, Ki-67 signal was not increased when miR-145 was overexpressed, which is in contrast to the increased metabolic intensity in this group in the WST-1 assay (Figure 25).

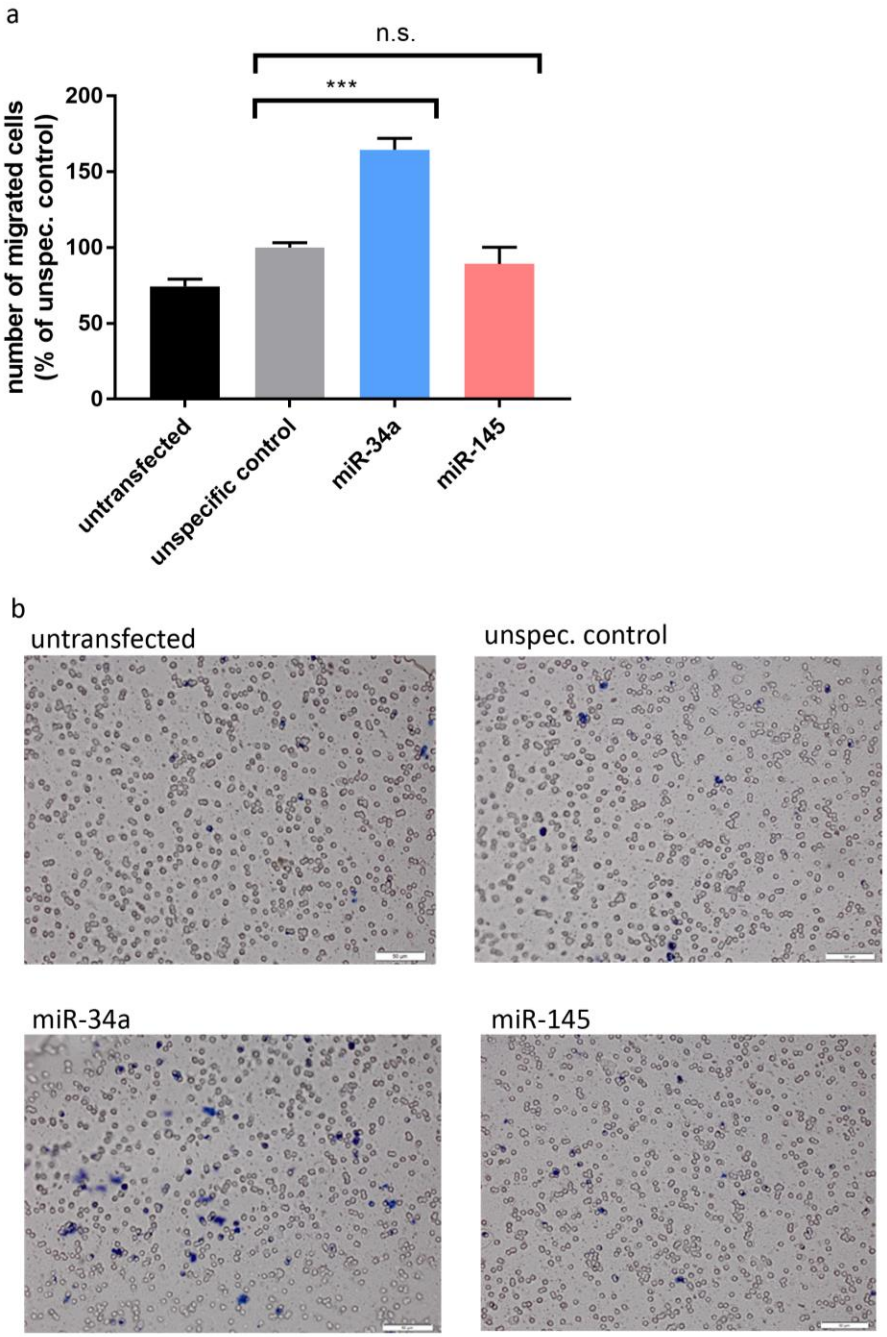

Figure 26: miR-34a increases cell migration of PA cells. GH3 cells were transfected with an unspecific miRNA (neg. control) or with specific mimics for mature miR-34a or miR-145. The assay was performed 24h after transfection.. Migration assays were conducted using the Boyden chamber and the migrated cells were stained with Toluidin Blue and counted. The experiment was independently performed twice each time with 3 technical replicates. Results are reported as the mean ±SEM (scale bar = 20µm); ***, $p<0.001$; n.s., not significant (by one-way ANOVA and Sidak's multiple comparisons test).

Assessment of cellular migration of GH3 cells is not an easy task, since these cells do not grow as a monolayer, which is the requirement for a wound healing assay. Therefore, this assay cannot not be conducted in GH3 cells. The transwell assay using the Boyden chamber was used as an

alternative measure of migration, although the semi-adherent phenotype of GH3 cells impairs this assay as well. Nevertheless, migration assays showed that GH3 cells transfected with the miR-34a mimic migrated significantly more than those transfected with the unspecific miRNA control, whereas transfection of miR-145 mimic had no effect on cell migration (Figure 26).

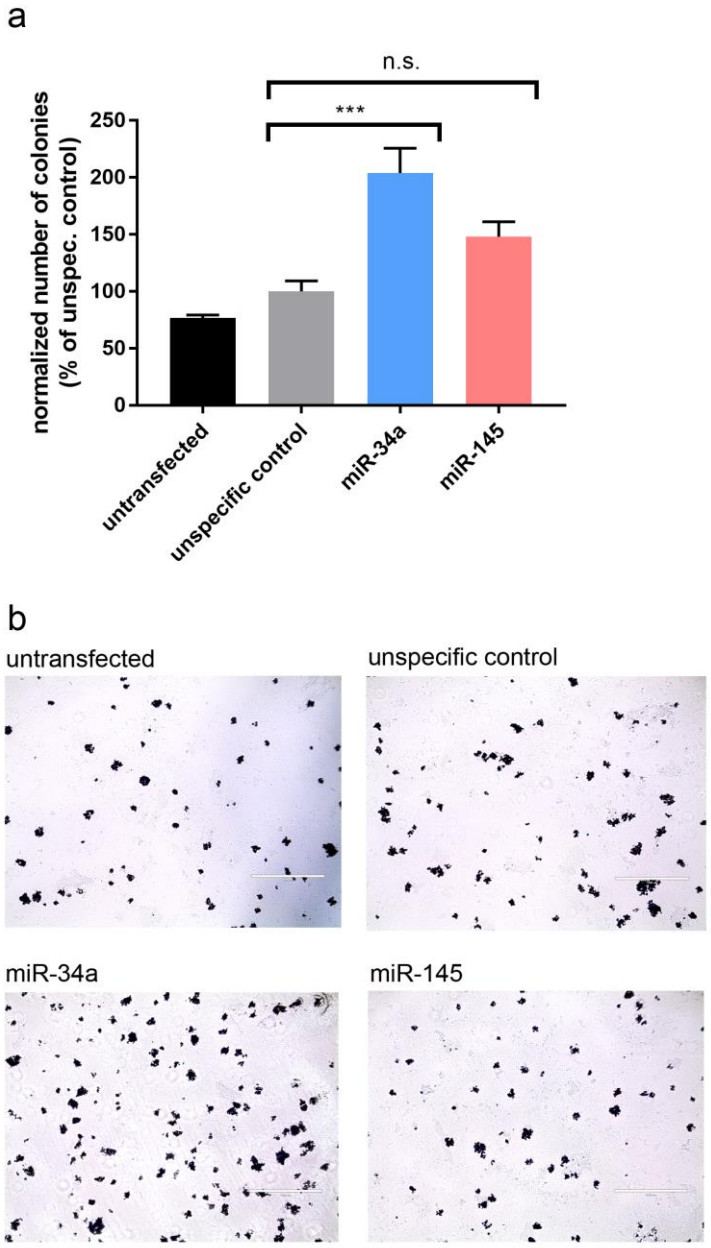

Figure 27: miR-34a increases clonogenic potential of PA cells. GH3 cells were transfected with an unspecific miRNA (neg. control) or with specific mimics for mature miR-34a or miR-145. Transfected GH3 cells were plated, seven days later the colonies were fixed, stained and those that reached a diameter >100µm were counted. The experiment was independently performed 3 times each with 3 technical replicates. Results are reported as the mean ± SEM.***, $p<0.001$; n.s., not significant (by one-way ANOVA and Sidak's multiple comparisons test).

The same obstacles, which were faced for the migration assay concerning GH3 cells do also apply for the colony formation assay. This assay monitors the cellular survival of cells that are plated in very low densities in order to form single clones. The clonogenic potential of these cells (i.e. the potential to grow colonies from single cells by clonal expansion) serve as another measure of oncogenic effects of miRNA overexpression. Transfection of miR-34a into GH3 cells increased by 2-fold the number of colonies (with a diameter >100µm) when compared with cells transfected with the unspecific miRNA control. In contrast, overexpression miR-145 did not significantly increase the clonogenic potential of GH3 cells (Figure 27). This is in line with the results of the Ki-67 intensity quantification and the migration assay, where also miR-34a, but not miR-145 showed a significant increase compared to an unspecific control miRNA.

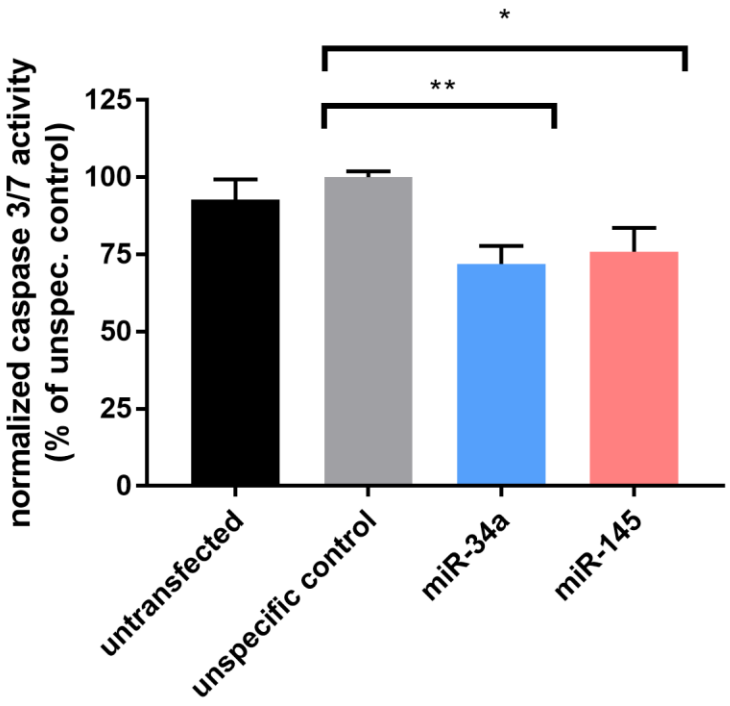

Figure 28: miR-34a and miR-145 reduce apoptosis, measured by caspase 3/7 activation, in PA cells. GH3 cells were transfected with an unspecific miRNA (neg. control) or with specific mimics for mature miR-34a or miR-145. Caspase 3/7 activity was measured 24h after transfection. The experiment was independently performed 3 times each with 2 technical replicates. Results are reported as the mean ±SEM. *, $p<0.05$; **, $p<0.01$ (by one-way ANOVA and Sidak's multiple comparisons test).

An important hallmark of cancer is the ability of tumor cells to resist cell death [167]. Thus, we wanted to see, whether miRNA overexpression changes the levels of apoptosis measured by the activation of caspase 3/7. Both miR-34a and miR-145 decreased caspase 3/7 activity, although the effect was more pronounced upon overexpression of miR-34a (Figure 28).

Altogether, high levels of miR-34a increased cell viability and proliferation, clonogenicity, migration and suppressed apoptosis of GH3 cells. miR-145 up-regulation only moderately promoted cell viability and decreased apoptosis of GH3 cells but had no effect on proliferation (Ki-67 staining intensity), migration nor on clonogenic potential.

3.6 Therapy response upon miRNA overexpression

It has been shown that FIPA patients carrying AIP mutations do not usually respond well to first generation somatostatin analogs such as octreotide, which target mainly somatostatin receptor 2 (SSTR2). As a consequence, these patients show a lack of normalization of hormone levels and no tumor shrinkage upon octreotide treatment [16, 19]. Given that mutations in AIP lead to upregulation of both miR-34a and miR-145 we decided to check whether the levels of these miRNAs play a role in the ability of PA cells to respond to octreotide. To this aim, GH3 cells were transfected with mimics of miR-34a, of miR-145 or with the unspecific miRNA control. Then, cells were treated with octreotide and cell proliferation was monitored.

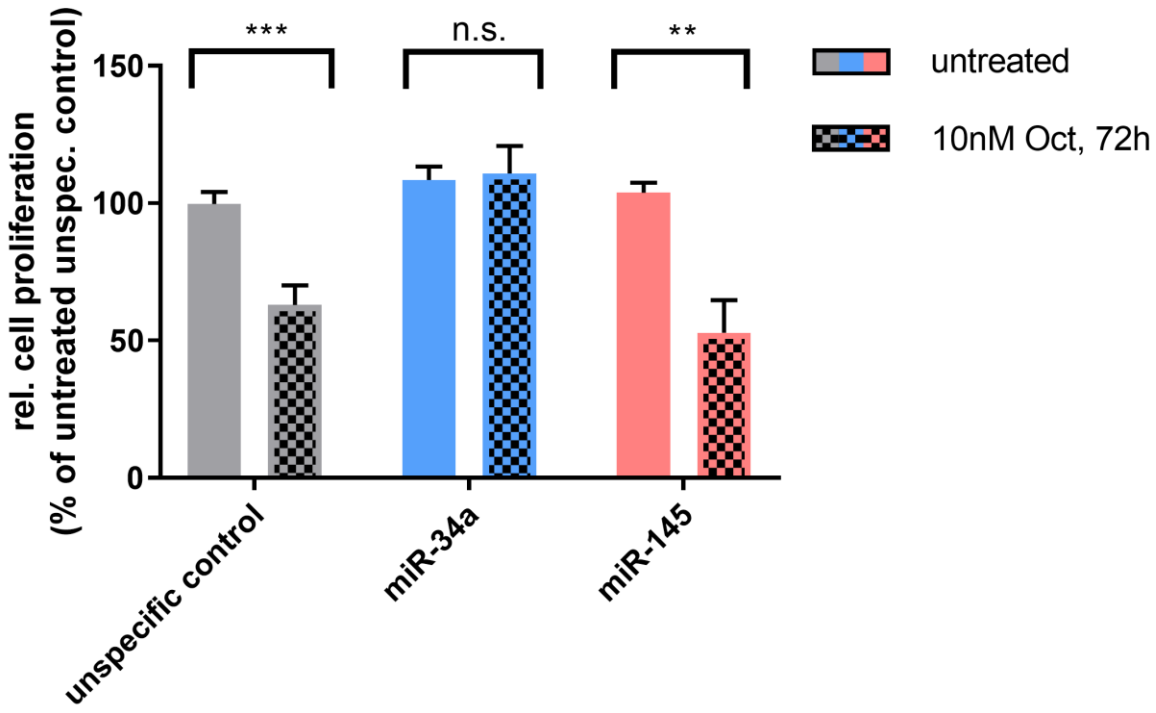

Figure 29: miR-34a abrogates the effect of octreotide treatment on the cell viability of GH3 cells. GH3 cells were transfected with an unspecific miRNA (neg. control) or with specific mimics for mature miR-34a or miR-145 and subsequently treated with 10nM octreotide (Oct) for 72h. Cell viability was then measured using the WST-1 assay. The experiments were independently performed 3 times with 6 technical replicates. Results are reported as the mean ± SEM. **, $p<0.01$; ***, $p<0.001$; n.s., not significant (by two-way ANOVA and Sidak's multiple comparisons test).

In cells overexpressing the unspecific miRNA control, a decrease in cell proliferation of approximately 30/40% when compared with untreated cells was observed following treatment with 10nM Oct for 72h (Figure 29) in agreement with previous reports [230, 231]. A comparable reduction in cell proliferation could also be observed in cells overexpressing miR-145 and treated with the same dose of octreotide, whereas no effect of octreotide on cell proliferation was detected upon miR-34a up-regulation (Figure 29). This suggests that high miR-34a levels abolish the octreotide-dependent inhibition of PA cell proliferation.

It has been reported that octreotide treatment suppresses GH secretion by GH3 cells in vitro [232]. AIP itself has also an effect on GH secretion since overexpression of wild-type AIP reduces secretion of GH in GH3 cells by decreasing cAMP levels [233]. Thus, GH was measured in the supernatant of GH3 cells transfected with the above miRNA mimics and treated with 100nM octreotide for 48h.

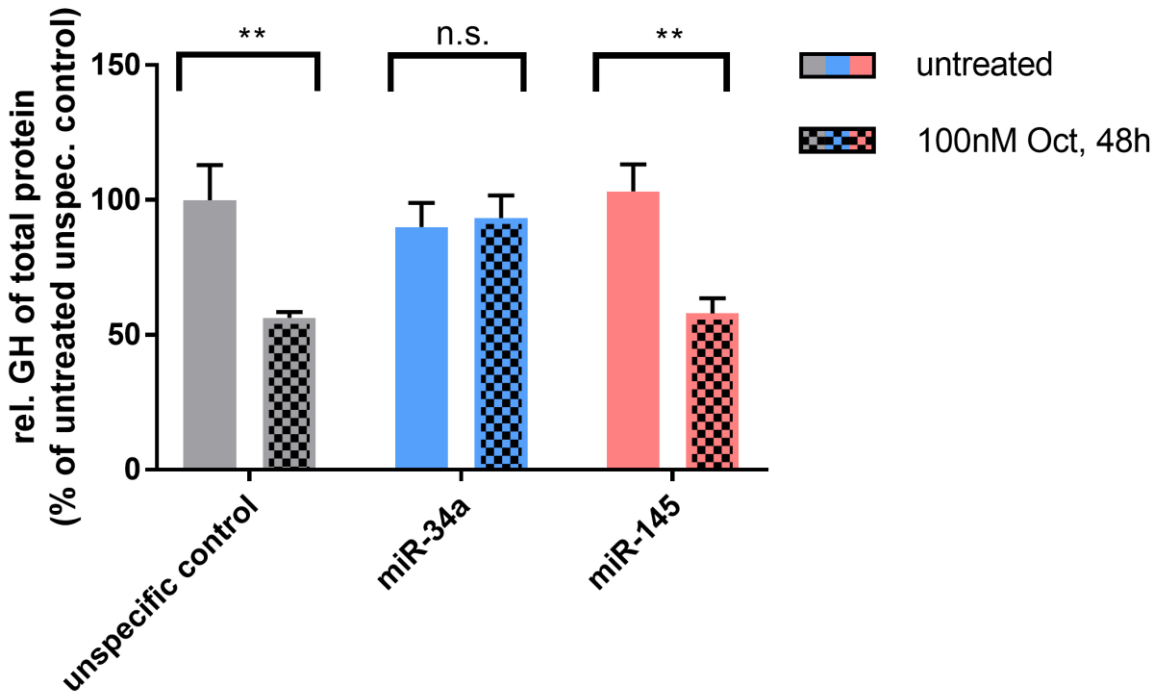

Figure 30: miR-34a abrogates the effect of octreotide treatment on the levels of secreted GH of GH3 cells. GH3 cells were transfected with an unspecific miRNA (neg. control) or with specific mimics for mature miR-34a or miR-145 and subsequently treated with 100nM octreotide (Oct) for 48h. GH secretion was then measured by ELISA. The experiments were independently performed 3 times with 2 technical replicates. Results are reported as the mean ± SEM. *, $p<0.05$; **, $p<0.01$; ***, $p<0.001$; n.s., not significant (by two-way ANOVA and Sidak's multiple comparisons test).

In agreement with previously reported data on parental cells, GH3 cells transfected with the unspecific miRNA control and treated with octreotide showed a reduction in the amount of

secreted GH upon incubation with octreotide (Figure 30). Similarly, a decrease in GH levels (-44%) was seen in the supernatant of cells transfected with miR-145 and treated with octreotide versus untreated cells (Figure 30). In contrast, overexpression of miR-34a led to a loss of octreotide-mediated suppression of GH secretion in these cells (Figure 30). Thus, miR-34a up-regulation or its downstream targets might mediate the lack of response of some tumors to octreotide treatment.

3.7 Involvement of the cAMP pathway

It has been previously described that an increase in cAMP levels is an important hallmark of neuroendocrine tumors including pituitary adenomas [234]. Moreover, cAMP signaling is dysregulated after AIP inactivation and this associates with somatotroph cells tumorigenesis [125].

Comparable levels of AIP-wt and AIP-R271W were confirmed by western blotting (Figure 31). As described before, four times more AIP-R271W than AIP-wt was used for the transfection (Figure 13).

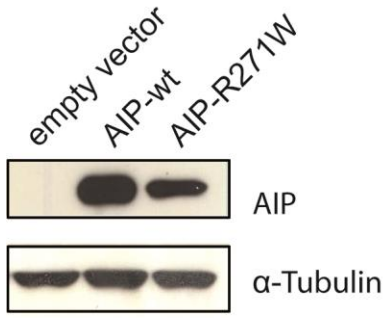

Figure 31: AIP protein levels after transfection of AIP plasmids in *AIP-/-* MEFs. *AIP-/-* MEFs were transfected with either the empty vector (4µg), AIP-wt (1µg+3µg empty vector) or AIP-R271W (4µg). Western blot was performed 24h after transfection using an anti-AIP antibody. α-Tubulin was used as loading control.

Intracellular levels of cAMP were assessed in MEFs, which are of course a physiologically different cell type than somatotroph cells of the pituitary, subsequently to transfection of AIP-wt or AIP-R271W. MEFs. In line with the previous reports, intracellular cAMP levels increased 2-fold upon AIP-R271W transfection compared to overexpression of AIP-wt (Figure 32).

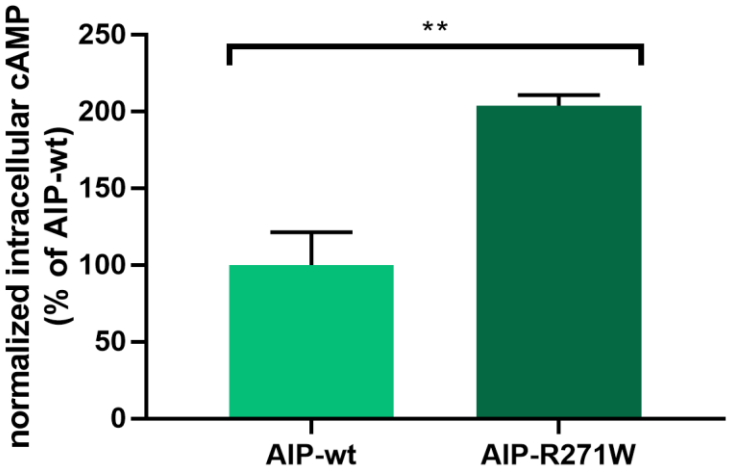

Figure 32: Mutant AIP increases intracellular cAMP levels of MEF *Aip-/-*. MEFs were transfected with either with AIP-wt or AIP-R271W. The assay was performed 24h after transfection. Results are reported as the mean ±SEM. The experiment was independently performed twice each time with 2 technical replicates. **, $p<0.01$ (by unpaired t-test, variances not significantly different (F test)).

However, intracellular cAMP levels after co-transfection of AIP-R271W with either anti-miR-34a, or anti-miR-145 did not change when compared to unspecific control inhibitor (Figure 33). This might imply that neither of these two miRNAs mediates the effect of mutant AIP in *Aip-/-* MEFs on cAMP levels. It needs to be considered that deregulation of cAMP levels in combination with AIP mutation is a phenomenon very specific for somatotroph PA cells [125, 233]. Therefore, even if in MEFs the selected miRNAs did not play a pole in the regulation of cAMP, the situation might be different in pituitary adenoma cells. For the reasons already discussed above, GH3 cells were also used to study the impact of candidate miRNAs on cAMP signaling.

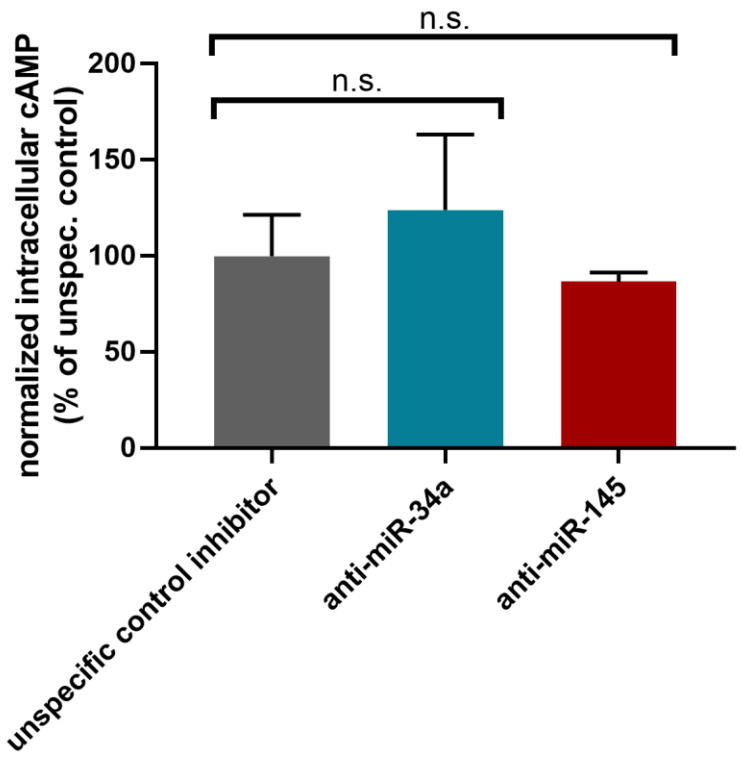

Figure 33: MEFs were co-transfected with the AIP-R271W construct and either an unspecific control inhibitor, an inhibitor for miR-34a or miR-145. The assay was performed 24h after transfection. Results are reported as the mean ±SEM. The experiment was independently performed twice each time with 2 technical replicates. n.s., not significant (by one-way ANOVA and Dunnett's multiple comparisons test).

cAMP levels were measured in GH3 cells transfected with miR-145, miR-34a mimics or with an unspecific miRNA control using an ELISA assay. Upon analysis of the AIP protein levels after transfection of miRNA mimics no change in AIP protein expression was observed (Figure 34).

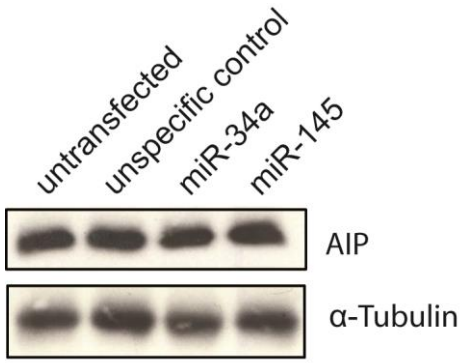

Figure 34: AIP protein levels after transfection miRNA mimics in GH3 cells. GH3 cells were left untransfected, transfected with either an unspecific control mimic, or specific mimics for miR-34a or miR-145. Western blot was performed 24h after transfection using an anti-AIP antibody. α-Tubulin was used as loading control.

We found that overexpression of miR-34a almost doubles the intracellular levels of cAMP in GH3 cells when compared with cells transfected with the unspecific negative control, whereas ectopic miR-145 expression had no effect on the amount of cAMP (Figure 35).

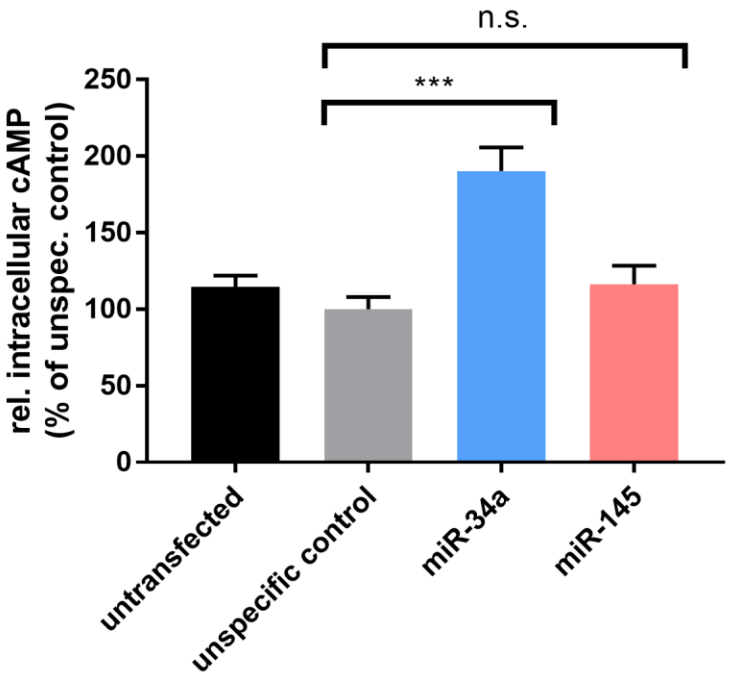

Figure 35: miR-34a increases levels of intracellular cAMP in GH3 cells. GH3 cells were transfected with an unspecific miRNA (neg. control) or with specific mimics for mature miR-34a or miR-145. Intracellular cAMP levels were measured 24h after transfection. The experiment was independently performed 5 times each with 2 technical replicates. Results are reported as the mean ±SEM. ***, $p<0.001$; n.s., not significant (by Kruskal-Wallis test and Dunn's multiple comparisons test; normality test (Shapiro-Wilk) failed).

cAMP has been reported to exert its mitogenic effect in somatotroph cells *via* phosphorylation of extracellular signal-regulated kinases (ERK1/2) [235, 236]. Therefore, the levels of total and phosphorylated ERK1/2 were assessed by western blotting and subsequently quantified. Overexpression of both miR-34a and miR-145 increased the levels of phosphorylated ERK1/2 compared to both untransfected cells and those transfected with the unspecific miRNA control (Figure 36a). The increase in ERK1/2 was more pronounced following miR-34a overexpression and this paralleled the higher levels of cAMP in cells transfected with this miRNA. miR-145 up-regulation also stimulated ERK1/2 phosphorylation in GH3 cells but this happens through pathways other than cAMP signaling. Although the increase is also obvious in the quantification of the western blot band, it did not reach a statistical significance (Figure 36b).

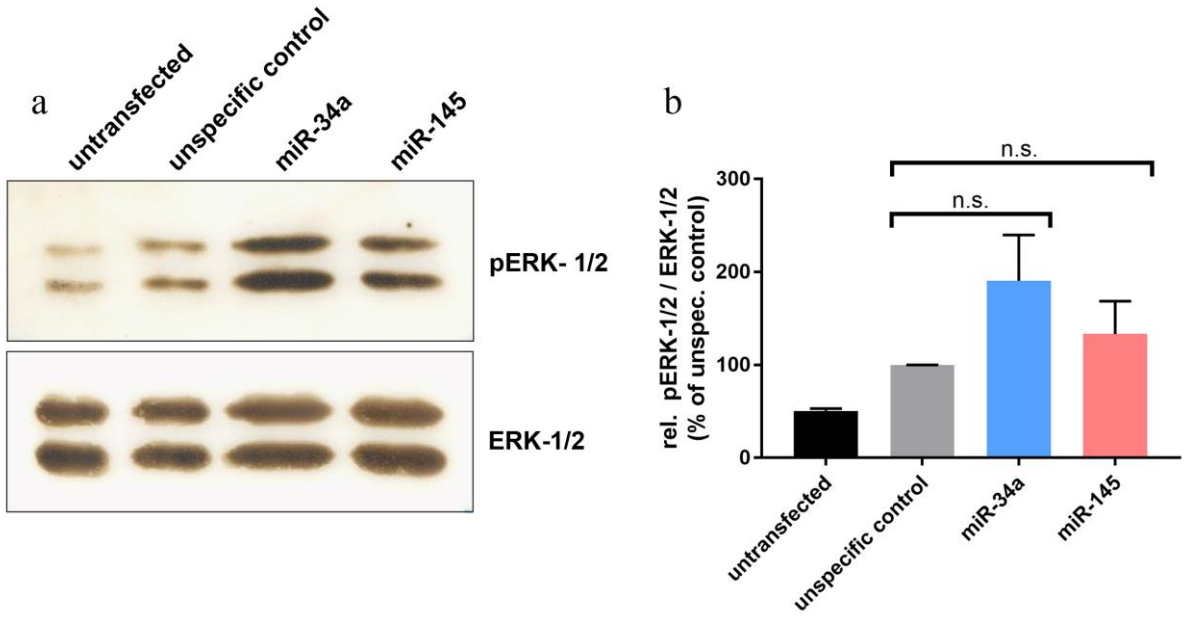

Figure 36: miR-34a and miR-145 show a trend towards elevated ERK1/2 activation. In samples parallel to those in Figure 32, western blot was performed 24h after transfection using an anti-p-ERK-1/2 antibody and an anti-ERK-1/2 antibody. The blot shown is representative of 2 independent experiments with similar results. (b) Ratio of the band intensities of the blots (n=2) described in (a). Results are reported as the mean ± SEM. ***, p<0.001; n.s., not significant (by one-way ANOVA and Dunnett's multiple comparisons test).

3.8 Mechanisms downstream of miR-34a

3.8.1 miRNA target prediction for miR-34a

We have shown that the presence of AIP mutations in PAs leads to up-regulation of miR-34a, which in turn promotes proliferation and cAMP signaling in PA cells *in vitro*. Since miRNAs exert their effect by regulating gene transcription, to better understand the function of miR-34a in PA cells we identified its predicted target genes. We used four different prediction tools (TargetScan, miRANDA-mirSVR, Diana tools, PITA). Whenever possible target genes were predicted for human, mouse and rat. Subsequently, only targets predicted in all three species at least by one algorithm were selected (Table 25). Since TargetScan considers only seed match and conservation for target prediction, and does not include free energy of miRNA binding nor site accessibility of the seed match (Table 24) [237], targets that were exclusively predicted by this algorithm were not considered.

Table 24: List of target prediction algorithms and the features that are used for the prediction (adapted from [237]).

Prediction algorithm	Seed match	Conservation	Free energy	Site accessibility	Target-site abundance	Machine learning	Online link
TargetScan 7.0	X	X					http://www.targetscan.org/vert_70/
miRANDA-mirSVR	X	X	X	X			http://www.microrna.org/microrna/home.do
DIANA tools	X	X	X	X	X	X	http://diana.imis.athena-innovation.gr/DianaTools/index.php
PITA	X	X	X	X	X		https://genie.weizmann.ac.il/pubs/mir07/mir07_prediction.html

In order to better explore the relationship between miR-34a and AIP, we compared the identified putative targets of miR-34a with known interaction partners of AIP. We specifically focused on genes involved in cAMP signaling, which is affected by both molecules (Table 25). Among the predicted targets of miR-34a were several members of the phosphodiesterase family including PDE4A, which is a known interaction partner of AIP [112]. In addition to phosphodiesterases, we observed that several predicted targets of miR-34a are genes coding for G-protein α-subunits members including GNAQ, encoding Guanine Nucleotide-Binding Protein G(Q) Subunit Alpha which is known to directly interact with AIP [114].

Table 25: Prediction of miRNA target gene for miR-34a by the indicated target prediction algorithms. Results were filtered for their involvement in cAMP signaling.

	human				rat			mouse			
	Target Scan	miRANDA	DIANA tools	PITA	Target Scan	miRANDA	DIANA tools	Target Scan	miRANDA	DIANA tools	PITA
AIP						X					
AhR		X							X		
PDE1a									X		X
PDE1b		X							X		
PDE1c						X	X		X		
PDE2a								X	X		
PDE3a	X				X			X			
PDE4a		X		X							X
PDE4b	X	X	X	X				X			
PDE4c		X									
PDE4d					X			X			
PDE4dip									X		X
PDE5a		X			X	X		X	X		
PDE6g									X		
PDE6h								X			
PDE7a	X		X	X					X		
PDE7b	X	X	X			X			X		
PDE8a					X			X			
PDE8b									X		
PDE10a					X			X		X	
PDE11a			X	X	X						
PDE12								X			
GNAO1	X	X			X			X	X		X
GNAI1					X			X	X		
GNAI2	X	X			X	X	X	X	X		X
GNAI3		X			X			X			X
GNA12		X		X			X				
GNAL	X	X							X		
GNAQ	X		X		X			X	X	X	
GNAS	X	X		X					X		
GNAT1		X							X		
GNAT2											
GNAZ		X		X		X					

If we consider the cAMP-related targets predicted in all three species by at least one software we are left with seven genes, i.e. *PDE3a, PDE5a, PDE7b, GNAO1, GNAI2, GNAI3, GNAQ* (Table 26). *PDE3a* was excluded since it was only predicted by TargetScan. The cGMP-specific *PDE5a* did not undergo further analysis. *PDE7b* is not expected to be a target of mir-34a and therefore downregulated in *AIP*mut+ PAs since it has been shown to be upregulated in *Aip* knockout cells [125]. Due to this reason, PDE7b was also excluded. For the remaining predicted targets, especially mRNAs of the inhibitory G alpha subunit family were of interest, because 1) differential has already been reported in *AIP*mut+ PAs [125] and 2) SSAs have been shown to exert its anti-proliferative and anti-secretory effects by activation of these proteins, which are coupled to SSTRs [51]. Therefore, members of this protein family were chosen as candidate target genes for establishment of a direct regulation by AIP via reporter assays.

Table 26: Candidate target genes of miR-34a predicted by at least one algorithm in each species.

	human				rat			mouse			
	Target Scan	miRANDA	DIANA tools	PITA	Target Scan	miRANDA	DIANA tools	Target Scan	miRANDA	DIANA tools	PITA
PDE3a	X				X			X			
PDE5a		X			X	X		X	X		
PDE7b	X	X	X			X			X		
GNAO1	X	X			X			X	X		
GNAI2	X	X			X	X	X	X	X		X
GNAI3		X			X			X			X
GNAQ	X		X		X				X		

3.8.2 mRNA and protein levels of GNAI2 and GNAI3 upon modulation of miR-34a levels

Members of the inhibitory G alpha subunit family, *GNAI2* and *GNAI3*, are promising candidate targets in the context of PAs. These genes encode Gαi subunits which inhibit adenylate cyclase (AC) activity, thereby leading to decreased cAMP levels [238]. We have shown that miR-34a levels increase in PA cells with mutant AIP. Assuming that miR-34a directly or indirectly targets *GNAI* genes and thereby decreases the amount of Gαi proteins, this would in turn increase AC activity and consequently cAMP levels in *AIP*mut+ cells, features associated with PA tumorigenesis. To verify whether *GNAI2* and *GNAI3* are indeed regulated by the level of miR-34a, we transfected the specific miR-34a mimic (overexpression) or a specific inhibitor anti-miR-34a (downregulation) in GH3 cells and then assessed the mRNA level of both genes by qRT-PCR.

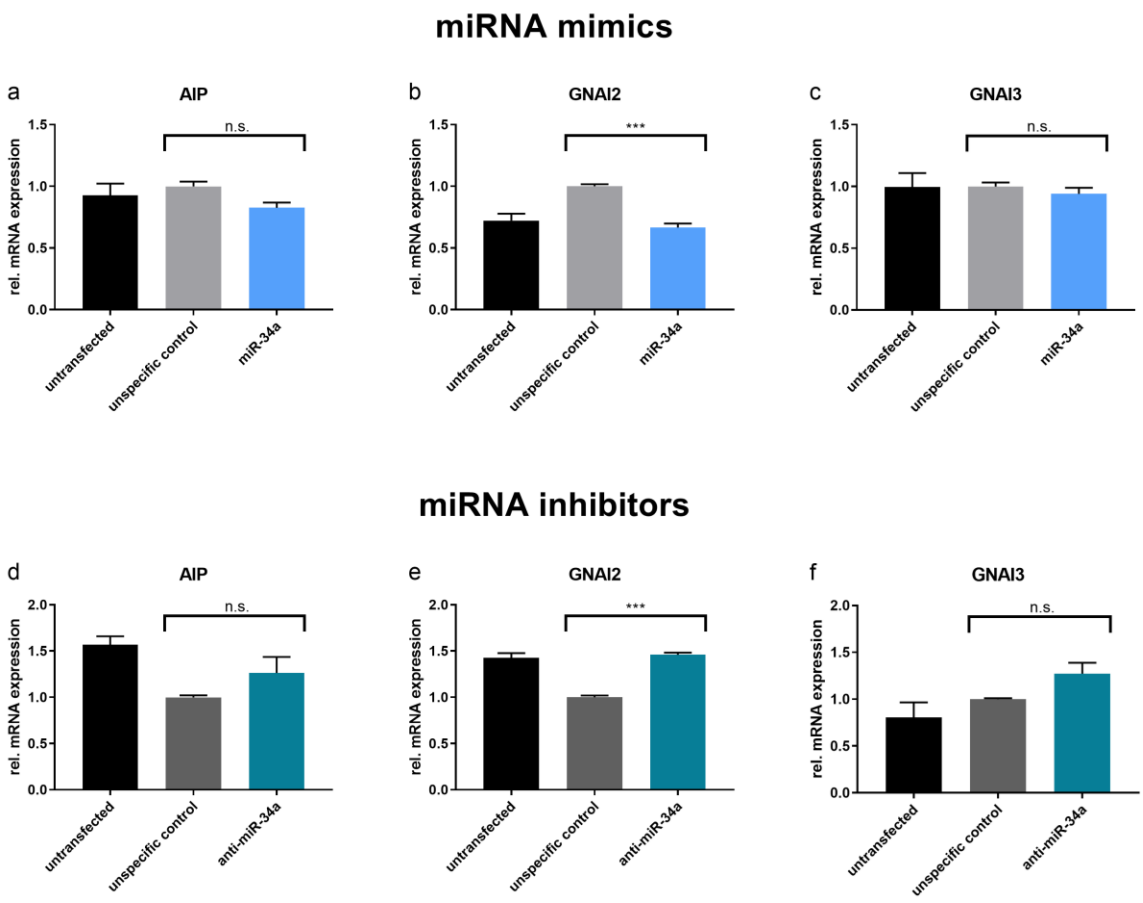

Figure 37: Effect of miR-34a modulation on the mRNA expression of *Aip*, *Gnai2* and *Gnai3*. GH3 cells were transfected with an unspecific miRNA (neg. control), with a specific mimic for mature miR-34a (a-c) or with an inhibitor of miR-34a (d-f). mRNA levels of *Aip* (a, d), *Gnai2* (b, e), or *Gnai3* (c, f) were determined 24h after transfection by qRT-PCR. Each amplification was independently performed 5 times each with 2 technical replicates. Results are reported as the mean ± SEM. ***, p<0.001; n.s., not significant (by one-way ANOVA and Dunnett's multiple comparisons test).

miR-34a overexpression decreased *Gnai2* mRNA levels by about 30 % when compared with cells transfected with unspecific miRNA negative control (Figure 37b), while its downregulation increased mRNA expression by about 1.5-fold (Figure 37e). No significant changes in *Gnai3* levels were observed after either overexpression (Figure 37c) or downregulation (Figure 37f) of miR-34a. Since *Aip* has been shown to be targeted by miR-34a in GH3 cells [191], the effect of overexpression (Figure 37a) and down-regulation (Figure 37d) on *Aip* mRNA levels was also assessed. No effect on *Aip* mRNA expression was observed in either condition.

miR-34a significantly affected *Gnai2* mRNA levels, therefore also the levels of the Gαi2 protein were examined. Although mRNA expression of *Gnai2* was clearly reduced or increased by miR-34a overexpression and inhibition respectively, both conditions did not alter Gαi2 levels up to 48 h after transfection of the cells. In addition, AIP protein levels were analyzed. Consistent with the observation of the mRNA level, AIP protein levels did not change upon modulation of miR-34a

expression. Denes and colleagues reported before that overexpression of miR-34a resulted in decrease of AIP protein expression while AIP mRNA levels remained unaffected [191]. This could not be reproduced in our study. Finally protein levels of ARNT were assessed, which were also unaffected by miR-34a expression (Figure 38). ARNT interacts with Ahr and the complex acts as a transcription factor in the context of the xenobiotic response [119]. In addition, ARNT may also be involved in PA formation and progression since its expression has been shown to be decreased in *AIP*mut+ PAs compared to PAs without *AIP* mutation [239] as well as in a heterozygous *Aip* mouse model (*Aip*+/- mice) [240]. In contrast, studies in homozygous *Aip*-/- MEFs and downregulation of AIP by siRNA in human cell lines provided no evidence of altered ARNT levels [239].

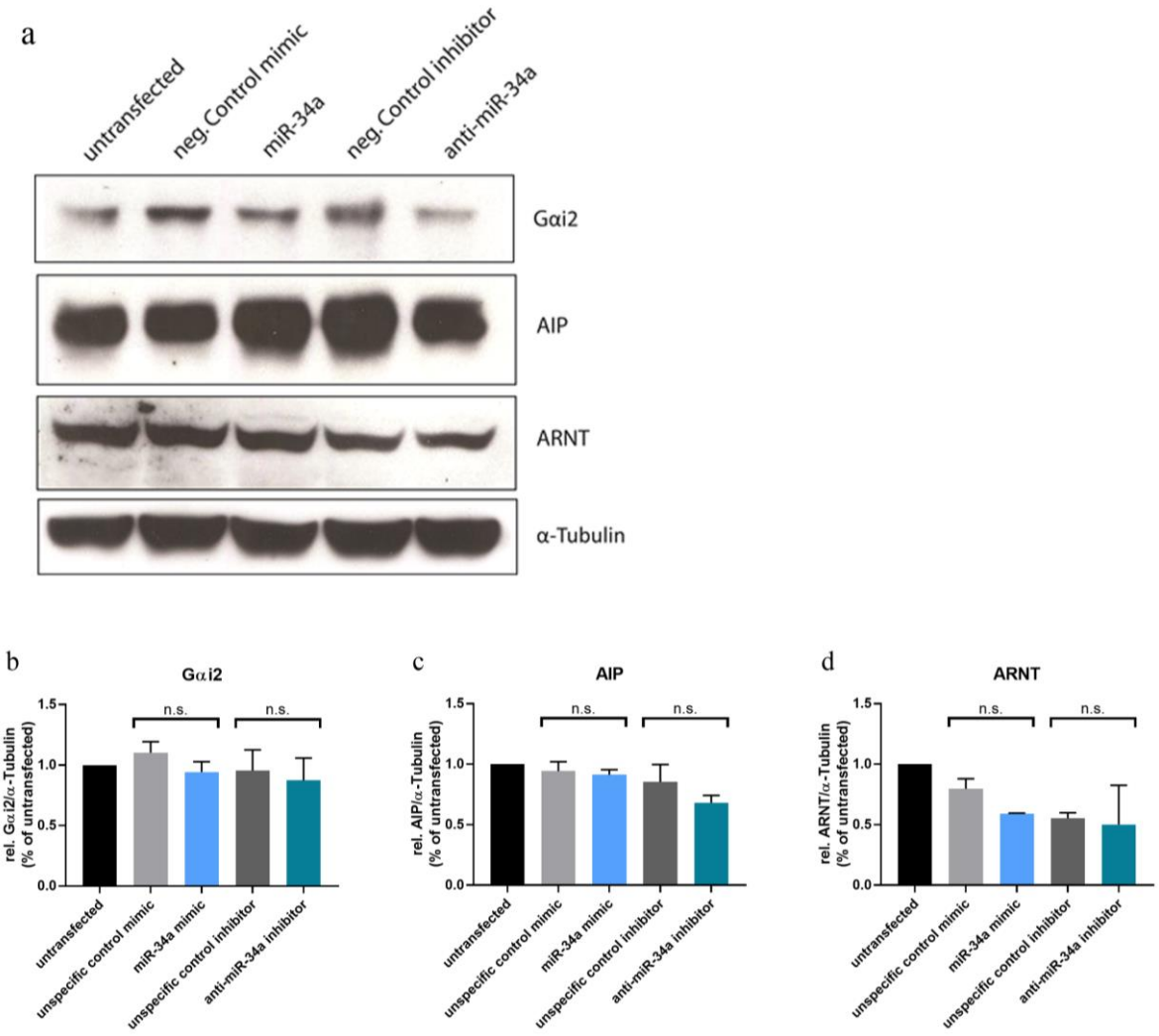

Figure 38: Effect of miR-34a modulation on the protein expression of Aip, Gnai2 and ARNT. (a) GH3 cells were either left untransfected of transfected with neg. Control mimic, miR-34a, a neg. Control inhibitor or a specific inhibitor against miR-34a (anti-miR-34a) and protein samples were subjected to Western Blot 48 h after transfection. Analysis of Gαi2, AIP and ARNT showed no major changes in protein levels between the groups. α-Tubulin was used as a loading control. The blot shown is representative of 3 independent experiments with similar results. (b-d) Ratio of the band intensities of the blots (n=3) described in (a). Results are reported as the mean ± SEM. n.s., not significant (by one-way ANOVA and Sidak's multiple comparisons test).

3.8.3 *Gnai2* as a direct target of miR-34a

Since qRT-PCR experiments indicated a possible regulation of *GNAI2* by miR-34a, we decided to test whether miR-34a directly targets this gene by conducting reporter gene assays.

The psiCHECK™-2 (Figure 7) vector was designed to allow monitoring of changes in expression of a target gene fused to a reporter gene. In this case, a fragment containing the predicted seed match of miR-34a in the 3'UTR of the rat GNAI2 gene from GH3 cells (Figure 39). was cloned into the multiple cloning site of the vector. *Renilla* luciferase (hRluc, ORF_1) is used as the primary

reporter gene, therefore, the seed match was cloned downstream of the gene. *Firefly* luciferase (hluc, ORF_2) served for internal normalization.

Figure 39: Partial sequences of the 3'UTR of the rat *Gnai2* gene that were cloned into reporter vectors. (a) The fragment that was cloned into the luciferase vector for the reporter gene assay and is highlighted in yellow. The predicted seed match that is located in the 3'UTR is highlighted in pink. (b) A mutated 3'UTR lacking the predicted seed match was cloned. The seed match deletion is indicated by the pink arrow.

We transfected the empty vector or the construct with the seed match together with anti-miR-34a or the unspecific control inhibitor in HEK293 cells and monitored luciferase activity 24h later. A decrease in luciferase activity was detected between cells co-transfected with empty vector and unspecific control miRNA inhibitor *versus* cells co-transfected with empty vector and anti-miR-34a inhibitor (Figure 40). In contrast, anti-miR-34a increased the luciferase activity of the construct containing the *Gnai2* seed match *versus* unspecific miRNA inhibitor by almost 30 % (Figure 40). Deletion of the seed region abolished the anti-miR-34a-mediated regulation of luciferase activity (Figure 40), thereby confirming that this miRNA indeed binds to the seed sequence in *Gnai2*.

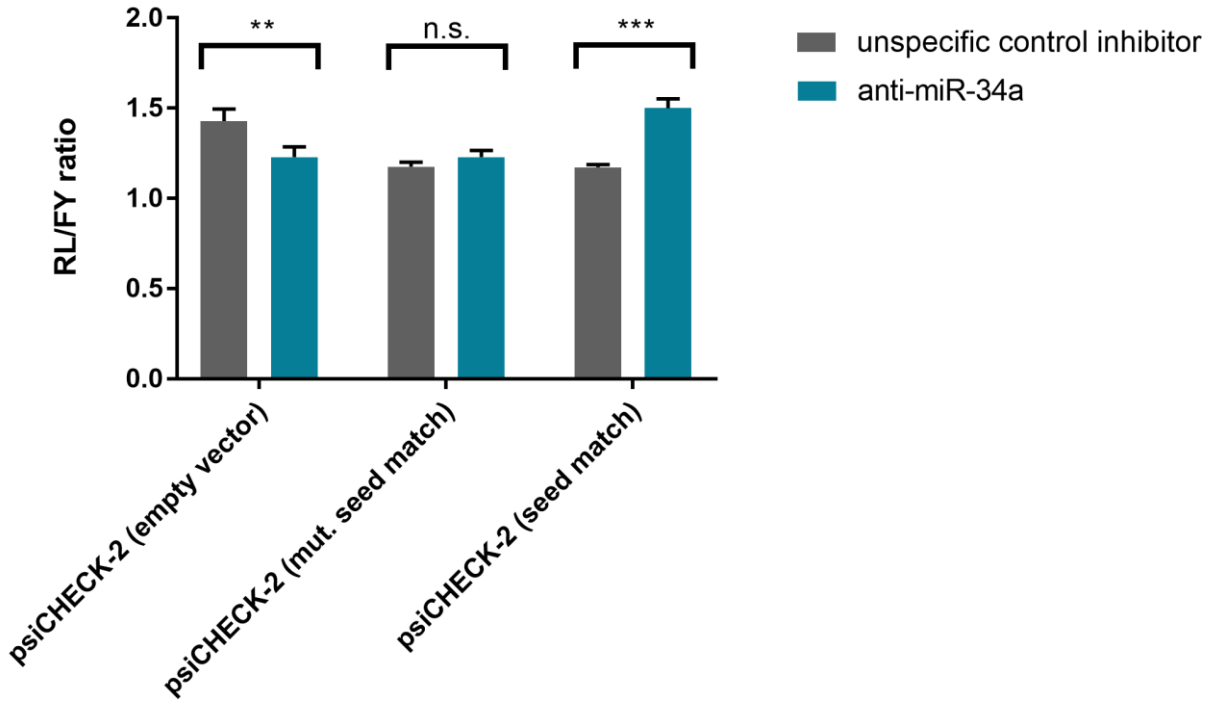

Figure 40: miR-34a inhibition increases the luciferase activity in cells transfected with the reporter vector containing the predicted seed match of the GNAI2 gene. HEK293 cells were co-transfected with either the empty psiCHECK-2, the vector containing the *Gnai2* seed match sequence or the vector with a mutated version of the seed match sequence together with either an unspecific control miRNA inhibitor or a specific miR-34a inhibitor. Data shown is the average of 3 independent experiments with 4 technical replicates. Results are reported as the mean ± SEM. *, p<0.05; ***, p<0.001; n.s., not significant (by two-way ANOVA and Sidak's multiple comparisons test).

3.8.4 Gαi2 and AIP expression levels in human pituitary adenomas

We demonstrated that miR-34a directly regulates *Gnai2* expression. Given that AIP mutated PAs show an increase in miR-34a expression, we next wondered whether these tumors also show reduced levels of expression of Gαi2. We conducted immunohistochemical staining (IHC) of all primary PA samples described above with antibodies against both AIP and Gαi2. Slides were then scored using a semi-quantitative assessment of the staining intensities (0, +, ++, +++). Examples of the staining intensities assigned to the various scores are depicted in Figure 41. A total of 40 samples could be assessed for Gαi2 expression (n=25 *AIP*mut-; n=15 *AIP*mut+) and 42 were scored for AIP expression (n=30 *AIP*mut-; n=12 *AIP*mut+).

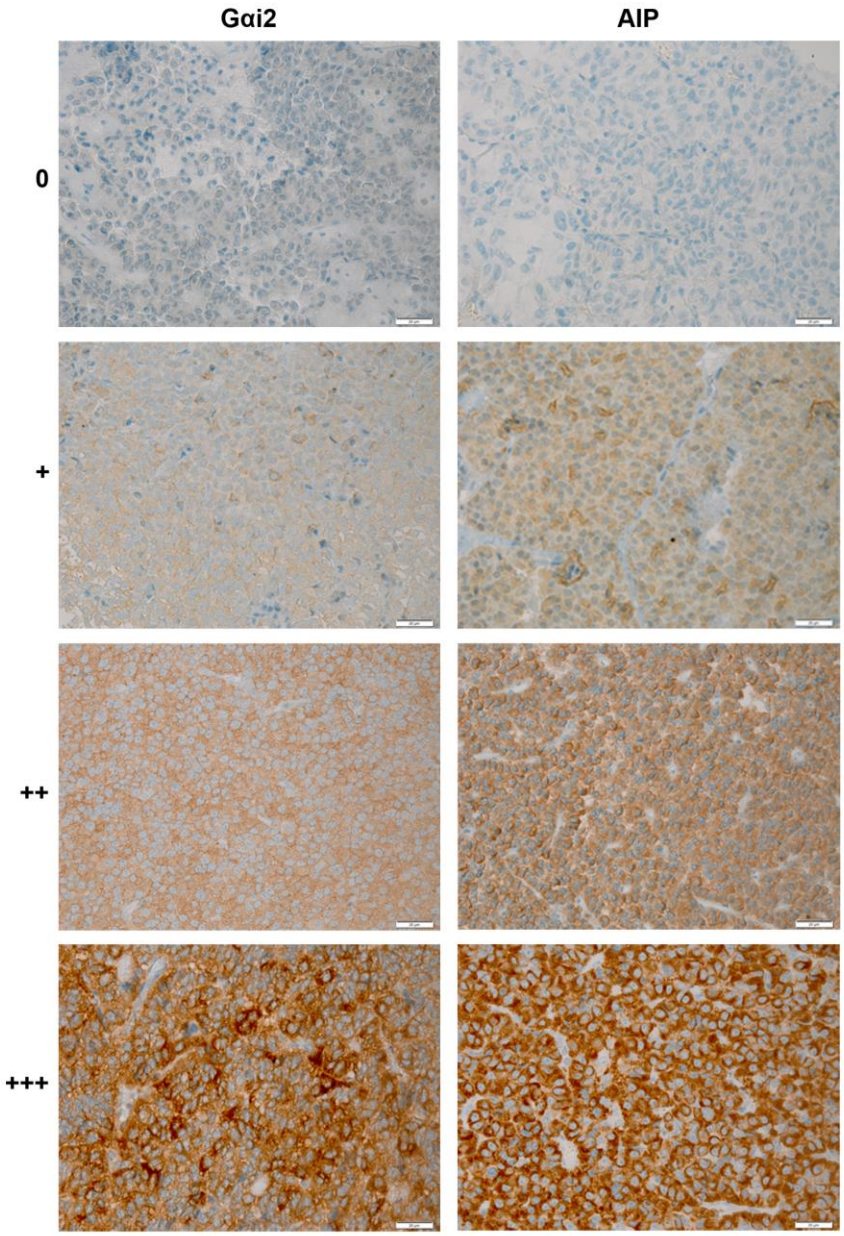

Figure 41: Semi-quantitative assessment of protein expression levels of Gαi2 and AIP. Immunohistochemical staining for Gαi2 and AIP in different primary PAs representative of the various scoring categories (Gαi2 or AIP) (0; +; ++; +++). PAs were from patients with and without AIP mutations (immunoperoxidase, x200) (scale bar = 20µm). Antibodies anti-Gαi2 (1/200) and anti-AIP (1/1000) were used.

Summary of the scores are reported in Figure 42a and Figure 42b.

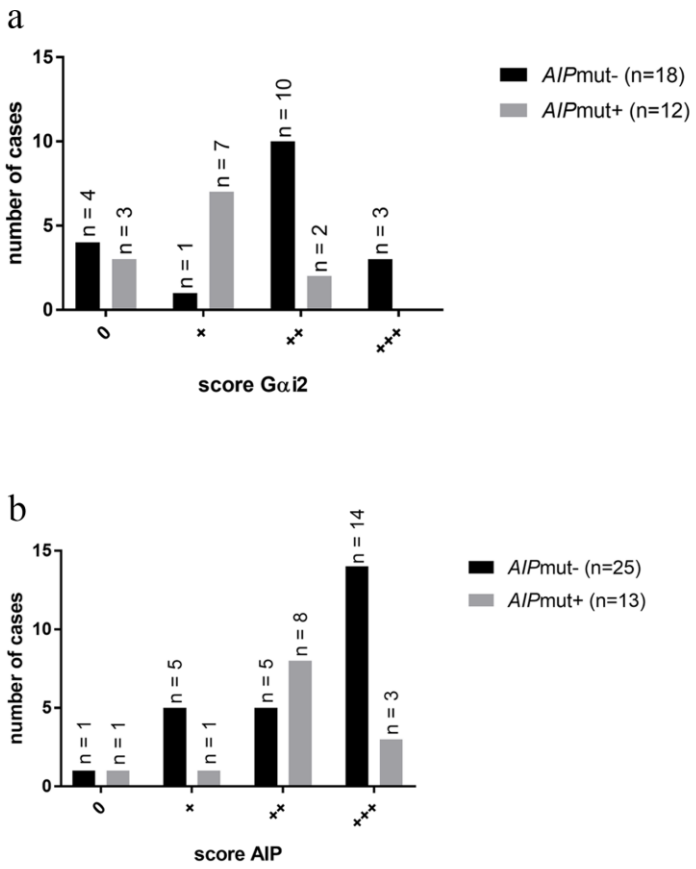

Figure 42: Semi-quantitative assessment of protein expression levels of Gαi2 and AIP. (a) expression levels of Gαi2 in our PA samples. (b) expression levels of AIP in our PA samples.

By dividing the samples in *AIP*mut- and *AIP*mut+, it can be appreciated that the levels of Gαi2 were significantly lower in *AIP*mut+ samples than in those without mutations (p=0,0344) (Figure 43a), whereas there was no statistically significant difference in AIP levels between the two sample groups (Figure 43b).

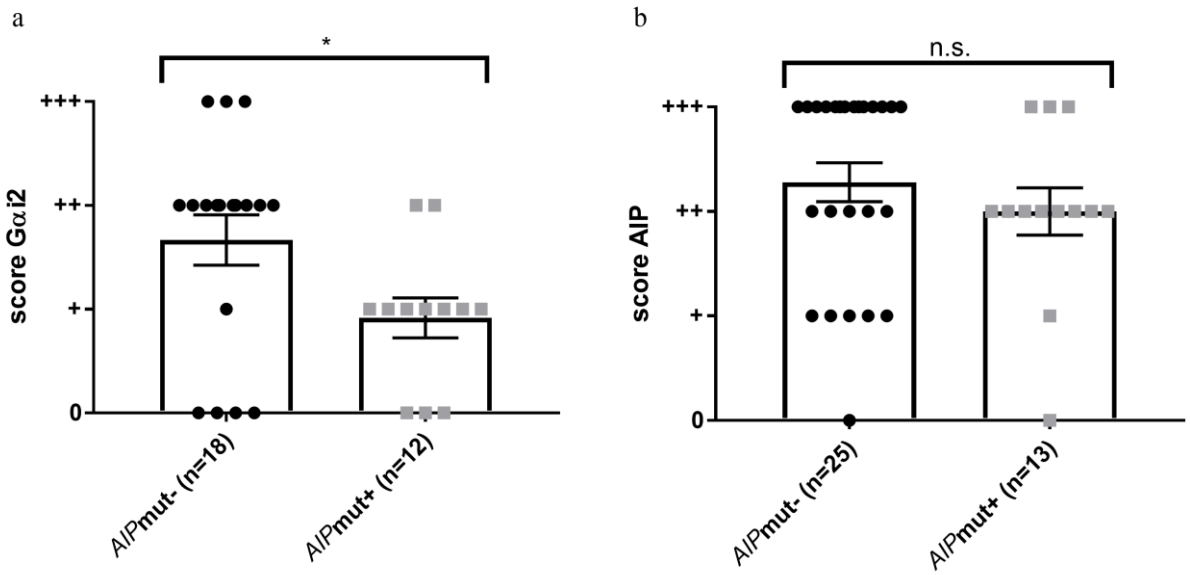

Figure 43: Gαi2, but not AIP scores are significantly decreased in *AIP*mut+ compared to *AIP*mut- PAs. Gαi2 (a) and AIP (b) scores in *AIP*mut- and in *AIP*mut+ PA samples. Results are reported as the mean ± SEM. *, p<0.05; n.s., not significant (by Mann-Whitney test; normality test (Shapiro-Wilk) failed).

If we only consider the somatotropinomas within our cohort (n=22, *AIP*mut-; n=15, *AIP*mut+), the decrease in score values of Gαi2 in *AIP*mut+ versus *AIP*mut- tumors was even more pronounced (p=0,0031) (Figure 44a). For the somatotropinomas a trend towards a reduction in AIP expression was detected between the two patient groups, but this failed to reach statistical significance (p=0,0553) (Figure 44b).

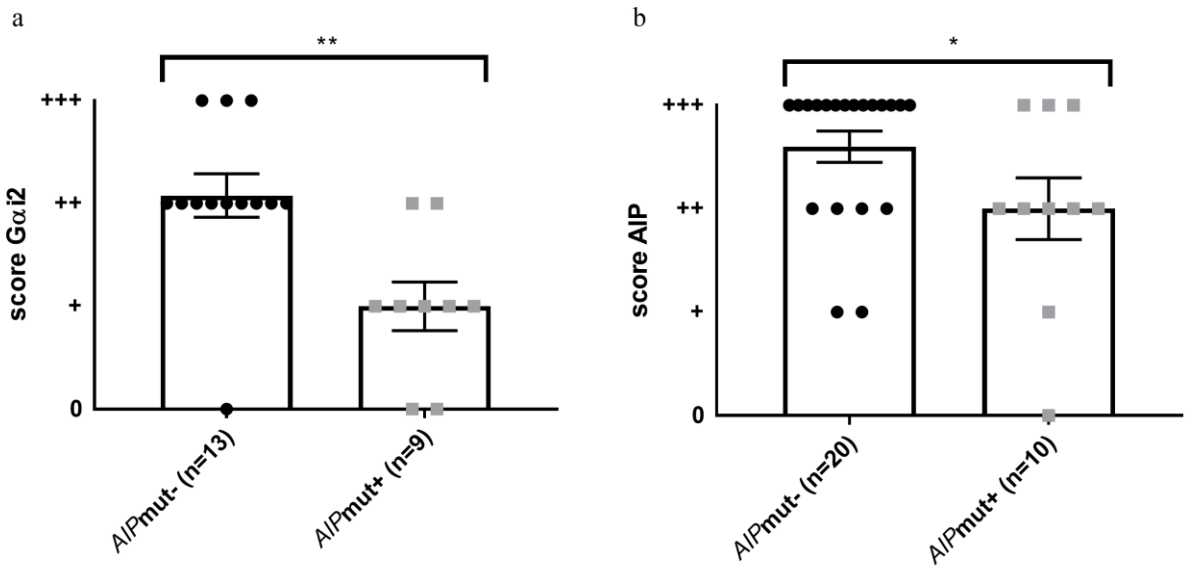

Figure 44: Gαi2 scores are significantly decreased and AIP scores show a trend towards a reduction in *AIP*mut+ compared to *AIP*mut- somatotropinomas. Gαi2 (a) and AIP (b) scores in *AIP*mut- and in *AIP*mut+ PA samples in somatotropinomas. Results are reported as the mean ± SEM. **, p<0.01; *, p<0.05 (by Mann-Whitney test; normality test (Shapiro-Wilk) failed).

Since the p.R271W mutation was very prevalent in our study (n=7) we investigated whether the expression levels of AIP and Gαi2 were comparable in patients with the same AIP mutation. We expected that the same mutation would have a similar effect on the protein expression levels, e.g. a global loss of protein expression. Surprisingly, the expression levels of AIP among the patient samples carrying the p.R271W mutation were very heterogeneous. Immunoreactivity for AIP was classified as +++, ++ or + depending on the staining intensity (Figure 45a). In addition, Gαi2 expression was also variable among the patients with the p.R271W mutation (Figure 45b).

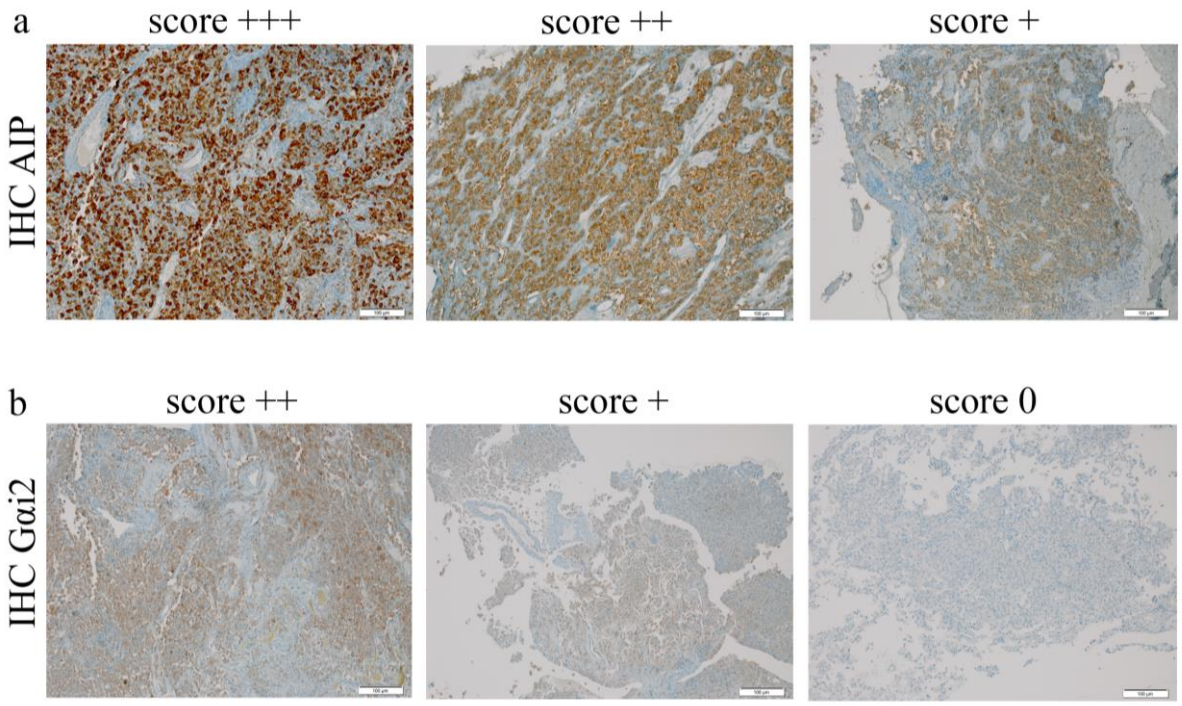

Figure 45: Variable expression levels in human somatotropinomas samples with the same mutation (R271W). (a) Immunhistochemical staining for AIP and (b) Gαi2 (scale bar = 100 µm. Antibodies anti-Gαi2 (1/200) and anti-AIP (1/1000) were used.

3.8.5 Correlations of protein expression scores with clinical parameters

A positive correlation between AIP and Gαi2 expression levels was observed in our sample cohort (p=0,0018; Figure 42a). The positive correlation implicates that an increased AIP IHC score went together with increased Gαi2 expression levels. There was no significant correlation if only somatotropinomas (Figure 42b) or only prolactinomas (Figure 42c) were taken into the analysis. AIPmut- PAs (somatotropinomas and prolactinomas) display a significant correlation between the IHC scores of the two proteins (p=0,0167; Figure 42d), whereas no significance was reached in case of AIPmut+ PAs (Figure 42e). When only considering the somatotropinomas, either AIPmut- (Figure 42f) or AIPmut+ somatotropinomas (Figure 42g) no significant correlation was generated. In case of the prolactinomas (n=8), the number of samples was too low to calculate a correlation.

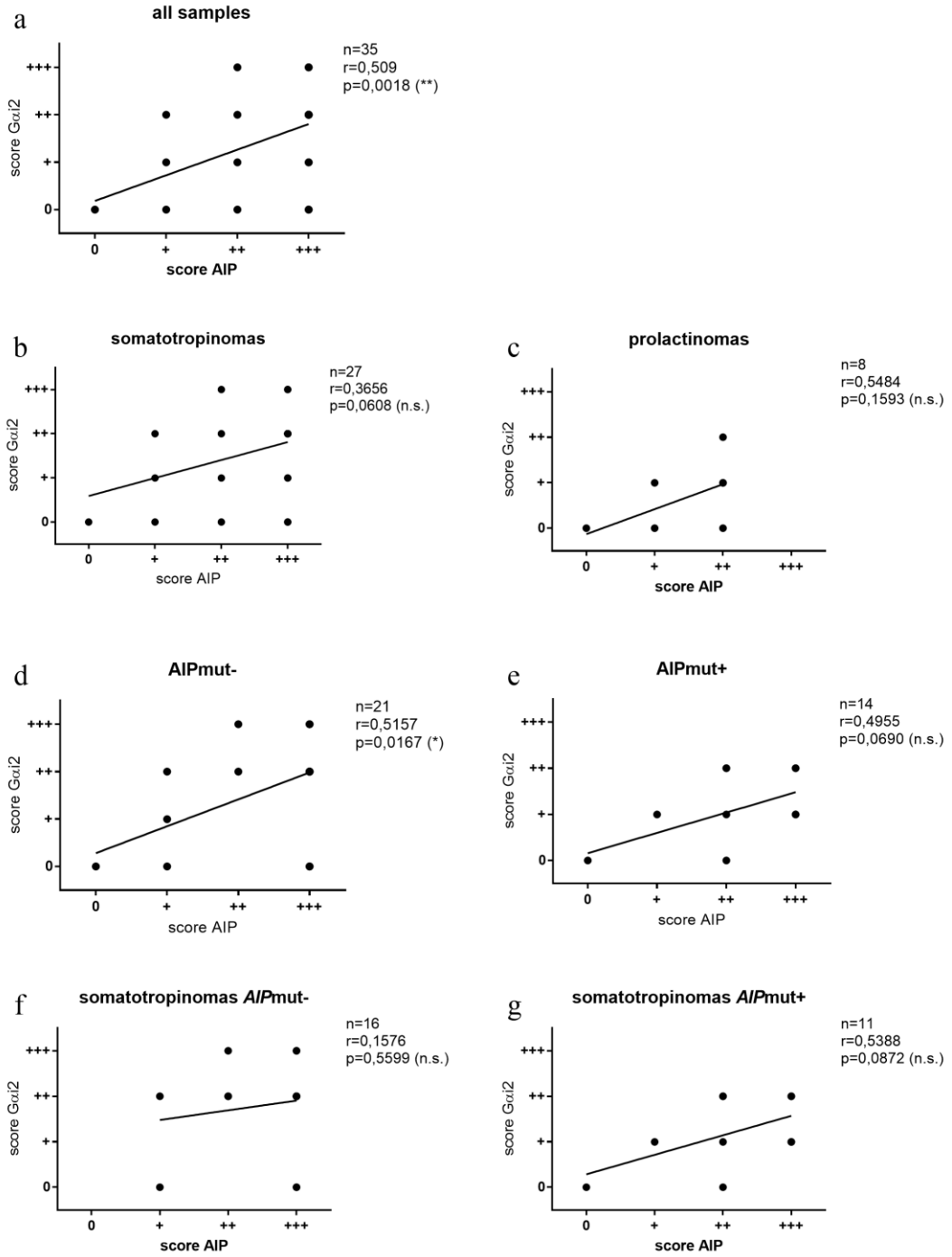

Figure 46: Correlations of IHC scores of AIP and Gαi2. Correlations for (a) all samples (n=35), (b) somatotropinomas (n=27), (c) prolactinomas (n=8), (d) *AIP*mut- PAs (somatotropinomas +prolactinomas; n=21), (e) *AIP*mut+ PAs (somatotropinomas +prolactinomas; n=14), (f) *AIP*mut- somatotropinomas (n=16), (g) *AIP*mut+ somatotropinomas. Pearson correlation coefficients and two-tailed p value were computed. Linear regression was applied on the correlation. **, p<0.01; *, p<0,05; n.s., not significant.

We further aimed to see whether AIP or Gαi2 scores correlate with any of the clinical characteristics of the patients listed in Table 11. AIP (Figure 47a), as well as Gαi2 (Figure 47d)

scores were significantly lower in prolactinomas compared to somatotropinomas when *AIP*mut- and *AIP*mut+ samples were taken together for the analysis. A reduction was observed in only *AIP*mut- (Figure 47b, e), it was even more pronounced in the case of AIP expression (Figure 47b). In contrary, for AIP and Gαi2 expression scores no difference between somatotropinomas and prolactinomas was found in *AIP*mut+ PAs (Figure 47c, f).

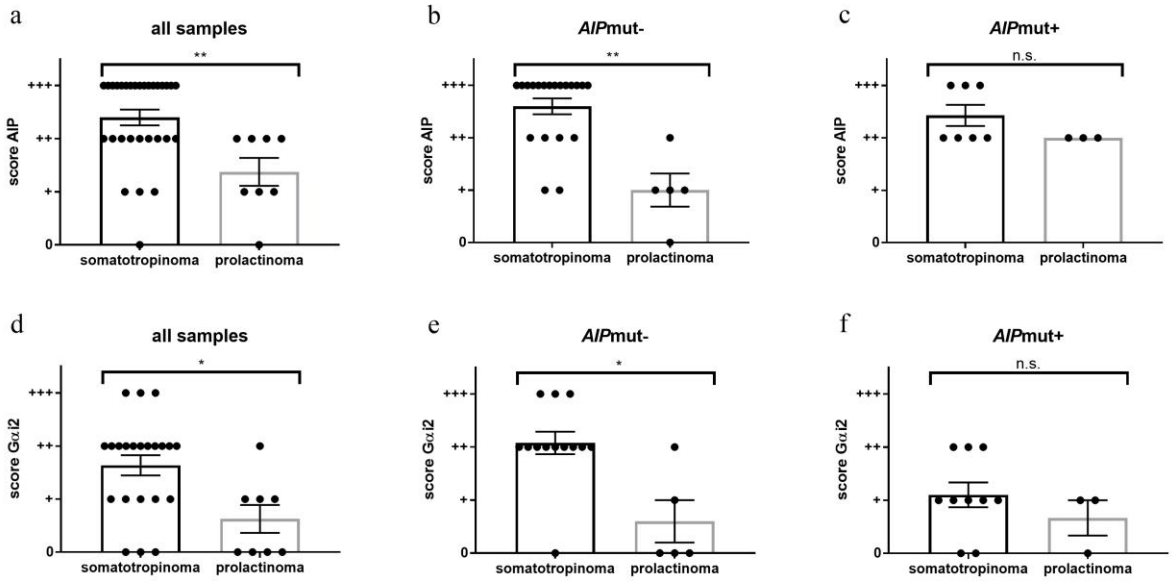

Figure 47: Reduced expression levels of AIP and Gαi2 in prolactinomas compared to somatotropinomas. (a-c) AIP expression scores, (d-f) Gαi2 expression scores. All samples (a, d), only *AIP*mut- (b, e) or only *AIP*mut+ (c, f) were taken into the analysis. Results are reported as the mean ± SEM. **, p<0.01; ***, p<0,001 n.s., not significant; (by Mann-Whitney test; normality test (Shapiro-Wilk) failed).

Neither AIP (Figure 48a) nor Gαi2 (Figure 48b) expression scores differed between female and male PA patients. No in-depth analysis concerning the *AIP* mutation status was possible in case of the gender of the patients due to the male preponderance among *AIP*mut+ patients. Therefore, the number of female *AIP*mut+ patients was not enough for a statistical analysis (Table 21).

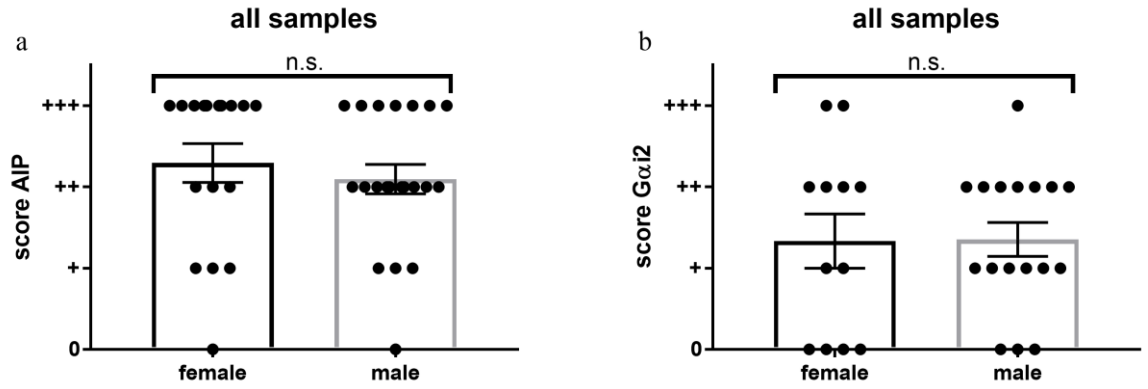

Figure 48: No difference in expression scores between female and male patients. AIP (a) and Gαi2 (b) expression scores in all PA samples (*AIP*mut- and *AIP*mut+). Results are reported as the mean ± SEM. n.s., not significant; (by Mann-Whitney test; normality test (Shapiro-Wilk) failed).

AIP and Gαi2 expression scores did not correlate with the tumor size of patients in all of the patients that were investigated (Figure 49a, d). Also in *AIP*mut- cases no statistically relevant correlation was calculated (Figure 49b, d). Nevertheless, a trend (p=0,0707) towards a negative correlation between AIP expression and tumor size can be found in *AIP*mut- cases (Figure 49b). This would imply that reduced AIP expression levels tend to occur in patients with large PA.

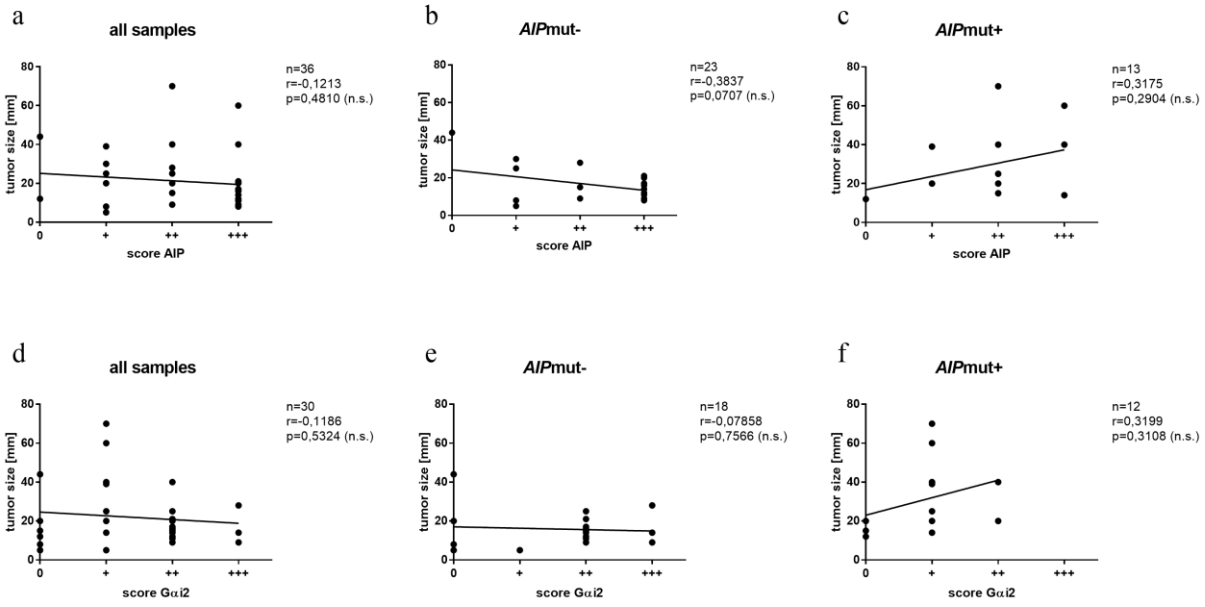

Figure 49: No correlation between the tumor size and AIP or Gαi2 expression scores. (a-c) AIP expression scores, (d-f) Gαi2 expression scores. All samples (a, d), only *AIP*mut- (b, e) or only *AIP*mut+ (c, f) were taken into the analysis. Pearson correlation coefficients and two-tailed p value were computed. Linear regression was applied on the correlation. n.s., not significant.

We further tested if invasion of surrounding tissue is associated with the expression levels of AIP or Gαi2. No correlation between invasion an expression score of AIP (Figure 50a) or Gαi2 (Figure 50d) was calculated in the whole patient cohort. If only *AIP*mut- patients were considered, no change in AIP and Gαi2 expression was found in invasive tumors (Figure 50b, e) as well as in *AIP*mut+ tumors, concerning either AIP or Gαi2 expression scores (Figure 50c, f).

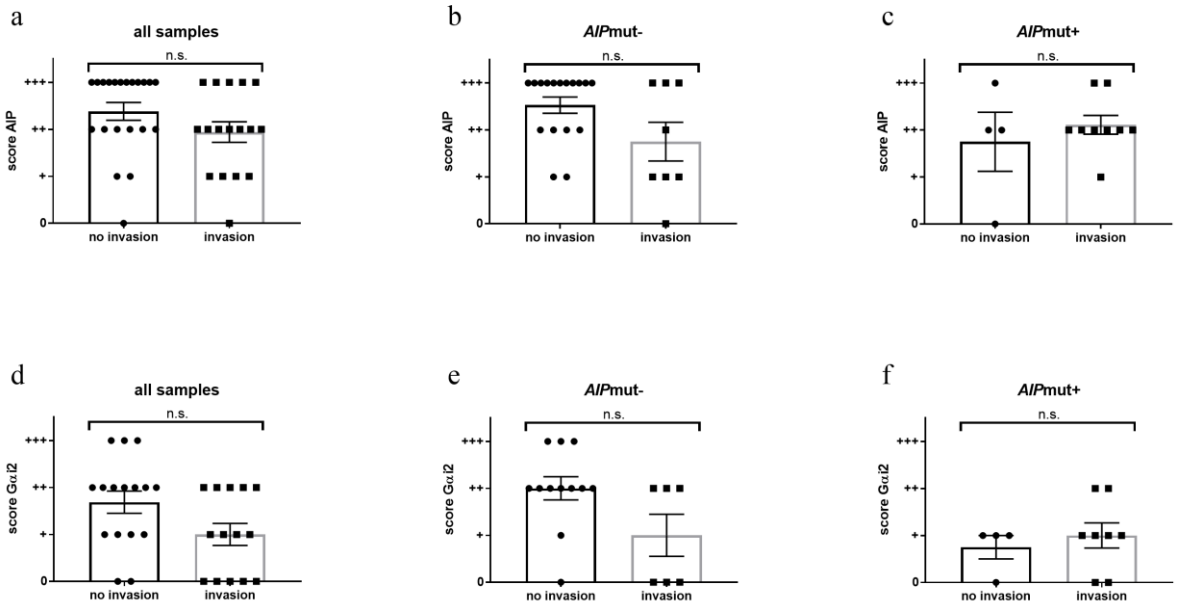

Figure 50: Invasion status does not associate with either AIP or Gαi2 expression levels. (a-c) AIP expression scores, (d-f) Gαi2 expression scores. All samples (a, d), only *AIP*mut- (b, e) or only *AIP*mut+ (c, f) were taken into the analysis. Results are reported as the mean ± SEM. n.s., not significant; (by Mann-Whitney test; normality test (Shapiro-Wilk) failed).

No significant correlation was found between age at diagnosis and expression of AIP (Figure 51a-c) or of Gαi2 (Figure 51d-f) in either patient group. Therefore, although a younger age at diagnosis is a feature of *AIP*mut+ patients, the level of AIP protein is not correlated with the age at diagnosis.

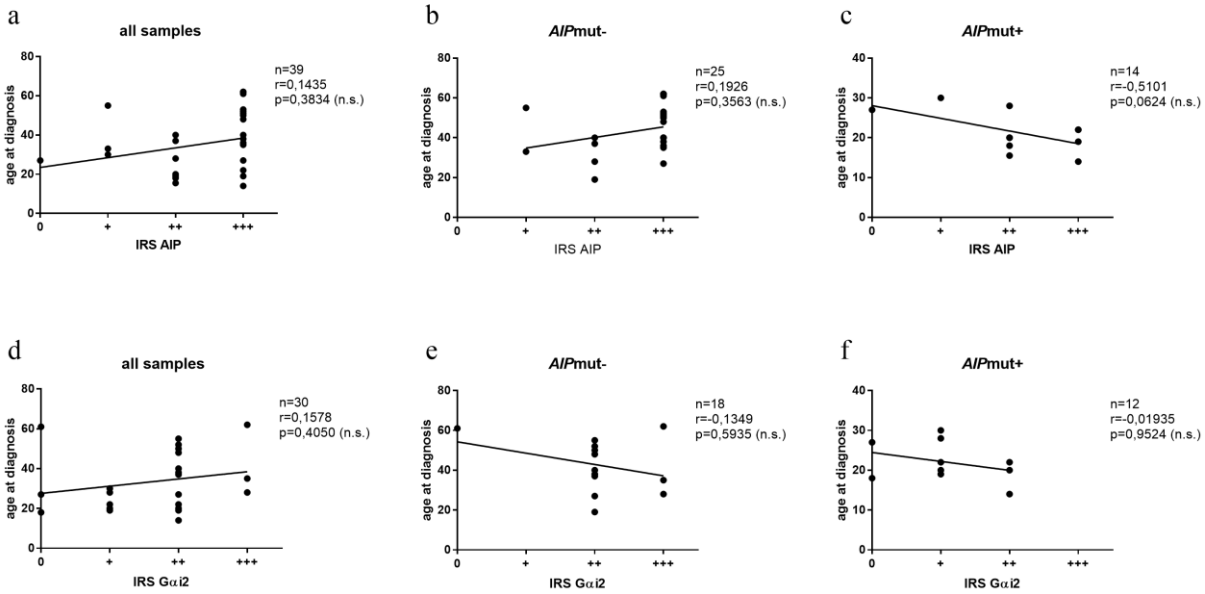

Figure 51: No dependency of the age at diagnosis on the expression levels of AIP or Gαi2. (a-c) AIP expression scores, (d-f) Gαi2 expression scores. All samples (a, d), only *AIP*mut- (b, e) or only *AIP*mut+ (c, f) were taken into the analysis. Pearson correlation coefficients and two-tailed p value were computed. Linear regression was applied on the correlation. n.s., not significant.

4 Discussion

In its cannonical function, aryl hydrocarbon receptor interacting protein (AIP) acts as a co-chaperone in cellular detoxification within the aryl hydrocarbon receptor (AhR) signaling pathway (Figure 3) [116-119]. The involvement of AIP mutations in pituitary tumorigenesis was initially reported in 2006 [81]: Germline *AIP* mutations were found to predispose to pituitary adenoma (PA) development. Since then, a multitude of studies have aimed at determining the role of AIP in pituitary tumor development. However, to date the molecular mechanisms underlying AIP-dependent tumorigenesis are only partially understood. Several studies show differential expression of miRNAs in PAs or certain PA histotypes compared to normal pituitary indicating that miRNAs are important for PA development [170-174]. AIP itself is a direct target of two miRNAs, miR-34a [191] and miR-107 [190]. In line with this, we decided to investigate whether mutation of *AIP* affects the miRNA profile of PAs.

The *AIP*mut+ samples used in this study had different mutations in AIP. The R271W mutation was by far the most prevalent mutation in our cohort, being present in seven out of 15 *AIP*mut+ PAs. Other mutations were found in only one or two samples: R56C (n=1), F269F (n=1), Q146S (n=2), L115W (n=1), R128H (n=1), M1I (n=1) and C238W (n=1). Reviewing the literature, the most common reported AIP mutations are R271W, R304X, R304Q, Q14X, F269F and R81X (Table 20). Most, albeit not all, AIP mutations are located in one of the three TPR domains at the C-terminus of the protein [107]. This also applies to R271W, which is located in the third TRP domain [14]. The TRP domains mediate protein-protein interactions [108], and residue R271 is especially vital for the interaction of AIP with PDE4A5 [112].

20 PAs were analyzed in miRNA expression arrays (8 PRL-, 12 GH-secreting; 10 *AIP*mut-, 10 *AIP*mut+). The miRNA expression arrays examined a subset of cellular miRNAs and established that some were differentially expressed between *AIP*mut+ *versus AIP*mut- tumors. The majority of these miRNAs have not been previously reported to be involved in PA formation.

Four miRNAs were subsequently validated by qRT-PCR. The expression levels of two miRNAs, namely miR-145 and miR-34a were shown to be modulated by forced overexpression of AIP-R271W compared to AIP-wt and therefore were further investigated. The AIP-R271W induced overexpression of miR-34a, and to a lesser extent of miR-145, increased the tumorigenic behavior of GH3 cells *in vitro*, increasing cell viability and migration, clonogenic potential and reducing apoptosis. In line with the features of *AIP*mut+ PA [15, 16, 19], miR-34a-overexpressing GH3 cells showed an impaired response to octreotide (Oct), concerning its influence on both cell viability

and GH secretion. The signaling pathway that mediates the increase in oncogenic features of GH3 cells was indicated as the cAMP pathway, since both cAMP levels and the activation of downstream targets such as ERK1/2 were increased upon overexpression of miR-34a in GH3 cells. *GNAI2*, encoding Gαi2 was predicted as a putative target gene of miR-34a, and direct targeting was confirmed by reporter gene assays. Gαi2 is the alpha subunit of a G proteins (guanine nucleotide binding proteins), which mediates the regulation of the adenylate cyclase. Ultimately, it was shown that expression levels of Gαi2 in AIPmut+ PAs were reduced compared to *AIP*mut- tumors.

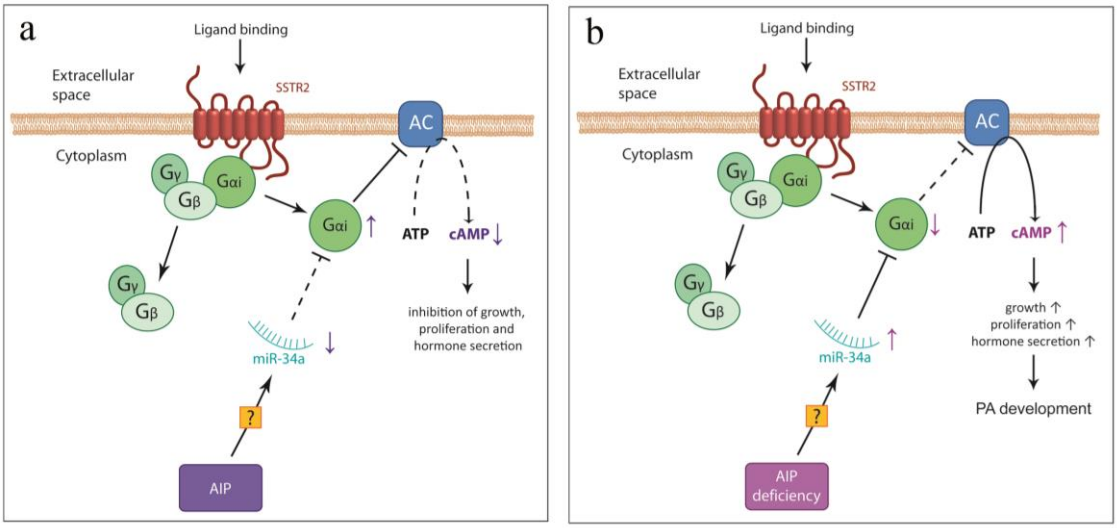

Figure 52: Model of the effect of AIP deficiency on intracellular processes. (a) physiological and (b) pathological scenario in which AIP deficiency leads to upregulation of miR-34a which in turn decreases Gαi2 levels. The inhibition of AC by Gαi2 is reduces and the AC produces non-physiological amounts of cAMP, which acts as an mitogenic signal in the cell.
Figure: Eva-Maria Bogner

4.1 AIP-R271W promotes the growth of PA cells

AIP is classified as a tumor suppressor [81] and accordingly wild-type AIP overexpression has been shown to reduce cell proliferation in three different cell lines, GH3 (lacking functional p27 protein), HEK293 (disrupted G1 regulation) and TIG3 fibroblasts [16]. In contrast, overexpression of mutant AIP-R271W promoted the growth of *Aip*-/- MEFs compared to wild-type AIP (Figure 12). This gain-of-function phenotype of mutated AIP-R271W does not fit with the classical definition of a tumor suppressor. An example of another tumor suppressor that can develop oncogenic mutations is p53. Missense mutations in the core binding domain of p53 interfere with differentiation [241, 242], apoptosis [243, 244] and growth arrest [245]. Strikingly, in patients with Li-Fraumeni syndrome tumor development occurred more often and earlier in patients with

missense mutations located in the binding core domain than in patients with truncating nonsense mutations that lead to absence or decreased levels of the protein [246]. This may also apply to AIP. Truncating mutations, like AIP-Q14X, accompanied by LOH, lead to no detectable protein expression in the tumor and therefore in this setting AIP acts as a classical tumor suppressor in the pituitary [81]. However, missense mutations, like AIP-R271W, especially when located in the TPR domains, might potentially acquire oncogenic features, which would lead to a higher incidence of tumors and an earlier age at onset in the patients. This assumption is strengthened by two findings: 1) AIP-R271W does not lead to a general loss of AIP protein expression in the tumor, but shows variable expression levels in different tumors (see below), 2) AIP-R271W increases cell viability, migration and cAMP levels *in vitro* which does not correspond to the definition of a tumor suppressor protein.

When transfected into *Aip*-/- MEFs, AIP-R271W appeared to be highly unstable. The treatment of transfected cells with cycloheximide (CHX), an inhibitor of *de novo* protein synthesis, led to a marked reduction of AIP-R271W levels already after 4 hours establishing that the mutant protein is quickly degraded (Figure 14). Given that the proteasome inhibitor epoxomicin (EPOX) partially rescued AIP-R271W levels in MEF cells, the mutant protein is presumably degraded at least in part by the proteasome (Figure 15). Our results showing low AIP-R271W *in vitro* stability are in agreement with a study of Hernández-Ramirez and colleagues [198] showing that the *in vitro* half-life of ectopic wild-type AIP transfected in HEK293 cells is 43.5 hours, whereas that of AIP-R271W was 8.2 hours. Additionally, they found a correlation between the predicted pathogenicity and the reduced half-life of the variant *in vitro* [198].

Surprisingly, we observed that tumors bearing the R271W mutation had different levels of expression of AIP (Figure 45). This suggests that the mutation is not associated to a loss of heterozygosity (LOH) of the wt allele. The reason why AIP has been initially classified as a tumor suppressor was that LOH was detected in patients with the AIP-Q14X variant [81]. Several studies also identified LOH in the tumor tissue of *AIP*mut+ PA patients [16, 17, 21, 22, 86, 89, 132, 199, 202, 210, 211, 215, 218, 222, 227]. On the other side, a multitude of reports have failed to find LOH in *AIP*mut+ PA patients [14, 15, 17, 20, 21, 90, 123, 203, 205, 247, 248]. Although LOH clearly is a strong hint for a more severe effect of an AIP variant on the patient's phenotype, the lack of evidence for LOH does not mean that the effect on the phenotype can be neglected. In case of AIP-R271W, the presence of LOH has not been tested [82, 92, 133, 134] or has not been found [14]. The development of tumors in *AIP*mut+ patients without LOH of the *AIP* gene may be possible since the expression of one wild-type allele may be insufficient in exerting its tumor suppressive function. This has already been described for class II tumor suppressor genes, which

are generally downregulated in the tumor compared to healthy tissue, instead of being mutated or deleted [249]. It has been assumed that impaired protein-protein interaction might mediate the tumorigenic potential of AIP mutations which might require a certain amount of functional (i.e. wild-type) AIP protein [16, 18].

4.2 miR-34a is an oncogenic miRNA (oncomiR) in PAs

Comparison of miRNA expression signatures revealed that miR-34a, amongst others, was upregulated in *AIP*mut+ compared to *AIP*mut- somatotropinomas (Figure 10). This upregulation was confirmed by qRT-PCR. We were able to show that miR-34a overexpression was at least in part mediated by mutated AIP since miR-34a was increased to a greater extent in *Aip*-/- MEFs transfected with AIP-R271W, compared to cells transfected with AIP-wt. Oncogenic features of miR-34a were investigated upon its overexpression in GH3 cells. Cells transfected with the miR-34a mimic had a significantly higher cell viability, assessed by the colorimetric WST-1 assay, compared to those transfected with an unspecific control miRNA (Figure 24). In order to assess cell proliferation independent of metabolic activity we stained transfected GH3 cells for Ki-67. In agreement with the results of the WST-1 assay, miR-34a-overexpressing cells showed elevated levels of Ki-67, confirming the higher proliferation rates (Figure 25). Conversely, miR-34a overexpression reduced apoptosis since caspase 3/7 activity was reduced in GH3 cells (Figure 28). The miR-34a-overexpressing GH3 cells also displayed a marked increase in cellular migration (Figure 26) as well as in their potential to form colonies (Figure 27). The results of the colony formation assay are of special interest since they support an oncogenic function of miR-34a in the long term in GH3 cells. Indeed, while all other assays were performed within 24 hours after transfection, the colony formation assay was analyzed seven days after transfection.

4.2.1 Dual role of miR-34a in other human cancers

In human cancers, miRNAs are often found to be globally downregulated [250]. This would suggest that these miRNAs act as tumor suppressors and, upon their downregulation, tumor development is enabled [251]. The members of the miR-34 family, namely miR-34a, miR-34b and miR-34c, were found to be directly up-regulated by p53 in wild-type and *p53*-/- MEFs [252]. Furthermore, the miR-34 family exhibited anti-proliferative behavior *in vitro* in a lung cancer and a colorectal carcinoma cell line [252]. The transcriptional activation of miR-34a by p53 has been simultaneously reported in other cell types [253-256]. Subsequently, miR-34a has been proposed to have tumor suppressor potential and to be downregulated in several tumor types, e.g. neuroblastoma [257], colon cancer [258], CLL [259], epithelial ovarian cancer [260], laryngeal carcinoma [261] and gastric cancer [262], especially after loss or mutation of p53. Within the p53

tumor suppressor network, miRNAs might be responsible for transcriptional repression of target genes indirectly mediated by p53, which is *per se* a transcriptional activator [252]. Upon cellular stressors such as DNA damage or telomere depletion p53 is activated and can in turn activate the transcription of genes [263]. These p53 target genes can either inhibit the cell cycle (p21), or inhibit the transcription of anti-apoptotic genes, (e.g. *BAX* or *BBC3* encoding PUMA) [264], therefore leading to death of the damaged cells. The targeting of miR-34a by p53 can be integrated into this model since miR-34a has been shown to target for example E2F3, a transcriptional inducer of cell cycle progression [257]. Therefore, miR-34a targets the same cellular pathways as p21 and complements its function. BAX and PUMA both inhibit BCL2, which is also a target of miR-34a [265] exhibiting also a synergistic role of the two pathways in increasing apoptosis. In addition, miR-34a targets and down-regulates known oncogenes such as c-MET [266] and MYC [267].

In contrast to the literature discussed above, other evidence shows miR-34a to be acting as an oncomiR. In gastric cancer [268] and in neoplasms of the central nervous system, including medulloblastoma [269], astrocytoma [270] and ependymoma [271] miR-34a has been shown to be overexpressed [272]. In transformed mycosis fungoides (T-MF), a cutaneous T-cell lymphoma, miR-34a was upregulated compared to normal control skin tissue [273, 274]. Elevated serum miR-34a levels have been described in patients with breast cancer [196], gastric cancer [275] and B cell lymphoma [276]. In osteosarcoma cell lines, miR-34a promotes chemoresistance [277, 278], and increased miR-34a expression was associated with docetaxel resistance in breast cancer cell lines [279]. These reports, together with the current study, indicate that miR-34a can also behave as an oncomiR, possibly in a cell type or mutation-dependent context.

Several other miRNAs have been described to act as oncomiRs or tumor suppressors depending on the context. miR-125b was shown to be an oncomiR in hematopoietic malignancies [250, 280, 281] but to behave as a tumor suppressor in solid tumors such as ovarian cancer [282] and hepatocellular carcinoma [283, 284]. This dual behavior may be explained by the multitude of genes, comprising both oncogenes and tumor suppressor genes that are targeted by one miRNA. The availability of certain target genes, or subsets of genes, and their expression level in a given tissue dictate whether a miRNA will promote or inhibit tumor initiation and progression [285]. Surprisingly, miRNAs can also have opposing functions within the same cell type. Perez-Añorve and colleagues [286] discovered a role for miR-122 as a tumor suppressor in parental breast cancer cells, while when the same cells acquire radioresistance, miR-122 acts as an oncomiR. They conclude that the change in miR-122 functions as a molecular adaptation to radiotherapy [286].

4.2.2 Dual role of miR-34a in PAs

Recently, an anti-proliferative and pro-apoptotic function of miR-34a in PA cells *in vitro* has been reported [287]. In that study, Yang *et al* report a downregulation of miR-34a in GH4C1 cells, a rat pituitary tumor cell line derived from GH3 cells [288], when compared to normal rat pituitary tissue. Ectopic overexpression of miR-34a was shown to inhibit GH4C1 cell proliferation, from day three to day five post-transfection. Clonogenic potential was impaired upon miR-34a overexpression. In line with these findings, apoptosis was induced by miR-34a in GH4C1 cells [287]. SOX7, a transcription factor gene that has been described both as an oncogene and a tumor suppressor gene in different cell types, was predicted and validated as a target of miR-34a in these cells and knock-down of SOX7 also decreased proliferation and induced apoptosis [287]. The discrepancy between these published results and our study may be explained by the different cell lines used. GH4C1 cells produce much lower basal levels of GH compared to GH3 cells [289]. In addition, they react differently towards IGF-1 stimulation: in GH3 cells, both GH and PRL mRNA levels are decreased upon IGF-1 treatment, while in GH4C1 cells PRL mRNA increased and GH mRNA levels were unaffected [289]. The decrease of GH mRNA expression and GH secretion upon IGF-1 stimulation has also been described in rat primary pituitary cells [290] and human primary pituitary tumor cells [291]. GH3 cells express higher levels of Magmas mRNA and protein compared to GH4C1 [292]. The levels of Magmas expression in GH4C1 is comparable to the levels in normal pituitary. The difference in Magmas expression leads to a reduced induction of apoptosis in GH3 compared to GH4C1 cells in response to Staurosporine treatment, as well as to improved cell viability in GH3 cells [292]. These profoundly different behaviors of GH3 and GH4C1 cells concerning cell viability and apoptosis upon Staurosporine treatment might be another hint that explains the conflicting results between our study and the report by Yang *et al* [287]. Apart from the different cell lines used, Yang and colleagues also investigated the effects of miR-34a in a different time frame when compared with our study. We focused on short-term (up to 24h) effects of miR-34a overexpression in order to capture the direct consequences of miR-34a modulation. While within this short time frame the effect of the miRNA are observable, analysis of long-term effects, as done by Yang *et al,* might be weakened by downstream, or even compensatory effects that are triggered as a cellular response towards modulation of miRNA levels.

Most interestingly, an oncogenic role of miR-34a in PA cells has already been described. Denes and colleagues found miR-34a to be highly expressed in sporadic somatotropinoma samples with low AIP expression levels [191]. They found a trend for higher miR-34a levels in invasive *versus* non-invasive somatotropinomas, with low miR-34a expression inversely correlating with disease

control after SSA treatment (OCT-LAR). Furthermore, they showed that miR-34a directly targets AIP in HEK293 cells [191].

4.2.3 Functions of miR-34a depend on cellular context

The literature concerning the role of miR-34a in cancer includes conflicting reports on whether it functions as a tumor suppressor or an oncomiR (see above).

As outlined before miR-34a may have a dual function in tumorigenesis depending on the cellular circumstances. A first hint of miR-34a switching its function was delivered by Sotillo and colleagues [293, 294]. miR-34a displayed anti-apoptotic effects by downregulating p53 only upon overexpression of Myc, whereas no effect of miR-34a on p53 levels could be observed in the absence of Myc. Therefore, they postulated an oncogenic role of miR-34a only in tumors with Myc rearrangements [293]. This might extend to PAs, since Myc has already been shown to play an important role in PA development. Myc overexpression occurred in a subset of PAs, across all histotypes [295] and has been shown to be downstream of the pituitary tumor-transforming gene (PTTG) [296], therefore being an important oncogene in the pituitary. Myc expression also correlates with increased aggressiveness in NFPAs [297]. Nevertheless, no change in phosphorylation of Myc or total Myc levels was reported in NFPAs, somatotropinomas or corticotropinomas by Dworakowska *et al* [298]. Myc overexpression seems to be a specific event in a subset of PAs, in which an oncogenic role of miR-34a might be facilitated.

4.3 The oncogenic role of miR-34a is mediated by increased intracellular cAMP

Under physiological conditions, cAMP signaling plays a crucial role in the pituitary [299]. cAMP facilitates the growth response of secretory cells of the anterior pituitary to signaling of hypothalamic hormones stimulating pituitary cells. Depending on the cell type, cAMP can have a stimulating or inhibiting effect. It has been established that in somatotroph cells cAMP increases proliferation [299], while, in cells of the lactotroph and gonadodroph lineage cAMP does not, or can even negatively affect proliferation [300, 301]. Overexpression of AIP-R271W in *Aip*-/- MEFs increased intracellular cAMP levels by 2-fold when compared with AIP-wt (Figure 32). In line with this, miR-34a overexpression in GH3 cells also increased intracellular cAMP levels when compared to transfection of an unspecific control miRNA (Figure 35). Since cAMP is a mitogenic signal in somatotroph cells, these results further strengthen the pro-tumorigenic role of miR-34a in GH3 cells.

A great variety of cellular functions is regulated by cyclic monophosphates like cAMP and cGMP. Therefore, an accurate temporal and spatial control of the concentrations of these second messengers is vital for the maintenance of cellular homeostasis. PDEs catalyze the hydrolysis of cAMP to 5'AMP and of cGMP to 5'GMP, thereby ending cAMP signaling after its activation by extracellular signals [120, 121] Two AIP interaction partners are found in the PDE family, the cAMP-specific PDE4A5 [112] as well as PDE2A3, which targets both cAMP and cGMP [113]. Among the predicted targets of miR-34a, which are relevant for cyclic monophosphate signaling are several members of the PDE family (Table 26).

AIP can be linked to the cAMP signaling pathway via its interaction partners, which partners can be found amongst PDEs [112, 113], G-protein subunits [114] as well as the cAMP-dependent protein kinase (PKA) [302]. AIP itself indirectly regulates cAMP levels and GH release in GH3 cells in a PDE-independent fashion. In these cells, wild-type AIP suppressed the forskolin-induced cAMP increase and the subsequent secretion of GH [233]. The negative impact of wt AIP on cAMP levels in somatotroph cells may explain its role as a tumor suppressor in this cell type. Since AIP mutations can affect its ability to bind interaction partners, mutant AIP might thereby also lose its capacity to decrease cAMP levels, which might explain its oncogenic features.

In the physiological state hypothalamic GHRH is released and binds the G-protein coupled receptor (GPCR) on the surface of somatotroph pituitary cells which causes the activation of the adenylate cyclase (AC) via the Gαs subunit [303]. G-proteins have been initially linked to PA tumorigenesis since approximately one third of sporadic somatotropinomas harbor gain-of-function mutation in the *GNAS* gene, encoding Gαs [43, 304]. These mutations turns *GNAS* into the *gsp* oncogene that causes constitutive activation of AC in the absence of hormone binding and therefore constant cAMP production [305]. Two members of the G-protein family have been reported to interact directly with AIP, Gα13 and Gαq [114]. The interaction of AIP with Gα13 inhibits the interaction of AIP with AhR, thereby prohibiting the AhR-mediated transcription and destabilizing AhR [114].

Tuominen *et al* [125] reported that the increase in cAMP levels in response to AIP deficiency they observed in *Aip*-/- MEFs was due to defective Gαi2 and Gαi3 proteins. These proteins usually limit stimulated cAMP production by inhibiting AC [238]. Gαi1-3 proteins mediate AC inhibition following hormonal stimulation leading to decreased cAMP levels, [306, 307] Gαi2, but not Gαi3 expression was reduced in both human *AIP*mut+ (n=4 *versus* 4 *AIP*mut-) and murine *Aip*-/- somatotropinomas [125]. Interestingly no loss-of-function mutations in the *GNAI1-3* loci have been identified in PAs

so far [308]. We expanded on the previously reported association between AIP and Gαi2 expression levels [199] by analyzing a larger cohort of patients (*AIP*mut+: n=12; *AIP*mut-: n=18).

Significantly, we found *GNAI2* to be among the predicted targets of miR-34a and we could prove direct targeting of *GNAI2* mRNA by miR-34a (Figure 40). Collectively, these results are in agreement with our hypothesis that miR-34a is upregulated upon AIP mutation/deficiency and subsequently directly targets *GNAI2,* thereby decreasing Gαi2 levels. Upon ligand binding, e.g. by somatostatin or SSAs, lower Gαi2 levels cannot effectively limit AC, and this in turn leads to excessive accumulation of intracellular cAMP, which in turn increases growth and proliferation, and ultimately leads to somatotropinoma development and progression (Figure 52).

A downstream target of cAMP known to be regulated by G-proteins and able to mediate cell proliferation is ERK1/2 [235]. cAMP can either activate or inhibit ERK1/2 in a cell type-dependent manner [235]. Besides the already mentioned pituitary cell types in which cAMP inhibits proliferation, also in adipocytes [309], endothelial cells [310] and hepatocytes [311] cAMP causes an inhibition of ERK1/2 and therefore a decrease in cell proliferation. On the other hand, in many cancer cells, such as LnCaP (human prostate cancer cells) [312], GH3/GH4C1 [313] and PC12 (pheochromocytoma cells) [314] cAMP activates ERK1/2 and therefore acts as a mitogenic signal. In human primary cultures of somatotropinomas and NFPAs, GHRH- and forskolin (FSK)-induced cAMP signaling increased ERK1/2 activity, with FSK doing so specifically in somatotropinomas. In line with these findings, we were able to show that miR-34a, which itself increased intracellular cAMP levels, also promoted ERK1/2 phosphorylation in GH3 cells (Figure 36). In contrast, previous studies have reported that cAMP does not increase ERK1/2 phosphorylation in a small sample of *AIP*mut+ somatotropinomas when compared to *AIP*mut- somatotropinomas [125]. Further analysis on primary PAs with or without *AIP* mutations are required to clarify whether cAMP acts through ERK1/2 in these tumors.

4.4 miR-34a impairs the therapeutic response to octreotide

Low AIP expression and the presence of AIP mutations in PA patients are predictors of resistance to first generation SSAs [315-318]. According to our hypothesis, miR-34a may mediate some clinical characteristics of *AIP*mut+ PAs, such as the increased aggressiveness and the impaired therapy response. Our studies of GH3 cells transfected with an unspecific miRNA or with a miR-34a mimic and then treated with octreotide support this hypothesis. Indeed, we observed that the octreotide-mediated suppression of cell proliferation and GH secretion was abolished upon overexpression of miR-34a (Figure 29, Figure 30). These results show that miR-34a may play an important role in mediating the response of GH3 cells to SSAs.

A suboptimal therapy response in PA patients results in no or marginal disease control, defined by no normalization of secreted hormones and no tumor shrinkage [15, 16, 19]. Since SSAs target SSTRs in order to mimic the inhibitory effect of somatostatin on hormone secretion and cell growth, one may hypothesize that increased expression of SSTRs, and especially of SSTR2, the main target of first generation SSAs, may play a role in the lack of therapy response. However, Chahal *et al* were able to prove that a reduction in SSTR expression was not the reason for the impaired therapy response in *AIP*mut+ PAs to SSAs [126].

AIP has long been believed to play an important role in SSA responses since AIP staining intensity positively correlated with SSA responsiveness [315], and AIP protein levels were upregulated in patients after lanreotide treatment [126]. Loss of another tumor suppressor, ZAC/Zac1 (PLAG1, Pleiomorphic Adenoma Gene-Like 1) was also reported to be involved in limiting the therapy response to SSAs. ZAC is highly expressed in normal pituitary tissue, whereas its expression in most PAs is downregulated [50]. In GH3 cells, octreotide treatment upregulated Zac1 and knockdown of Zac1 abolished the antiproliferative effect of octreotide [17, 51]. Overexpression of wild-type but not mutant AIP increased Zac1 expression, whereas AIP knockdown decreases it while also increasing cell viability and clonogenic potential of GH3 cells [126]. These results indicate a link between AIP and ZAC in mediating SSA effects in the tumor cells. Pertussis toxin (PT) treatment of the cells prevents Zac1 upregulation, which implicates that the increase in Zac1 protein levels in response to SSAs is mediated by Gαi subunits [51]. PT causes the ADP-ribosylation of Gαi subunits, therefore keeping these subunits in an inactive state, in which they cannot inhibit AC and in turn cannot decrease intracellular cAMP levels [319]. Gαi subunits are involved in somatostatin signal transduction and subsequent AC inhibition following hormonal stimulation leading to decreased cAMP levels [306, 307, 320, 321]. Finally, somatostatin treatment has been shown to activate the ERK1/2 pathway [322, 323]. With the current study yet another component is added to this network. miR-34a was shown to directly target the 3'UTR of rat *Gnai2* (Figure 40). Downregulation of *GNAI2* expression by miR-34a, which is itself upregulated in *AIP*mut+ PAs, might explain the reduced expression of Gαi2 in *AIP*mut+ PAs that has been observed by us (Figure 43, Figure 44) and others [125].

4.5 Expression of AIP and Gαi2 in somatotropinomas

To our knowledge this is the first study examining AIP expression levels in a large collection of *AIP*mut+ PA samples. Previous studies reported that AIP mutations were usually accompanied by a reduction or even loss of AIP expression levels in the tumor tissues [15, 17, 81, 206]. We were not able to confirm these results, since in our sample series *AIP*mut+ PAs did not exhibit reduced

AIP IHC scores (Figure 43b). Nevertheless, when exclusively considering somatotropinomas, a trend for a reduction in AIP IHC scores can be observed in the mutant samples although it is not significant (Figure 43d).

Surprisingly, we found variable levels of AIP expression in tumors of patients carrying the same AIP mutation (R271W) (Figure 45a). It is clear that the R271W missense mutation is not generally associated to a loss of AIP expression. The retained expression of AIP in *AIP*mut+ cases might be due to the retention of the wt allele of AIP which is expressed when no LOH is present in the tumor cells. It is also possible, that some mutations, like the missense mutation AIP-R271W, do not lead to a loss of protein expression in the tumor cells, and this would result in the expression of the mutant protein. This might indicate a gain-of function effect in addition to an impaired protein-protein interaction. This is supported by our findings of an increase in cell proliferation upon overexpression of AIP-R271W in *Aip*-/- MEFs. Further studies are needed to clarify this implication. Concerning *AIP*mut- patients, AIP expression was significantly higher in somatotropinomas compared to prolactinomas, whereas no significant reduction could be observed within the *AIP*mut+ patient group (Figure 47b, c). A possible explanation might be that the overall AIP expression is already reduced in *AIP*mut+ *versus AIP*mut- somatotropinoma cases. Therefore, *AIP*mut+ somatotropinomas approximate the Gαi2 and AIP expression levels of prolactinoma samples, which attenuates the effect between somatotropinomas and prolactinomas within the *AIP*mut+ patient group. The trend towards a negative correlation between AIP expression score and tumor size (Figure 49b) is in line with previous reports, in which a correlation has in fact been described [318, 324, 325]. An important feature of aggressive tumors is the ability to grow invasively. AIP scores were significantly lower in invasive PAs in *AIP*mut- samples than in non-invasive samples (Figure 50b). *AIP*mut+ samples showed no reduction in AIP or scores in invasive *versus* non-invasive PAs (Figure 50c).

In case of Gαi2 IHC, we can confirm and extend previous studies reporting that *AIP* mutations are accompanied by a reduction in Gαi2 expression levels [125, 199]. A reduction of Gαi2 expression in *AIP*mut+ compared to *AIP*mut- cases was evident when either somatotropinomas or prolactinomas were analyzed (Figure 43a), but was even more pronounced by only considering the somatotropinomas (Figure 44a). As already described for AIP, Gαi2 IHC scores were variable in different patients carrying the same mutation (R271W) (Figure 45b). Gαi2 scores were significantly higher in somatotropinomas compared to proactinomas in *AIP*mut-, but not in *AIP*mut+ patients (Figure 47e, f). As described before for AIP, the reason for this might be the already reduces Gαi2 expression in *AIP*mut+ somatotropinomas, leading to equal expression levels of Gαi2 in somatotropinomas and prolactinomas. Another parallel between Gαi2 and AIP

expression levels is that Gαi2 levels are reduced in invasive, compared to non-invasive PAs only in *AIP*mut+ patients.

AIP and Gαi2 IHC scores were positively correlated in *AIP*mut- but not in *AIP*mut+ patients (Figure 46). This might be due to the generally lower Gαi2 expression in *AIP*mut+ *versus AIP*mut- patients. Similar findings have already been published in a cohort of somatotropinomas by Ritvonen e*t al* [199]. In contrast, *AIP*mut+ PAs do not show a significant correlation. Decreased Gαi2 expression was associated with a trend towards reduced AIP expression levels, and this is known to be a predictor for impaired therapy response to SSAs. These results suggest a role of Gαi2 in SSA response, but further studies are needed in order to clarify the underlying mechanism.

4.6 The link between AIP and miR-34a

Our finding that miR-34a is a regulator of Gαi2 nicely complements already published data on the regulation of AIP expression by miR-34a. An association between the miRNA expression and *AIP* mutation status has been demonstrated in *Aip*-/- MEFs (Figure 17). Since AIP itself does not have a DNA-binding domain, we propose that the regulation of miR-34a must be indirect. Preliminary analysis revealed that several aryl hydrocarbon response elements (AHRE) are located in the vicinity of the rat MiR34a promoter (data not shown). This might imply a possible regulation of miR-34a by ARNT, a binding partner of AhR (Figure 3). Since ARNT is downregulated both in tumor tissue of *Aip*-/- mice [240] and in GH3 cells after AIP silencing [239], it could also be reduced in *AIP*mut+ cells. Further experiments are needed to clarify this issue.

4.7 Conclusion and outlook

In summary, our experiments reveal that in *AIP*mut+ PAs the expression of miR-34a was upregulated and has oncogenic potential. Overexpression of miR-34a was shown to impair therapy response to SSAs, accompanied by a modulation of cAMP levels in transfected PA cells. The miR-34a directly targets *Gnai2*. Gαi2 is downregulated in *AIP*mut+ compared to *AIP*mut- primary somatotropinomas and prolactinomas.

miR-34a has been extensively described to be a tumor suppressor in a variety of cancers and is currently under examination for applications in cancer therapy. Our results draw attention to the fact that miR-34a has an oncogenic function in PA cells, as well as in other cell types. Therefore, the use of miR-34a overexpression for therapeutic purposes has to be pursued with great caution. Our results are helpful in strengthening the connection between AIP and Gαi2, which has been already described in PAs. By providing a functional model for downregulation of Gαi2 in PA cells, our study contributes to clarifying the molecular mechanisms by which the therapy response is

impaired in *AIP*mut+ PAs. Therefore, we can only speculate that wt AIP directly or indirectly influences miR-34a in somatotroph cells leading to relatively low levels of miR-34a. The mechanism by which this interaction takes place remains to be uncovered. Gαi2 is directly targeted by miR-34a. Therefore, upon miR-34a downregulation Gαi2 levels in the cells increase. Since Gαi2 inhibits AC, the increased levels of Gαi2 due to AIP loss would lead to a decrease in intracellular cAMP levels after binding of a ligand to the GPCR with which Gαi2 is associated. cAMP acts as a mitogen in somatotroph cells of the pituitary, hence it reduces proliferation and limits hormone secretion from these cells (Figure 52a). However, in case of AIP deficiency (mutation or loss of the *AIP* gene), miR-34a is available at high levels is the cells. This leads to increased transcriptional inhibition of Gαi2 expression. Accordingly, inhibition of AC by Gαi2 is impaired, causing an excess of cAMP. cAMP increases proliferation and hormone secretion of somatotroph pituitary cells and ultimately leads to the development of PA (Figure 52b).

We have demonstrated that AIP-R271W, leads to an upregulation of miR-34a and Denes and colleagues [191] show that wt AIP is a direct target and therefore downregulated by miR-34a. Taking these two studies together we hypothesize that mutant AIP indirectly downregulates wt AIP via upregulation of miR-34a, which further facilitates the pro-tumorigenic potential of the mutant protein. In addition, we propose that AIP-R271W is an oncogenic mutation of the tumor suppressor AIP which increases *in vitro* tumorigenic behavior by indirectly increasing cAMP signaling. In patients with this mutation tumor development might not only be facilitated by the loss of the wt AIP tumor suppressor but in addition by the mitogenic signaling which is caused by AIP-R271W.

The mechanism of AIP-dependent tumorigenesis is still not fully elucidated. As already proposed, a possible regulation of miR-34a by ARNT can be tested in the future. Since only octreotide, a first generation SSA, was used in our study, repeating the therapy response experiments with multi-receptor SSAs, like pasireotide, is of great interest. Pasireotide targets several SSTRs and has been shown to be more effective than octreotide in *AIP*mut+ PA patients. Assessment of the therapy response to multi-receptor SSAs would clarify whether the loss of treatment efficacy we observed in GH3 cells upon miR-34a overexpression is limited tp SSAs specifically targeting SSTR2. In order to clarify whether only one or both alleles are expressed in the *AIP*mut+ PAs LOH analysis can be done so the competing presence of wt AIP can be ruled out. Alternatively, wt and mutant alleles can be distinguished by (q)RT-PCR to see whether mutation of AIP can lead to the expression of the protein.

Our model of the effect of AIP deficiency in regulating miR-34a and, further downstream, Gαi2, depicted in Figure 52, may help to discover novel therapeutic targets, which regulate cAMP levels in PA cells. These might be members of the G-protein family, like Gαi2, which directly reduces cAMP levels by inhibiting the AC: Targeting these or related components of the cAMP pathway might help to overcome the resistance to SSAs observed in many *AIP*mut+ PA patients.

5 List of Figures

6 List of Tables

7 Literature

1. Larkin, S. and O. Ansorge, *Development And Microscopic Anatomy Of The Pituitary Gland*, in *Endotext*, K.R. Feingold, et al., Editors. 2000: South Dartmouth (MA).
2. Bargmann, W. and E. Scharrer, *The site of origin of the hormones of the posterior pituitary.* Am Sci, 1951. **39**(2): p. 255-9.
3. Scharrer, E., *Neurosecretion and anterior pituitary in the dog.* Experientia, 1954. **10**(6): p. 264-6.
4. Bear, M.H. and P.C. Bollu, *Neuroanatomy, Hypothalamus*, in *StatPearls*. 2019: Treasure Island (FL).
5. Guillemin, R., *Hypothalamic hormones a.k.a. hypothalamic releasing factors.* J Endocrinol, 2005. **184**(1): p. 11-28.
6. Yeung, C.M., et al., *Cells of the anterior pituitary.* Int J Biochem Cell Biol, 2006. **38**(9): p. 1441-9.
7. Rinehart, J.F. and M.G. Farquhar, *The fine vascular organization of the anterior pituitary gland; an electron microscopic study with histochemical correlations.* Anat Rec, 1955. **121**(2): p. 207-39.
8. Inoue, K., et al., *The structure and function of folliculo-stellate cells in the anterior pituitary gland.* Arch Histol Cytol, 1999. **62**(3): p. 205-18.
9. Alexander, J.M., et al., *Clinically nonfunctioning pituitary tumors are monoclonal in origin.* J Clin Invest, 1990. **86**(1): p. 336-40.
10. Herman, V., et al., *Clonal origin of pituitary adenomas.* J Clin Endocrinol Metab, 1990. **71**(6): p. 1427-33.
11. Gsponer, J., et al., *Diagnosis, treatment, and outcome of pituitary tumors and other abnormal intrasellar masses. Retrospective analysis of 353 patients.* Medicine (Baltimore), 1999. **78**(4): p. 236-69.
12. Arafah, B.M. and M.P. Nasrallah, *Pituitary tumors: pathophysiology, clinical manifestations and management.* Endocr Relat Cancer, 2001. **8**(4): p. 287-305.
13. Daly, A.F., et al., *Clinical characterization of familial isolated pituitary adenomas.* J Clin Endocrinol Metab, 2006. **91**(9): p. 3316-23.
14. Daly, A.F., et al., *Aryl hydrocarbon receptor-interacting protein gene mutations in familial isolated pituitary adenomas: analysis in 73 families.* J Clin Endocrinol Metab, 2007. **92**(5): p. 1891-6.
15. Georgitsi, M., et al., *Molecular diagnosis of pituitary adenoma predisposition caused by aryl hydrocarbon receptor-interacting protein gene mutations.* Proc Natl Acad Sci U S A, 2007. **104**(10): p. 4101-5.
16. Leontiou, C.A., et al., *The role of the aryl hydrocarbon receptor-interacting protein gene in familial and sporadic pituitary adenomas.* J Clin Endocrinol Metab, 2008. **93**(6): p. 2390-401.
17. Jaffrain-Rea, M.L., et al., *Expression of aryl hydrocarbon receptor (AHR) and AHR-interacting protein in pituitary adenomas: pathological and clinical implications.* Endocr Relat Cancer, 2009. **16**(3): p. 1029-43.
18. Igreja, S., et al., *Characterization of aryl hydrocarbon receptor interacting protein (AIP) mutations in familial isolated pituitary adenoma families.* Hum Mutat, 2010. **31**(8): p. 950-60.
19. Daly, A.F., et al., *Clinical characteristics and therapeutic responses in patients with germ-line AIP mutations and pituitary adenomas: an international collaborative study.* J Clin Endocrinol Metab, 2010. **95**(11): p. E373-83.
20. Cazabat, L., et al., *Germline AIP mutations in apparently sporadic pituitary adenomas: prevalence in a prospective single-center cohort of 443 patients.* J Clin Endocrinol Metab, 2012. **97**(4): p. E663-70.
21. Cai, F., et al., *Screening for AIP gene mutations in a Han Chinese pituitary adenoma cohort followed by LOH analysis.* Eur J Endocrinol, 2013. **169**(6): p. 867-84.

22. Araujo, P.B., et al., *AIP mutations in Brazilian patients with sporadic pituitary adenomas: a single-center evaluation.* Endocr Connect, 2017. **6**(8): p. 914-925.
23. Tuncer, F.N., et al., *Screening of AIP Gene Variations in a Cohort of Turkish Patients with Young-Onset Sporadic Hormone-Secreting Pituitary Adenomas.* Genet Test Mol Biomarkers, 2018.
24. Cushing, H., *III. Partial Hypophysectomy for Acromegaly: With Remarks on the Function of the Hypophysis.* Ann Surg, 1909. **50**(6): p. 1002-17.
25. Colao, A., et al., *Systemic complications of acromegaly: epidemiology, pathogenesis, and management.* Endocr Rev, 2004. **25**(1): p. 102-52.
26. Jane, J.A., Jr., M.P. Catalino, and E.R. Laws, Jr., *Surgical Treatment of Pituitary Adenomas*, in *Endotext*, K.R. Feingold, et al., Editors. 2000: South Dartmouth (MA).
27. Rim, C.H., et al., *Radiotherapy for pituitary adenomas: long-term outcome and complications.* Radiat Oncol J, 2011. **29**(3): p. 156-63.
28. Loeffler, J.S. and H.A. Shih, *Radiation therapy in the management of pituitary adenomas.* J Clin Endocrinol Metab, 2011. **96**(7): p. 1992-2003.
29. Ji, Y., R.I. Vogel, and E. Lou, *Temozolomide treatment of pituitary carcinomas and atypical adenomas: systematic review of case reports.* Neurooncol Pract, 2016. **3**(3): p. 188-195.
30. Syro, L.V., et al., *65 YEARS OF THE DOUBLE HELIX: Treatment of pituitary tumors with temozolomide: an update.* Endocr Relat Cancer, 2018. **25**(8): p. T159-T169.
31. Giustina, A., et al., *Guidelines for the treatment of growth hormone excess and growth hormone deficiency in adults.* J Endocrinol Invest, 2008. **31**(9): p. 820-38.
32. van der Lely, A.J., et al., *Long-term safety of pegvisomant in patients with acromegaly: comprehensive review of 1288 subjects in ACROSTUDY.* J Clin Endocrinol Metab, 2012. **97**(5): p. 1589-97.
33. Sandret, L., P. Maison, and P. Chanson, *Place of cabergoline in acromegaly: a meta-analysis.* J Clin Endocrinol Metab, 2011. **96**(5): p. 1327-35.
34. Casanueva, F.F., et al., *Guidelines of the Pituitary Society for the diagnosis and management of prolactinomas.* Clin Endocrinol (Oxf), 2006. **65**(2): p. 265-73.
35. Melmed, S., et al., *Diagnosis and treatment of hyperprolactinemia: an Endocrine Society clinical practice guideline.* J Clin Endocrinol Metab, 2011. **96**(2): p. 273-88.
36. Dai, C., et al., *The Treatment of Refractory Pituitary Adenomas.* Front Endocrinol (Lausanne), 2019. **10**: p. 334.
37. Colao, A., et al., *Medical therapy for clinically non-functioning pituitary adenomas.* Endocr Relat Cancer, 2008. **15**(4): p. 905-15.
38. Colao, A., et al., *A 12-month phase 3 study of pasireotide in Cushing's disease.* N Engl J Med, 2012. **366**(10): p. 914-24.
39. Fleseriu, M., et al., *Mifepristone, a glucocorticoid receptor antagonist, produces clinical and metabolic benefits in patients with Cushing's syndrome.* J Clin Endocrinol Metab, 2012. **97**(6): p. 2039-49.
40. Vilar, L., et al., *Effectiveness of cabergoline in monotherapy and combined with ketoconazole in the management of Cushing's disease.* Pituitary, 2010. **13**(2): p. 123-9.
41. Bertagna, X. and L. Guignat, *Approach to the Cushing's disease patient with persistent/recurrent hypercortisolism after pituitary surgery.* J Clin Endocrinol Metab, 2013. **98**(4): p. 1307-18.
42. Beck-Peccoz, P., et al., *2013 European thyroid association guidelines for the diagnosis and treatment of thyrotropin-secreting pituitary tumors.* Eur Thyroid J, 2013. **2**(2): p. 76-82.
43. Landis, C.A., et al., *GTPase inhibiting mutations activate the alpha chain of Gs and stimulate adenylyl cyclase in human pituitary tumours.* Nature, 1989. **340**(6236): p. 692-6.
44. Weinstein, L.S., et al., *Activating mutations of the stimulatory G protein in the McCune-Albright syndrome.* N Engl J Med, 1991. **325**(24): p. 1688-95.

45. Hibberts, N.A., et al., *Analysis of cyclin D1 (CCND1) allelic imbalance and overexpression in sporadic human pituitary tumors.* Clin Cancer Res, 1999. **5**(8): p. 2133-9.
46. Simpson, D.J., et al., *Hypermethylation of the p16/CDKN2A/MTSI gene and loss of protein expression is associated with nonfunctional pituitary adenomas but not somatotrophinomas.* Genes Chromosomes Cancer, 1999. **24**(4): p. 328-36.
47. Kirsch, M., et al., *Frequent loss of the CDKN2C (p18INK4c) gene product in pituitary adenomas.* Genes Chromosomes Cancer, 2009. **48**(2): p. 143-54.
48. Buckley, N., et al., *P53 protein accumulates in Cushings adenomas and invasive non-functional adenomas.* J Clin Endocrinol Metab, 1995. **80**(2): p. 4 p following 692.
49. Harvey, M., et al., *Mice deficient in both p53 and Rb develop tumors primarily of endocrine origin.* Cancer Res, 1995. **55**(5): p. 1146-51.
50. Pagotto, U., et al., *The expression of the antiproliferative gene ZAC is lost or highly reduced in nonfunctioning pituitary adenomas.* Cancer Res, 2000. **60**(24): p. 6794-9.
51. Theodoropoulou, M., et al., *Octreotide, a somatostatin analogue, mediates its antiproliferative action in pituitary tumor cells by altering phosphatidylinositol 3-kinase signaling and inducing Zac1 expression.* Cancer Res, 2006. **66**(3): p. 1576-82.
52. Scheithauer, B.W., et al., *Pituitary adenomas of the multiple endocrine neoplasia type I syndrome.* Semin Diagn Pathol, 1987. **4**(3): p. 205-11.
53. Vasilev, V., et al., *Familial pituitary tumor syndromes.* Endocr Pract, 2011. **17 Suppl 3**: p. 41-6.
54. Tichomirowa, M.A., A.F. Daly, and A. Beckers, *Familial pituitary adenomas.* J Intern Med, 2009. **266**(1): p. 5-18.
55. Wermer, P., *Genetic aspects of adenomatosis of endocrine glands.* Am J Med, 1954. **16**(3): p. 363-71.
56. Larsson, C., et al., *Multiple endocrine neoplasia type 1 gene maps to chromosome 11 and is lost in insulinoma.* Nature, 1988. **332**(6159): p. 85-7.
57. Chandrasekharappa, S.C., et al., *Positional cloning of the gene for multiple endocrine neoplasia-type 1.* Science, 1997. **276**(5311): p. 404-7.
58. Skogseid, B., et al., *Multiple endocrine neoplasia type 1: a 10-year prospective screening study in four kindreds.* J Clin Endocrinol Metab, 1991. **73**(2): p. 281-7.
59. Burgess, J.R., et al., *Spectrum of pituitary disease in multiple endocrine neoplasia type 1 (MEN 1): clinical, biochemical, and radiological features of pituitary disease in a large MEN 1 kindred.* J Clin Endocrinol Metab, 1996. **81**(7): p. 2642-6.
60. Fritz, A., et al., *Recessive transmission of a multiple endocrine neoplasia syndrome in the rat.* Cancer Res, 2002. **62**(11): p. 3048-51.
61. Piotrowska, K., et al., *Mapping of a novel MEN-like syndrome locus to rat chromosome 4.* Mamm Genome, 2004. **15**(2): p. 135-41.
62. Pellegata, N.S., et al., *Germ-line mutations in p27Kip1 cause a multiple endocrine neoplasia syndrome in rats and humans.* Proc Natl Acad Sci U S A, 2006. **103**(42): p. 15558-63.
63. Georgitsi, M., et al., *Germline CDKN1B/p27Kip1 mutation in multiple endocrine neoplasia.* J Clin Endocrinol Metab, 2007. **92**(8): p. 3321-5.
64. Molatore, S., et al., *A novel germline CDKN1B mutation causing multiple endocrine tumors: clinical, genetic and functional characterization.* Hum Mutat, 2010. **31**(11): p. E1825-35.
65. Sambugaro, S., et al., *Early onset acromegaly associated with a novel deletion in CDKN1B 5'UTR region.* Endocrine, 2015. **49**(1): p. 58-64.
66. Carney, J.A., et al., *Dominant inheritance of the complex of myxomas, spotty pigmentation, and endocrine overactivity.* Mayo Clin Proc, 1986. **61**(3): p. 165-72.
67. Casey, M., et al., *Identification of a novel genetic locus for familial cardiac myxomas and Carney complex.* Circulation, 1998. **98**(23): p. 2560-6.

68. Casey, M., et al., *Mutations in the protein kinase A R1alpha regulatory subunit cause familial cardiac myxomas and Carney complex.* J Clin Invest, 2000. **106**(5): p. R31-8.
69. Kirschner, L.S., et al., *Mutations of the gene encoding the protein kinase A type I-alpha regulatory subunit in patients with the Carney complex.* Nat Genet, 2000. **26**(1): p. 89-92.
70. Stratakis, C.A., et al., *Carney complex, a familial multiple neoplasia and lentiginosis syndrome. Analysis of 11 kindreds and linkage to the short arm of chromosome 2.* J Clin Invest, 1996. **97**(3): p. 699-705.
71. Verloes, A., et al., *Familial acromegaly: case report and review of the literature.* Pituitary, 1999. **1**(3-4): p. 273-7.
72. Pestell, R.G., F.P. Alford, and J.D. Best, *Familial acromegaly.* Acta Endocrinol (Copenh), 1989. **121**(2): p. 286-9.
73. Tanaka, C., et al., *Absence of germ-line mutations of the multiple endocrine neoplasia type 1 (MEN1) gene in familial pituitary adenoma in contrast to MEN1 in Japanese.* J Clin Endocrinol Metab, 1998. **83**(3): p. 960-5.
74. Soares, B.S. and L.A. Frohman, *Isolated familial somatotropinoma.* Pituitary, 2004. **7**(2): p. 95-101.
75. Cameron, F.J. and G.L. Warne, *Familial Cushing's disease with severe weight loss occurring in late childhood.* J Paediatr Child Health, 1997. **33**(1): p. 74-7.
76. Salti, I.S. and I.S. Mufarrij, *Familial Cushing Disease.* Am J Med Genet, 1981. **8**(1): p. 91-4.
77. Berezin, M. and A. Karasik, *Familial prolactinoma.* Clin Endocrinol (Oxf), 1995. **42**(5): p. 483-6.
78. Yuasa, H., et al., *Familial pituitary adenoma--report of four cases from two unrelated families.* Neurol Med Chir (Tokyo), 1990. **30**(13): p. 1016-9.
79. Beckers, A., et al., *Familial isolated pituitary adenomas (FIPA) and the pituitary adenoma predisposition due to mutations in the aryl hydrocarbon receptor interacting protein (AIP) gene.* Endocr Rev, 2013. **34**(2): p. 239-77.
80. Gadelha, M.R., et al., *Isolated familial somatotropinomas: establishment of linkage to chromosome 11q13.1-11q13.3 and evidence for a potential second locus at chromosome 2p16-12.* J Clin Endocrinol Metab, 2000. **85**(2): p. 707-14.
81. Vierimaa, O., et al., *Pituitary adenoma predisposition caused by germline mutations in the AIP gene.* Science, 2006. **312**(5777): p. 1228-30.
82. Hernandez-Ramirez, L.C., et al., *Landscape of Familial Isolated and Young-Onset Pituitary Adenomas: Prospective Diagnosis in AIP Mutation Carriers.* J Clin Endocrinol Metab, 2015. **100**(9): p. E1242-54.
83. Yu, R., et al., *Aryl hydrocarbon receptor interacting protein variants in sporadic pituitary adenomas.* J Clin Endocrinol Metab, 2006. **91**(12): p. 5126-9.
84. DiGiovanni, R., et al., *AIP Mutations are not identified in patients with sporadic pituitary adenomas.* Endocr Pathol, 2007. **18**(2): p. 76-8.
85. Yarman, S., Y.D. Ogret, and F.S. Oguz, *Do the aryl hydrocarbon receptor interacting protein variants (Q228K and Q307R) play a role in patients with familial and sporadic hormone-secreting pituitary adenomas?* Genet Test Mol Biomarkers, 2015. **19**(7): p. 394-8.
86. Barlier, A., et al., *Mutations in the aryl hydrocarbon receptor interacting protein gene are not highly prevalent among subjects with sporadic pituitary adenomas.* J Clin Endocrinol Metab, 2007. **92**(5): p. 1952-5.
87. Iwata, T., et al., *The aryl hydrocarbon receptor-interacting protein gene is rarely mutated in sporadic GH-secreting adenomas.* Clin Endocrinol (Oxf), 2007. **66**(4): p. 499-502.
88. Raitila, A., et al., *No evidence of somatic aryl hydrocarbon receptor interacting protein mutations in sporadic endocrine neoplasia.* Endocr Relat Cancer, 2007. **14**(3): p. 901-6.
89. Georgitsi, M., et al., *Aryl hydrocarbon receptor interacting protein (AIP) gene mutation analysis in children and adolescents with sporadic pituitary adenomas.* Clin Endocrinol (Oxf), 2008. **69**(4): p. 621-7.

90. Buchbinder, S., et al., *Aryl hydrocarbon receptor interacting protein gene (AIP) mutations are rare in patients with hormone secreting or non-secreting pituitary adenomas.* Exp Clin Endocrinol Diabetes, 2008. **116**(10): p. 625-8.
91. Occhi, G., et al., *Prevalence of AIP mutations in a large series of sporadic Italian acromegalic patients and evaluation of CDKN1B status in acromegalic patients with multiple endocrine neoplasia.* Eur J Endocrinol, 2010. **163**(3): p. 369-76.
92. Tichomirowa, M.A., et al., *High prevalence of AIP gene mutations following focused screening in young patients with sporadic pituitary macroadenomas.* Eur J Endocrinol, 2011. **165**(4): p. 509-15.
93. Cuny, T., et al., *Genetic analysis in young patients with sporadic pituitary macroadenomas: besides AIP don't forget MEN1 genetic analysis.* Eur J Endocrinol, 2013. **168**(4): p. 533-41.
94. Preda, V., et al., *Low rate of germline AIP mutations in patients with apparently sporadic pituitary adenomas before the age of 40: a single-centre adult cohort.* Eur J Endocrinol, 2014. **171**(5): p. 659-66.
95. Lecoq, A.L., et al., *Very low frequency of germline GPR101 genetic variation and no biallelic defects with AIP in a large cohort of patients with sporadic pituitary adenomas.* Eur J Endocrinol, 2016. **174**(4): p. 523-30.
96. Matsumoto, R., et al., *Genetic and clinical characteristics of Japanese patients with sporadic somatotropinoma.* Endocr J, 2016. **63**(11): p. 953-963.
97. Foltran, R.K., et al., *Study of major genetic factors involved in pituitary tumorigenesis and their impact on clinical and biological characteristics of sporadic somatotropinomas and non-functioning pituitary adenomas.* Braz J Med Biol Res, 2018. **51**(9): p. e7427.
98. Trivellin, G., et al., *Gigantism and acromegaly due to Xq26 microduplications and GPR101 mutation.* N Engl J Med, 2014. **371**(25): p. 2363-74.
99. Trivellin, G., et al., *An orphan G-protein-coupled receptor causes human gigantism and/or acromegaly: Molecular biology and clinical correlations.* Best Pract Res Clin Endocrinol Metab, 2018. **32**(2): p. 125-140.
100. Rostomyan, L., et al., *Clinical and genetic characterization of pituitary gigantism: an international collaborative study in 208 patients.* Endocr Relat Cancer, 2015. **22**(5): p. 745-57.
101. Ma, Q. and J.P. Whitlock, Jr., *A novel cytoplasmic protein that interacts with the Ah receptor, contains tetratricopeptide repeat motifs, and augments the transcriptional response to 2,3,7,8-tetrachlorodibenzo-p-dioxin.* J Biol Chem, 1997. **272**(14): p. 8878-84.
102. Kuzhandaivelu, N., et al., *XAP2, a novel hepatitis B virus X-associated protein that inhibits X transactivation.* Nucleic Acids Res, 1996. **24**(23): p. 4741-50.
103. Meyer, B.K., et al., *Hepatitis B virus X-associated protein 2 is a subunit of the unliganded aryl hydrocarbon receptor core complex and exhibits transcriptional enhancer activity.* Mol Cell Biol, 1998. **18**(2): p. 978-88.
104. Carver, L.A. and C.A. Bradfield, *Ligand-dependent interaction of the aryl hydrocarbon receptor with a novel immunophilin homolog in vivo.* J Biol Chem, 1997. **272**(17): p. 11452-6.
105. Linnert, M., et al., *NMR assignments of the FKBP-type PPIase domain of the human aryl-hydrocarbon receptor-interacting protein (AIP).* Biomol NMR Assign, 2012. **6**(2): p. 209-12.
106. Laenger, A., et al., *XAP2 inhibits glucocorticoid receptor activity in mammalian cells.* FEBS Lett, 2009. **583**(9): p. 1493-8.
107. Morgan, R.M., et al., *Structure of the TPR domain of AIP: lack of client protein interaction with the C-terminal alpha-7 helix of the TPR domain of AIP is sufficient for pituitary adenoma predisposition.* PLoS One, 2012. **7**(12): p. e53339.
108. Blatch, G.L. and M. Lassle, *The tetratricopeptide repeat: a structural motif mediating protein-protein interactions.* Bioessays, 1999. **21**(11): p. 932-9.
109. Trivellin, G. and M. Korbonits, *AIP and its interacting partners.* J Endocrinol, 2011. **210**(2): p. 137-55.

110. Perdew, G.H., *Association of the Ah receptor with the 90-kDa heat shock protein.* J Biol Chem, 1988. **263**(27): p. 13802-5.
111. Denis, M., et al., *Association of the dioxin receptor with the Mr 90,000 heat shock protein: a structural kinship with the glucocorticoid receptor.* Biochem Biophys Res Commun, 1988. **155**(2): p. 801-7.
112. Bolger, G.B., et al., *Attenuation of the activity of the cAMP-specific phosphodiesterase PDE4A5 by interaction with the immunophilin XAP2.* J Biol Chem, 2003. **278**(35): p. 33351-63.
113. de Oliveira, S.K., et al., *Phosphodiesterase 2A forms a complex with the co-chaperone XAP2 and regulates nuclear translocation of the aryl hydrocarbon receptor.* J Biol Chem, 2007. **282**(18): p. 13656-63.
114. Nakata, A., et al., *G-protein signalling negatively regulates the stability of aryl hydrocarbon receptor.* EMBO Rep, 2009. **10**(6): p. 622-8.
115. Kazlauskas, A., L. Poellinger, and I. Pongratz, *Evidence that the co-chaperone p23 regulates ligand responsiveness of the dioxin (Aryl hydrocarbon) receptor.* J Biol Chem, 1999. **274**(19): p. 13519-24.
116. Meyer, B.K. and G.H. Perdew, *Characterization of the AhR-hsp90-XAP2 core complex and the role of the immunophilin-related protein XAP2 in AhR stabilization.* Biochemistry, 1999. **38**(28): p. 8907-17.
117. LaPres, J.J., et al., *ARA9 modifies agonist signaling through an increase in cytosolic aryl hydrocarbon receptor.* J Biol Chem, 2000. **275**(9): p. 6153-9.
118. Kazlauskas, A., L. Poellinger, and I. Pongratz, *The immunophilin-like protein XAP2 regulates ubiquitination and subcellular localization of the dioxin receptor.* J Biol Chem, 2000. **275**(52): p. 41317-24.
119. Reyes, H., S. Reisz-Porszasz, and O. Hankinson, *Identification of the Ah receptor nuclear translocator protein (Arnt) as a component of the DNA binding form of the Ah receptor.* Science, 1992. **256**(5060): p. 1193-5.
120. Sutherland, E.W. and T.W. Rall, *Fractionation and characterization of a cyclic adenine ribonucleotide formed by tissue particles.* J Biol Chem, 1958. **232**(2): p. 1077-91.
121. Drummond, G.I. and S. Perrott-Yee, *Enzymatic hydrolysis of adenosine 3',5'-phosphoric acid.* J Biol Chem, 1961. **236**: p. 1126-9.
122. Zaccolo, M. and M.A. Movsesian, *cAMP and cGMP signaling cross-talk: role of phosphodiesterases and implications for cardiac pathophysiology.* Circ Res, 2007. **100**(11): p. 1569-78.
123. Cazabat, L., et al., *Germline inactivating mutations of the aryl hydrocarbon receptor-interacting protein gene in a large cohort of sporadic acromegaly: mutations are found in a subset of young patients with macroadenomas.* Eur J Endocrinol, 2007. **157**(1): p. 1-8.
124. Daly, A.F. and A. Beckers, *The role of AIP mutations in pituitary adenomas: 10 years on.* Endocrine, 2017. **55**(2): p. 333-335.
125. Tuominen, I., et al., *AIP inactivation leads to pituitary tumorigenesis through defective Galphai-cAMP signaling.* Oncogene, 2015. **34**(9): p. 1174-84.
126. Chahal, H.S., et al., *Somatostatin analogs modulate AIP in somatotroph adenomas: the role of the ZAC1 pathway.* J Clin Endocrinol Metab, 2012. **97**(8): p. E1411-20.
127. Theodoropoulou, M., et al., *Tumor ZAC1 expression is associated with the response to somatostatin analog therapy in patients with acromegaly.* Int J Cancer, 2009. **125**(9): p. 2122-6.
128. Ferrau, F., et al., *Analysis of GPR101 and AIP genes mutations in acromegaly: a multicentric study.* Endocrine, 2016. **54**(3): p. 762-767.
129. Schofl, C., et al., *Frequency of AIP gene mutations in young patients with acromegaly: a registry-based study.* J Clin Endocrinol Metab, 2014. **99**(12): p. E2789-93.
130. Petrulis, J.R. and G.H. Perdew, *The role of chaperone proteins in the aryl hydrocarbon receptor core complex.* Chem Biol Interact, 2002. **141**(1-2): p. 25-40.

131. Bell, D.R. and A. Poland, *Binding of aryl hydrocarbon receptor (AhR) to AhR-interacting protein. The role of hsp90.* J Biol Chem, 2000. **275**(46): p. 36407-14.
132. Occhi, G., et al., *The R304X mutation of the aryl hydrocarbon receptor interacting protein gene in familial isolated pituitary adenomas: Mutational hot-spot or founder effect?* J Endocrinol Invest, 2010. **33**(11): p. 800-5.
133. De Sousa, S.M.C., et al., *Germline variants in familial pituitary tumour syndrome genes are common in young patients and families with additional endocrine tumours.* Eur J Endocrinol, 2017. **176**(5): p. 635-644.
134. Jennings, J.E., et al., *Aggressive pituitary adenomas occurring in young patients in a large Polynesian kindred with a germline R271W mutation in the AIP gene.* Eur J Endocrinol, 2009. **161**(5): p. 799-804.
135. He, L. and G.J. Hannon, *MicroRNAs: small RNAs with a big role in gene regulation.* Nat Rev Genet, 2004. **5**(7): p. 522-31.
136. Ambros, V., *The functions of animal microRNAs.* Nature, 2004. **431**(7006): p. 350-5.
137. Lee, Y., et al., *MicroRNA maturation: stepwise processing and subcellular localization.* EMBO J, 2002. **21**(17): p. 4663-70.
138. Lee, Y., et al., *The nuclear RNase III Drosha initiates microRNA processing.* Nature, 2003. **425**(6956): p. 415-9.
139. Lund, E., et al., *Nuclear export of microRNA precursors.* Science, 2004. **303**(5654): p. 95-8.
140. Bohnsack, M.T., K. Czaplinski, and D. Gorlich, *Exportin 5 is a RanGTP-dependent dsRNA-binding protein that mediates nuclear export of pre-miRNAs.* RNA, 2004. **10**(2): p. 185-91.
141. Hutvagner, G., et al., *A cellular function for the RNA-interference enzyme Dicer in the maturation of the let-7 small temporal RNA.* Science, 2001. **293**(5531): p. 834-8.
142. Grishok, A., et al., *Genes and mechanisms related to RNA interference regulate expression of the small temporal RNAs that control C. elegans developmental timing.* Cell, 2001. **106**(1): p. 23-34.
143. Ketting, R.F., et al., *Dicer functions in RNA interference and in synthesis of small RNA involved in developmental timing in C. elegans.* Genes Dev, 2001. **15**(20): p. 2654-9.
144. Hammond, S.M., et al., *Argonaute2, a link between genetic and biochemical analyses of RNAi.* Science, 2001. **293**(5532): p. 1146-50.
145. Schwarz, D.S., et al., *Asymmetry in the assembly of the RNAi enzyme complex.* Cell, 2003. **115**(2): p. 199-208.
146. Khvorova, A., A. Reynolds, and S.D. Jayasena, *Functional siRNAs and miRNAs exhibit strand bias.* Cell, 2003. **115**(2): p. 209-16.
147. Wu, H., et al., *Alternative processing of primary microRNA transcripts by Drosha generates 5' end variation of mature microRNA.* PLoS One, 2009. **4**(10): p. e7566.
148. Lagos-Quintana, M., et al., *Identification of novel genes coding for small expressed RNAs.* Science, 2001. **294**(5543): p. 853-8.
149. Lagos-Quintana, M., et al., *Identification of tissue-specific microRNAs from mouse.* Curr Biol, 2002. **12**(9): p. 735-9.
150. Lau, N.C., et al., *An abundant class of tiny RNAs with probable regulatory roles in Caenorhabditis elegans.* Science, 2001. **294**(5543): p. 858-62.
151. Baskerville, S. and D.P. Bartel, *Microarray profiling of microRNAs reveals frequent coexpression with neighboring miRNAs and host genes.* RNA, 2005. **11**(3): p. 241-7.
152. Monteys, A.M., et al., *Structure and activity of putative intronic miRNA promoters.* RNA, 2010. **16**(3): p. 495-505.
153. Rodriguez, A., et al., *Identification of mammalian microRNA host genes and transcription units.* Genome Res, 2004. **14**(10A): p. 1902-10.
154. Lagos-Quintana, M., et al., *New microRNAs from mouse and human.* RNA, 2003. **9**(2): p. 175-9.

155. Lee, Y., et al., *MicroRNA genes are transcribed by RNA polymerase II.* EMBO J, 2004. **23**(20): p. 4051-60.
156. Cai, X., C.H. Hagedorn, and B.R. Cullen, *Human microRNAs are processed from capped, polyadenylated transcripts that can also function as mRNAs.* RNA, 2004. **10**(12): p. 1957-66.
157. Hutvagner, G. and P.D. Zamore, *RNAi: nature abhors a double-strand.* Curr Opin Genet Dev, 2002. **12**(2): p. 225-32.
158. Doench, J.G., C.P. Petersen, and P.A. Sharp, *siRNAs can function as miRNAs.* Genes Dev, 2003. **17**(4): p. 438-42.
159. Zeng, Y., E.J. Wagner, and B.R. Cullen, *Both natural and designed micro RNAs can inhibit the expression of cognate mRNAs when expressed in human cells.* Mol Cell, 2002. **9**(6): p. 1327-33.
160. Zeng, Y. and B.R. Cullen, *Sequence requirements for micro RNA processing and function in human cells.* RNA, 2003. **9**(1): p. 112-23.
161. Friedman, R.C., et al., *Most mammalian mRNAs are conserved targets of microRNAs.* Genome Res, 2009. **19**(1): p. 92-105.
162. Brennecke, J., et al., *Principles of microRNA-target recognition.* PLoS Biol, 2005. **3**(3): p. e85.
163. Krek, A., et al., *Combinatorial microRNA target predictions.* Nat Genet, 2005. **37**(5): p. 495-500.
164. Tan, L., et al., *Genome-wide serum microRNA expression profiling identifies serum biomarkers for Alzheimer's disease.* J Alzheimers Dis, 2014. **40**(4): p. 1017-27.
165. Junker, A., et al., *MicroRNA profiling of multiple sclerosis lesions identifies modulators of the regulatory protein CD47.* Brain, 2009. **132**(Pt 12): p. 3342-52.
166. Gartel, A.L. and E.S. Kandel, *miRNAs: Little known mediators of oncogenesis.* Semin Cancer Biol, 2008. **18**(2): p. 103-10.
167. Hanahan, D. and R.A. Weinberg, *Hallmarks of cancer: the next generation.* Cell, 2011. **144**(5): p. 646-74.
168. Calin, G.A., et al., *MiR-15a and miR-16-1 cluster functions in human leukemia.* Proc Natl Acad Sci U S A, 2008. **105**(13): p. 5166-71.
169. Peng, Y. and C.M. Croce, *The role of MicroRNAs in human cancer.* Signal Transduct Target Ther, 2016. **1**: p. 15004.
170. Mao, Z.G., et al., *Differential expression of microRNAs in GH-secreting pituitary adenomas.* Diagn Pathol, 2010. **5**: p. 79.
171. Bottoni, A., et al., *miR-15a and miR-16-1 down-regulation in pituitary adenomas.* J Cell Physiol, 2005. **204**(1): p. 280-5.
172. Bottoni, A., et al., *Identification of differentially expressed microRNAs by microarray: a possible role for microRNA genes in pituitary adenomas.* J Cell Physiol, 2007. **210**(2): p. 370-7.
173. Butz, H., et al., *MicroRNA profile indicates downregulation of the TGFbeta pathway in sporadic non-functioning pituitary adenomas.* Pituitary, 2011. **14**(2): p. 112-24.
174. Amaral, F.C., et al., *MicroRNAs differentially expressed in ACTH-secreting pituitary tumors.* J Clin Endocrinol Metab, 2009. **94**(1): p. 320-3.
175. Desvignes, T., et al., *miRNA Nomenclature: A View Incorporating Genetic Origins, Biosynthetic Pathways, and Sequence Variants.* Trends Genet, 2015. **31**(11): p. 613-626.
176. D'Angelo, D., et al., *Altered microRNA expression profile in human pituitary GH adenomas: down-regulation of miRNA targeting HMGA1, HMGA2, and E2F1.* J Clin Endocrinol Metab, 2012. **97**(7): p. E1128-38.
177. He, Z., et al., *Next-generation sequencing of microRNAs reveals a unique expression pattern in different types of pituitary adenomas.* Endocr J, 2019.
178. Stilling, G., et al., *MicroRNA expression in ACTH-producing pituitary tumors: up-regulation of microRNA-122 and -493 in pituitary carcinomas.* Endocrine, 2010. **38**(1): p. 67-75.
179. Leone, V., et al., *Thyrotropin regulates thyroid cell proliferation by up-regulating miR-23b and miR-29b that target SMAD3.* J Clin Endocrinol Metab, 2012. **97**(9): p. 3292-301.

180. Leone, V., et al., *miR-130b-3p Upregulation Contributes to the Development of Thyroid Adenomas Targeting CCDC6 Gene.* Eur Thyroid J, 2015. **4**(4): p. 213-21.
181. Leone, V., et al., *Mir-23b and miR-130b expression is downregulated in pituitary adenomas.* Mol Cell Endocrinol, 2014. **390**(1-2): p. 1-7.
182. Lines, K.E., et al., *MiR-15a/miR-16-1 expression inversely correlates with cyclin D1 levels in Men1 pituitary NETs.* J Endocrinol, 2018.
183. Renjie, W. and L. Haiqian, *MiR-132, miR-15a and miR-16 synergistically inhibit pituitary tumor cell proliferation, invasion and migration by targeting Sox5.* Cancer Lett, 2015. **356**(2 Pt B): p. 568-78.
184. Fan, X., et al., *Expression of somatostatin receptor subtype 2 in growth hormone-secreting pituitary adenoma and the regulation of miR-185.* J Endocrinol Invest, 2015. **38**(10): p. 1117-28.
185. Zhou, K., et al., *MicroRNA-106b promotes pituitary tumor cell proliferation and invasion through PI3K/AKT signaling pathway by targeting PTEN.* Tumour Biol, 2016. **37**(10): p. 13469-13477.
186. Lee, Y.J., et al., *Increased miR-338-3p expression correlates with invasiveness of GH-producing pituitary adenomas.* Endocrine, 2017. **58**(1): p. 184-189.
187. Wang, D.S., et al., *miR-133 inhibits pituitary tumor cell migration and invasion via down-regulating FOXC1 expression.* Genet Mol Res, 2016. **15**(1).
188. Zhao, Z.R., et al., *MiRNA153 induces pituitary tumor MMQ cell line apoptosis through down-regulating Skp protein expression.* Eur Rev Med Pharmacol Sci, 2017. **21**(6): p. 1270-1275.
189. Zhen, W., et al., *MicroRNA-524-5p Functions as a Tumor Suppressor in a Human Pituitary Tumor-Derived Cell Line.* Horm Metab Res, 2017. **49**(7): p. 550-557.
190. Trivellin, G., et al., *MicroRNA miR-107 is overexpressed in pituitary adenomas and inhibits the expression of aryl hydrocarbon receptor-interacting protein in vitro.* Am J Physiol Endocrinol Metab, 2012. **303**(6): p. E708-19.
191. Denes, J., et al., *Regulation of aryl hydrocarbon receptor interacting protein (AIP) protein expression by MiR-34a in sporadic somatotropinomas.* PLoS One, 2015. **10**(2): p. e0117107.
192. Nakahama, T., et al., *Aryl hydrocarbon receptor-mediated induction of the microRNA-132/212 cluster promotes interleukin-17-producing T-helper cell differentiation.* Proc Natl Acad Sci U S A, 2013. **110**(29): p. 11964-9.
193. Hanieh, H., *Aryl hydrocarbon receptor-microRNA-212/132 axis in human breast cancer suppresses metastasis by targeting SOX4.* Mol Cancer, 2015. **14**: p. 172.
194. Rogers, S., et al., *Aryl hydrocarbon receptor (AhR)-dependent regulation of pulmonary miRNA by chronic cigarette smoke exposure.* Sci Rep, 2017. **7**: p. 40539.
195. Robinson, J.T., et al., *Integrative genomics viewer.* Nat Biotechnol, 2011. **29**(1): p. 24-6.
196. Roth, C., et al., *Circulating microRNAs as blood-based markers for patients with primary and metastatic breast cancer.* Breast Cancer Res, 2010. **12**(6): p. R90.
197. Rainer, J., et al., *CARMAweb: comprehensive R- and bioconductor-based web service for microarray data analysis.* Nucleic Acids Res, 2006. **34**(Web Server issue): p. W498-503.
198. Hernandez-Ramirez, L.C., et al., *Rapid Proteasomal Degradation of Mutant Proteins Is the Primary Mechanism Leading to Tumorigenesis in Patients With Missense AIP Mutations.* J Clin Endocrinol Metab, 2016. **101**(8): p. 3144-54.
199. Ritvonen, E., et al., *Impact of AIP and inhibitory G protein alpha 2 proteins on clinical features of sporadic GH-secreting pituitary adenomas.* Eur J Endocrinol, 2017. **176**(2): p. 243-252.
200. Ozkaya, H.M., et al., *Germline mutations of aryl hydrocarbon receptor-interacting protein (AIP) gene and somatostatin receptor 1-5 and AIP immunostaining in patients with sporadic acromegaly with poor versus good response to somatostatin analogues.* Pituitary, 2018. **21**(4): p. 335-346.
201. Niyazoglu, M., et al., *Familial acromegaly due to aryl hydrocarbon receptor-interacting protein (AIP) gene mutation in a Turkish cohort.* Pituitary, 2014. **17**(3): p. 220-6.
202. Ramirez-Renteria, C., et al., *AIP mutations in young patients with acromegaly and the Tampico Giant: the Mexican experience.* Endocrine, 2016. **53**(2): p. 402-11.

203. Chahal, H.S., et al., *AIP mutation in pituitary adenomas in the 18th century and today.* N Engl J Med, 2011. **364**(1): p. 43-50.
204. Radian, S., et al., *Increased Population Risk of AIP-Related Acromegaly and Gigantism in Ireland.* Hum Mutat, 2017. **38**(1): p. 78-85.
205. Stratakis, C.A., et al., *The role of germline AIP, MEN1, PRKAR1A, CDKN1B and CDKN2C mutations in causing pituitary adenomas in a large cohort of children, adolescents, and patients with genetic syndromes.* Clin Genet, 2010. **78**(5): p. 457-63.
206. Naves, L.A., et al., *Variable pathological and clinical features of a large Brazilian family harboring a mutation in the aryl hydrocarbon receptor-interacting protein gene.* Eur J Endocrinol, 2007. **157**(4): p. 383-91.
207. Toledo, R.A., et al., *Germline mutation in the aryl hydrocarbon receptor interacting protein gene in familial somatotropinoma.* J Clin Endocrinol Metab, 2007. **92**(5): p. 1934-7.
208. Oriola, J., et al., *Germline mutations of AIP gene in somatotropinomas resistant to somatostatin analogues.* Eur J Endocrinol, 2013. **168**(1): p. 9-13.
209. Pinho, L.K., et al., *Familial isolated pituitary adenomas experience at a single center: clinical importance of AIP mutation screening.* Arq Bras Endocrinol Metabol, 2010. **54**(8): p. 698-704.
210. Toledo, R.A., et al., *Isolated familial somatotropinoma: 11q13-loh and gene/protein expression analysis suggests a possible involvement of aip also in non-pituitary tumorigenesis.* Clinics (Sao Paulo), 2010. **65**(4): p. 407-15.
211. Dutta, P., et al., *Surgery, octreotide, temozolomide, bevacizumab, radiotherapy and pegvisomant treatment of an AIP mutation positive child.* J Clin Endocrinol Metab, 2019.
212. Georgitsi, M., et al., *Large genomic deletions in AIP in pituitary adenoma predisposition.* J Clin Endocrinol Metab, 2008. **93**(10): p. 4146-51.
213. Khoo, S.K., et al., *Genome-wide scan identifies novel modifier loci of acromegalic phenotypes for isolated familial somatotropinoma.* Endocr Relat Cancer, 2009. **16**(3): p. 1057-63.
214. Naves, L.A., et al., *Aggressive prolactinoma in a child related to germline mutation in the ARYL hydrocarbon receptor interacting protein (AIP) gene.* Arq Bras Endocrinol Metabol, 2010. **54**(8): p. 761-7.
215. Villa, C., et al., *Hyperplasia-adenoma sequence in pituitary tumorigenesis related to aryl hydrocarbon receptor interacting protein gene mutation.* Endocr Relat Cancer, 2011. **18**(3): p. 347-56.
216. Personnier, C., et al., *Clinical features and treatment of pediatric somatotropinoma: case study of an aggressive tumor due to a new AIP mutation and extensive literature review.* Horm Res Paediatr, 2011. **75**(6): p. 392-402.
217. Salvatori, R., et al., *In-frame seven amino-acid duplication in AIP arose over the last 3000 years, disrupts protein interaction and stability and is associated with gigantism.* Eur J Endocrinol, 2017. **177**(3): p. 257-266.
218. Garcia-Arnes, J.A., et al., *Familial isolated pituitary adenoma caused by a Aip gene mutation not described before in a family context.* Endocr Pathol, 2013. **24**(4): p. 234-8.
219. Belar, O., et al., *Novel mutations in MEN1, CDKN1B and AIP genes in patients with multiple endocrine neoplasia type 1 syndrome in Spain.* Clin Endocrinol (Oxf), 2012. **76**(5): p. 719-24.
220. Xekouki, P., et al., *Familial pituitary apoplexy as the only presentation of a novel AIP mutation.* Endocr Relat Cancer, 2013. **20**(5): p. L11-4.
221. Urbani, C., et al., *A novel germline mutation in the aryl hydrocarbon receptor-interacting protein (AIP) gene in an Italian family with gigantism.* J Endocrinol Invest, 2014. **37**(10): p. 949-55.
222. Salvatori, R., et al., *A clinically novel AIP mutation in a patient with a very large, apparently sporadic somatotrope adenoma.* Endocrinol Diabetes Metab Case Rep, 2014. **2014**: p. 140048.

223. Iwata, T., et al., *A novel C-terminal nonsense mutation, Q315X, of the aryl hydrocarbon receptor-interacting protein gene in a Japanese familial isolated pituitary adenoma family.* Endocr Pathol, 2014. **25**(3): p. 273-81.
224. Karaca, Z., et al., *Prevalence of AIP mutations in a series of Turkish acromegalic patients: are synonymous AIP mutations relevant?* Pituitary, 2015. **18**(6): p. 831-7.
225. Mangupli, R., et al., *Combined treatment with octreotide LAR and pegvisomant in patients with pituitary gigantism: clinical evaluation and genetic screening.* Pituitary, 2016. **19**(5): p. 507-14.
226. Cansu, G.B., et al., *A novel truncating AIP mutation, p.W279*, in a familial isolated pituitary adenoma (FIPA) kindred.* Hormones (Athens), 2016. **15**(3): p. 441-444.
227. Imran, S.A., et al., *Unusual AIP mutation and phenocopy in the family of a young patient with acromegalic gigantism.* Endocrinol Diabetes Metab Case Rep, 2018. **2018**.
228. Cai, F., et al., *A Novel Mutation of Aryl Hydrocarbon Receptor Interacting Protein Gene Associated with Familial Isolated Pituitary Adenoma Mediates Tumor Invasion and Growth Hormone Hypersecretion.* World Neurosurg, 2019. **123**: p. e45-e59.
229. Heier, C.R. and C.J. DiDonato, *Translational readthrough by the aminoglycoside geneticin (G418) modulates SMN stability in vitro and improves motor function in SMA mice in vivo.* Hum Mol Genet, 2009. **18**(7): p. 1310-22.
230. Cheung, N.W. and S.C. Boyages, *Somatostatin-14 and its analog octreotide exert a cytostatic effect on GH3 rat pituitary tumor cell proliferation via a transient G0/G1 cell cycle block.* Endocrinology, 1995. **136**(10): p. 4174-81.
231. Pelicci, G., et al., *Inhibitory effect of the somatostatin analog octreotide on rat pituitary tumor cell (GH3) proliferation in vitro.* J Endocrinol Invest, 1990. **13**(8): p. 657-62.
232. Zatelli, M.C., et al., *In vitro testing of new somatostatin analogs on pituitary tumor cells.* Mol Cell Endocrinol, 2008. **286**(1-2): p. 187-91.
233. Formosa, R., A. Xuereb-Anastasi, and J. Vassallo, *Aip regulates cAMP signalling and GH secretion in GH3 cells.* Endocr Relat Cancer, 2013. **20**(4): p. 495-505.
234. Vallar, L., A. Spada, and G. Giannattasio, *Altered Gs and adenylate cyclase activity in human GH-secreting pituitary adenomas.* Nature, 1987. **330**(6148): p. 566-8.
235. Lania, A., et al., *Effects of hypothalamic neuropeptides on extracellular signal-regulated kinase (ERK1 and ERK2) cascade in human tumoral pituitary cells.* J Clin Endocrinol Metab, 2003. **88**(4): p. 1692-6.
236. Pertuit, M., et al., *Signalling pathway alterations in pituitary adenomas: involvement of Gsalpha, cAMP and mitogen-activated protein kinases.* J Neuroendocrinol, 2009. **21**(11): p. 869-77.
237. Peterson, S.M., et al., *Common features of microRNA target prediction tools.* Front Genet, 2014. **5**: p. 23.
238. Birnbaumer, L., *Expansion of signal transduction by G proteins. The second 15 years or so: from 3 to 16 alpha subunits plus betagamma dimers.* Biochim Biophys Acta, 2007. **1768**(4): p. 772-93.
239. Heliovaara, E., et al., *The expression of AIP-related molecules in elucidation of cellular pathways in pituitary adenomas.* Am J Pathol, 2009. **175**(6): p. 2501-7.
240. Raitila, A., et al., *Mice with inactivation of aryl hydrocarbon receptor-interacting protein (Aip) display complete penetrance of pituitary adenomas with aberrant ARNT expression.* Am J Pathol, 2010. **177**(4): p. 1969-76.
241. Aloni-Grinstein, R., et al., *Wild type p53 functions as a control protein in the differentiation pathway of the B-cell lineage.* Oncogene, 1993. **8**(12): p. 3297-305.
242. Soddu, S., et al., *Interference with p53 protein inhibits hematopoietic and muscle differentiation.* J Cell Biol, 1996. **134**(1): p. 193-204.
243. Lotem, J. and L. Sachs, *Regulation by bcl-2, c-myc, and p53 of susceptibility to induction of apoptosis by heat shock and cancer chemotherapy compounds in differentiation-competent and -defective myeloid leukemic cells.* Cell Growth Differ, 1993. **4**(1): p. 41-7.

244. Gottlieb, E., et al., *Down-regulation of wild-type p53 activity interferes with apoptosis of IL-3-dependent hematopoietic cells following IL-3 withdrawal.* EMBO J, 1994. **13**(6): p. 1368-74.
245. Aloni-Grinstein, R., D. Schwartz, and V. Rotter, *Accumulation of wild-type p53 protein upon gamma-irradiation induces a G2 arrest-dependent immunoglobulin kappa light chain gene expression.* EMBO J, 1995. **14**(7): p. 1392-401.
246. Birch, J.M., et al., *Cancer phenotype correlates with constitutional TP53 genotype in families with the Li-Fraumeni syndrome.* Oncogene, 1998. **17**(9): p. 1061-8.
247. Rowlands, J.C., et al., *An evaluation of single nucleotide polymorphisms in the human aryl hydrocarbon receptor-interacting protein (AIP) gene.* Drug Metab Pharmacokinet, 2011. **26**(4): p. 431-9.
248. Dinesen, P.T., et al., *An unusual case of an ACTH-secreting macroadenoma with a germline variant in the aryl hydrocarbon receptor-interacting protein (AIP) gene.* Endocrinol Diabetes Metab Case Rep, 2015. **2015**: p. 140105.
249. Sager, R., *Expression genetics in cancer: shifting the focus from DNA to RNA.* Proc Natl Acad Sci U S A, 1997. **94**(3): p. 952-5.
250. Klusmann, J.H., et al., *miR-125b-2 is a potential oncomiR on human chromosome 21 in megakaryoblastic leukemia.* Genes Dev, 2010. **24**(5): p. 478-90.
251. Williams, M., et al., *Exploring Mechanisms of MicroRNA Downregulation in Cancer.* Microrna, 2017. **6**(1): p. 2-16.
252. He, L., et al., *A microRNA component of the p53 tumour suppressor network.* Nature, 2007. **447**(7148): p. 1130-4.
253. Bommer, G.T., et al., *p53-mediated activation of miRNA34 candidate tumor-suppressor genes.* Curr Biol, 2007. **17**(15): p. 1298-307.
254. Chang, T.C., et al., *Transactivation of miR-34a by p53 broadly influences gene expression and promotes apoptosis.* Mol Cell, 2007. **26**(5): p. 745-52.
255. Raver-Shapira, N., et al., *Transcriptional activation of miR-34a contributes to p53-mediated apoptosis.* Mol Cell, 2007. **26**(5): p. 731-43.
256. Tarasov, V., et al., *Differential regulation of microRNAs by p53 revealed by massively parallel sequencing: miR-34a is a p53 target that induces apoptosis and G1-arrest.* Cell Cycle, 2007. **6**(13): p. 1586-93.
257. Welch, C., Y. Chen, and R.L. Stallings, *MicroRNA-34a functions as a potential tumor suppressor by inducing apoptosis in neuroblastoma cells.* Oncogene, 2007. **26**(34): p. 5017-22.
258. Tazawa, H., et al., *Tumor-suppressive miR-34a induces senescence-like growth arrest through modulation of the E2F pathway in human colon cancer cells.* Proc Natl Acad Sci U S A, 2007. **104**(39): p. 15472-7.
259. Mraz, M., et al., *miR-34a, miR-29c and miR-17-5p are downregulated in CLL patients with TP53 abnormalities.* Leukemia, 2009. **23**(6): p. 1159-63.
260. Corney, D.C., et al., *Frequent downregulation of miR-34 family in human ovarian cancers.* Clin Cancer Res, 2010. **16**(4): p. 1119-28.
261. Wang, J.X., et al., *Effect and mechanism of miR-34a on proliferation, apoptosis and invasion of laryngeal carcinoma cells.* Asian Pac J Trop Med, 2016. **9**(5): p. 494-8.
262. Deng, X., et al., *MicroRNA-34a regulates proliferation and apoptosis of gastric cancer cells by targeting silent information regulator 1.* Exp Ther Med, 2018. **15**(4): p. 3705-3714.
263. Hahn, W.C. and R.A. Weinberg, *Modelling the molecular circuitry of cancer.* Nat Rev Cancer, 2002. **2**(5): p. 331-41.
264. Munsch, D., et al., *Human and mouse Fas (APO-1/CD95) death receptor genes each contain a p53-responsive element that is activated by p53 mutants unable to induce apoptosis.* J Biol Chem, 2000. **275**(6): p. 3867-72.

265. Lin, X., et al., *Downregulation of Bcl-2 expression by miR-34a mediates palmitate-induced Min6 cells apoptosis.* J Diabetes Res, 2014. **2014**: p. 258695.
266. Yan, D., et al., *MicroRNA-34a inhibits uveal melanoma cell proliferation and migration through downregulation of c-Met.* Invest Ophthalmol Vis Sci, 2009. **50**(4): p. 1559-65.
267. Christoffersen, N.R., et al., *p53-independent upregulation of miR-34a during oncogene-induced senescence represses MYC.* Cell Death Differ, 2010. **17**(2): p. 236-45.
268. Yao, Y., et al., *MicroRNA profiling of human gastric cancer.* Mol Med Rep, 2009. **2**(6): p. 963-70.
269. Ferretti, E., et al., *MicroRNA profiling in human medulloblastoma.* Int J Cancer, 2009. **124**(3): p. 568-77.
270. Ruiz Esparza-Garrido, R., et al., *A proteomic approach of pediatric astrocytomas: MiRNAs and network insight.* J Proteomics, 2013. **94**: p. 162-75.
271. Costa, F.F., et al., *Identification of microRNAs as potential prognostic markers in ependymoma.* PLoS One, 2011. **6**(10): p. e25114.
272. Braoudaki, M., et al., *Microrna expression signatures predict patient progression and disease outcome in pediatric embryonal central nervous system neoplasms.* J Hematol Oncol, 2014. **7**: p. 96.
273. Marosvari, D., et al., *Altered microRNA expression in folliculotropic and transformed mycosis fungoides.* Pathol Oncol Res, 2015. **21**(3): p. 821-5.
274. Papadavid, E., et al., *Aberrant microRNA expression in tumor mycosis fungoides.* Tumour Biol, 2016. **37**(11): p. 14667-14675.
275. Liu, R., et al., *A five-microRNA signature identified from genome-wide serum microRNA expression profiling serves as a fingerprint for gastric cancer diagnosis.* Eur J Cancer, 2011. **47**(5): p. 784-91.
276. Fang, C., et al., *Serum microRNAs are promising novel biomarkers for diffuse large B cell lymphoma.* Ann Hematol, 2012. **91**(4): p. 553-9.
277. Pu, Y., et al., *MiR-34a-5p promotes multi-chemoresistance of osteosarcoma through down-regulation of the DLL1 gene.* Sci Rep, 2017. **7**: p. 44218.
278. Pu, Y., et al., *The miR-34a-5p promotes the multi-chemoresistance of osteosarcoma via repression of the AGTR1 gene.* BMC Cancer, 2017. **17**(1): p. 45.
279. Kastl, L., I. Brown, and A.C. Schofield, *miRNA-34a is associated with docetaxel resistance in human breast cancer cells.* Breast Cancer Res Treat, 2012. **131**(2): p. 445-54.
280. Bousquet, M., et al., *Myeloid cell differentiation arrest by miR-125b-1 in myelodysplastic syndrome and acute myeloid leukemia with the t(2;11)(p21;q23) translocation.* J Exp Med, 2008. **205**(11): p. 2499-506.
281. Surdziel, E., et al., *Enforced expression of miR-125b affects myelopoiesis by targeting multiple signaling pathways.* Blood, 2011. **117**(16): p. 4338-48.
282. Guan, Y., et al., *MiR-125b targets BCL3 and suppresses ovarian cancer proliferation.* Int J Cancer, 2011. **128**(10): p. 2274-83.
283. Bi, Q., et al., *Ectopic expression of MiR-125a inhibits the proliferation and metastasis of hepatocellular carcinoma by targeting MMP11 and VEGF.* PLoS One, 2012. **7**(6): p. e40169.
284. Liang, L., et al., *MicroRNA-125b suppressesed human liver cancer cell proliferation and metastasis by directly targeting oncogene LIN28B2.* Hepatology, 2010. **52**(5): p. 1731-40.
285. Svoronos, A.A., D.M. Engelman, and F.J. Slack, *OncomiR or Tumor Suppressor? The Duplicity of MicroRNAs in Cancer.* Cancer Res, 2016. **76**(13): p. 3666-70.
286. Perez-Anorve, I.X., et al., *New insights into radioresistance in breast cancer identify a dual function of miR-122 as a tumor suppressor and oncomiR.* Mol Oncol, 2019. **13**(5): p. 1249-1267.
287. Yang, Z., et al., *Overexpression of microRNA-34a Attenuates Proliferation and Induces Apoptosis in Pituitary Adenoma Cells via SOX7.* Mol Ther Oncolytics, 2018. **10**: p. 40-47.
288. Tashjian, A.H., Jr., et al., *Establishment of clonal strains of rat pituitary tumor cells that secrete growth hormone.* Endocrinology, 1968. **82**(2): p. 342-52.

289. Castillo, A.I. and A. Aranda, *Differential regulation of pituitary-specific gene expression by insulin-like growth factor 1 in rat pituitary GH4C1 and GH3 cells.* Endocrinology, 1997. **138**(12): p. 5442-51.
290. Yamashita, S. and S. Melmed, *Insulin-like growth factor I action on rat anterior pituitary cells: suppression of growth hormone secretion and messenger ribonucleic acid levels.* Endocrinology, 1986. **118**(1): p. 176-82.
291. Yamashita, S., M. Weiss, and S. Melmed, *Insulin-like growth factor I regulates growth hormone secretion and messenger ribonucleic acid levels in human pituitary tumor cells.* J Clin Endocrinol Metab, 1986. **63**(3): p. 730-5.
292. Tagliati, F., et al., *Magmas overexpression inhibits staurosporine induced apoptosis in rat pituitary adenoma cell lines.* PLoS One, 2013. **8**(9): p. e75194.
293. Sotillo, E., et al., *Myc overexpression brings out unexpected antiapoptotic effects of miR-34a.* Oncogene, 2011. **30**(22): p. 2587-94.
294. Rizzo, M., et al., *The over-expression of miR-34a fails to block DoHH2 lymphoma cell proliferation by reducing p53 via c-MYC down-regulation.* Nucleic Acid Ther, 2012. **22**(4): p. 283-8.
295. Woloschak, M., J.L. Roberts, and K. Post, *c-myc, c-fos, and c-myb gene expression in human pituitary adenomas.* J Clin Endocrinol Metab, 1994. **79**(1): p. 253-7.
296. Pei, L., *Identification of c-myc as a down-stream target for pituitary tumor-transforming gene.* J Biol Chem, 2001. **276**(11): p. 8484-91.
297. Liu, C., et al., *Increased betacatenin and c-myc expression predict aggressive growth of non-functioning pituitary adenomas: An assessment using a tissue microarray-based approach.* Mol Med Rep, 2017. **15**(4): p. 1793-1799.
298. Dworakowska, D., et al., *Activation of RAF/MEK/ERK and PI3K/AKT/mTOR pathways in pituitary adenomas and their effects on downstream effectors.* Endocr Relat Cancer, 2009. **16**(4): p. 1329-38.
299. Stork, P.J. and J.M. Schmitt, *Crosstalk between cAMP and MAP kinase signaling in the regulation of cell proliferation.* Trends Cell Biol, 2002. **12**(6): p. 258-66.
300. Mantovani, G., et al., *Effect of cyclic adenosine 3',5'-monophosphate/protein kinase a pathway on markers of cell proliferation in nonfunctioning pituitary adenomas.* J Clin Endocrinol Metab, 2005. **90**(12): p. 6721-4.
301. Vitali, E., et al., *Cyclic adenosine 3'-5'-monophosphate (cAMP) exerts proliferative and anti-proliferative effects in pituitary cells of different types by activating both cAMP-dependent protein kinase A (PKA) and exchange proteins directly activated by cAMP (Epac).* Mol Cell Endocrinol, 2014. **383**(1-2): p. 193-202.
302. Schernthaner-Reiter, M.H., G. Trivellin, and C.A. Stratakis, *Interaction of AIP with protein kinase A (cAMP-dependent protein kinase).* Hum Mol Genet, 2018.
303. Vezzosi, D. and J. Bertherat, *Phosphodiesterases in endocrine physiology and disease.* Eur J Endocrinol, 2011. **165**(2): p. 177-88.
304. Lyons, J., et al., *Two G protein oncogenes in human endocrine tumors.* Science, 1990. **249**(4969): p. 655-9.
305. Hayward, B.E., et al., *Imprinting of the G(s)alpha gene GNAS1 in the pathogenesis of acromegaly.* J Clin Invest, 2001. **107**(6): p. R31-6.
306. Kobayashi, I., et al., *Purification and characterization of five different alpha subunits of guanine-nucleotide-binding proteins in bovine brain membranes. Their physiological properties concerning the activities of adenylate cyclase and atrial muscarinic K+ channels.* Eur J Biochem, 1990. **191**(2): p. 499-506.
307. Peverelli, E., et al., *Specific roles of G(i) protein family members revealed by dissecting SST5 coupling in human pituitary cells.* J Cell Sci, 2013. **126**(Pt 2): p. 638-44.

308. Demir, H., et al., *Mutation analysis of inhibitory guanine nucleotide binding protein alpha (GNAI) loci in young and familial pituitary adenomas.* PLoS One, 2014. **9**(10): p. e109897.
309. Sevetson, B.R., X. Kong, and J.C. Lawrence, Jr., *Increasing cAMP attenuates activation of mitogen-activated protein kinase.* Proc Natl Acad Sci U S A, 1993. **90**(21): p. 10305-9.
310. D'Angelo, G., H. Lee, and R.I. Weiner, *cAMP-dependent protein kinase inhibits the mitogenic action of vascular endothelial growth factor and fibroblast growth factor in capillary endothelial cells by blocking Raf activation.* J Cell Biochem, 1997. **67**(3): p. 353-66.
311. Thoresen, G.H., E.J. Johasen, and T. Christoffersen, *Effects of cAMP on ERK mitogen-activated protein kinase activity in hepatocytes do not parallel the bidirectional regulation of DNA synthesis.* Cell Biol Int, 1999. **23**(1): p. 13-20.
312. Deeble, P.D., et al., *Interleukin-6- and cyclic AMP-mediated signaling potentiates neuroendocrine differentiation of LNCaP prostate tumor cells.* Mol Cell Biol, 2001. **21**(24): p. 8471-82.
313. Yonehara, T., et al., *Involvement of mitogen-activated protein kinase in cyclic adenosine 3',5'-monophosphate-induced hormone gene expression in rat pituitary GH(3) cells.* Endocrinology, 2001. **142**(7): p. 2811-9.
314. Arslan, G. and B.B. Fredholm, *Stimulatory and inhibitory effects of adenosine A(2A) receptors on nerve growth factor-induced phosphorylation of extracellular regulated kinases 1/2 in PC12 cells.* Neurosci Lett, 2000. **292**(3): p. 183-6.
315. Kasuki, L., et al., *AIP expression in sporadic somatotropinomas is a predictor of the response to octreotide LAR therapy independent of SSTR2 expression.* Endocr Relat Cancer, 2012. **19**(3): p. L25-9.
316. Kasuki, L., et al., *Resistance to octreotide LAR in acromegalic patients with high SSTR2 expression: analysis of AIP expression.* Arq Bras Endocrinol Metabol, 2012. **56**(8): p. 501-6.
317. Iacovazzo, D., et al., *Factors predicting pasireotide responsiveness in somatotroph pituitary adenomas resistant to first-generation somatostatin analogues: an immunohistochemical study.* Eur J Endocrinol, 2016. **174**(2): p. 241-50.
318. Jaffrain-Rea, M.L., et al., *Somatostatin analogues increase AIP expression in somatotropinomas, irrespective of Gsp mutations.* Endocr Relat Cancer, 2013. **20**(5): p. 753-66.
319. Burns, D.L., *Subunit structure and enzymic activity of pertussis toxin.* Microbiol Sci, 1988. **5**(9): p. 285-7.
320. Pan, M.G., T. Florio, and P.J. Stork, *G protein activation of a hormone-stimulated phosphatase in human tumor cells.* Science, 1992. **256**(5060): p. 1215-7.
321. Dent, P., et al., *Inactivation of raf-1 by a protein-tyrosine phosphatase stimulated by GTP and reconstituted by Galphai/o subunits.* J Biol Chem, 1996. **271**(6): p. 3119-23.
322. Florio, T., et al., *Somatostatin activation of mitogen-activated protein kinase via somatostatin receptor 1 (SSTR1).* Mol Endocrinol, 1999. **13**(1): p. 24-37.
323. Lahlou, H., et al., *sst2 Somatostatin receptor inhibits cell proliferation through Ras-, Rap1-, and B-Raf-dependent ERK2 activation.* J Biol Chem, 2003. **278**(41): p. 39356-71.
324. Kasuki Jomori de Pinho, L., et al., *Low aryl hydrocarbon receptor-interacting protein expression is a better marker of invasiveness in somatotropinomas than Ki-67 and p53.* Neuroendocrinology, 2011. **94**(1): p. 39-48.
325. Daly, A., et al., *AIP and MEN1 mutations and AIP immunohistochemistry in pituitary adenomas in a tertiary referral center.* Endocr Connect, 2019.

8 Acknowledgements

First of all, I want to thank **Prof. Dr. Natalia Pellegata** for giving me the opportunity to conduct my dissertation under her guidance and supervision. I am grateful for her scientific advice, her support and understanding.

I am very thankful to **Prof. Dr. Michael Atkinson** for his critical evaluation of this manuscript and his constant support during the project within the annual thesis committee meetings. Furthermore, I am very grateful to **Prof. Dr. Joachim Graw** for his participation at the thesis committee meetings.

Thanks to **Prof. Dr. Stephan Herzig** and the whole **Institute for Diabetes and Cancer** for the inclusion of our group and the unobstructed transition into this institute. This facilitated a multitude of new options to develop my project further and get new perspectives on the work. Thank you!

I want to express my gratitude to **Dr. Adrian Daly** for providing the human tissues and therefore facilitating this study. I am very thankful for your input and help! Thanks to **Dr. Auli Kahru** fpr providing cells for the study.

For their contribution to the present work I want to thank my former colleagues **Dr. Sara Molatore**, for the cloning of the AIP plasmids and preliminary experiments, and **Dr. Nikolai Falk**, for performing the miRNA assay. Thanks to **Dr. Martin Irmler** for the analysis of the miRNA array.

To my colleagues and friends **Dr. Tobi Wiedemann, Dr. Hermine Mohr, Nina Minaskan, Swapna Satam** and **Sebastian Gulde** and my former colleague **Dr. Andrea Richter** for all the fun, support and fruitful discussions. Working with you was always a pleasure! Thank you!

Thanks to **Elke Pulz** and **Elisabeth Weiß** for all their efforts and support in the lab!

Sincere thanks to my loved ones, **Manuel**, **Fritz** and **Rudi**, for making my life more joyful, exciting and much more exhausting over the last years. **Manuel**, thanks for your support and understanding during the last years, which were not always easy, but nevertheless, we made it! Thanks to my **family** and **friends** for always supporting me although I did not always have enough time for you.